Real-Time Three-Dimensional Acoustic Imaging System with a Reflector and Its Applications

by

Hirofumi Taki

Acknowledgments

The author wishes to express his appreciation to Professor Toru Sato for his constant guidance and constructive discussions throughout the present work. It would have been impossible to accomplish this thesis without his suggestions and criticisms. The author deeply thanks to Profs. Tetsuya Matsuda and Toshitaka Tsuda for their advice and suggestions for the present work.

The author thanks Associate Professor Seiji Norimatsu and Research Associate Takuya Sakamoto for their helpful advice and continuous encouragement. The author thanks the colleagues of Prof. Sato's Laboratory for their collaborative discussions and for participating the experiment of tactile stimulation. Especially the author deeply appreciates the members of radar research group for their useful suggestions and comments.

This work was partly supported by the 21st century center of excellence (COE) program (Grant No. 14213201).

Preface

The presentation of detailed environmental information allows the visually impaired to live their lives independently. To realize a robust vision substitute system with high time and spatial resolution, we propose a through-air acoustic imaging system with a reflector mirror and a 2-D element array. In the proposed system, a transmitter radiates a wide beam to the entire measurement field. The echo from a target is gathered by a concave mirror. The distance between the reflector mirror and the element array is fixed, and thus the defocused image is distributed along the array. The image of the target is reconstructed from the received signal on the array by numerical back projection. Since the proposed imager measures the entire target field in a transmit and receive event, the imager has significantly high time resolution. Furthermore, in this system most of the echo arriving at the mirror is gathered and received on the array. Thus the proposed imager has higher spatial resolution than that of a conventional imager with the same size element array. In this paper we evaluate the spatial resolution of the proposed imager using numerical calculation based on physical optics.

In order to transfer detailed environmental information to the visually impaired, we propose two stimulation methods to enhance transfer information using a 2-D tactile array. In the first method, stimulators are divided into several groups. Since each stimulator group is activated alternately, the interval of stimulations can be shortened to less than the two-point discrimination threshold. In cases in which stimulators are divided into two and four groups, for example, the number of stimulators increases to two and four times, respectively, of that in the case of the two-point discrimination threshold. In the second method, a user selects the measurement range and then the system presents targets within the range. The user acquires spatial information of the entire measurement area by changing the measurement range. This method can accurately present a range of targets. We examine and confirm these methods experimentally.

For the further improvement of medical diagnoses, real-time 3-D medical acoustic imagers are necessary. We propose a 3-D acoustic imager with a reflector and a 2-D dense element array for high time and spatial resolution. All elements on a small dense array are excited with proper time delays to transmit a broad beam similar to that of a single element transmitter. In this method, a wide beam with high power is radiated, and thus the proposed imager has a high signal-to-noise ratio. The echo is gathered by a concave reflector and received by the dense array. The image of the target is reconstructed by

numerical back projection from the de-focused image distributed on the array. With this scheme, images of the entire measurement field can be reconstructed from a single transmit and receive event. For sidelobe suppression, the reflection ratio of the reflector mirror is tapered off in the image reconstruction from the received signal. The synthesized transmit point can be changed in this system, and thus the coherent integration of multiple receive signals of different transmit points improves spatial resolution by using the synthetic aperture technique. We also evaluate the spatial resolution of the proposed imager using numerical calculation based on physical optics.

Contents

List of Tables

List of Figures

Chapter 1

General Introduction

1.1 Instruction

In 2001, the number of visually handicapped citizens in Japan was more than 300 thousand, and of these 60 % are severely visually impaired. Their blindness is caused mainly by diabetes, glaucoma, cataracts, retinitis pigmentosa, pathologic myopia, or macular degeneration. Regarding diabetes, recent changes in the cultural and social environments have caused an increase in its occurrence. Since cataracts and macular degenerations naturally occur by aging, the occurrence of these diseases will increase in Japan, an increasingly aging society. Therefore, in the future the number of totally blind citizens will increase, and thus the improvement of quality of life of the blind will become a serious issue. Many researchers have investigated mobility aid systems for the blind. For the blind, in order to go a destination it is necessary to detect and avoid obstacles. Particularly in cases of visiting a new place, such as when traveling, the real-time detection and discernment of many obstacles is needed to decide one 's next action, such as avoidance, waiting, or searching for an alternate route. Current means for mobility aid can be classified into two groups. The first group relies on the presence of an attendant or a guide dog, that is, the aid of a human being or an animal with vision. The other group relies on mobility aid instruments. Of these means, travel with an attendant is the safest. However, it also prevents the blind from living their own lives. As for travel with a guide dog, it also has many problems with respect to training and keeping the dog. Thus, the second group, mobility aid instruments, is very important for the blind. Mobility aid instruments can be further divided roughly into three types. The first is used for obstacle detection. The second is to transfer environmental information. The last is a guidance system to guide the blind to their destination. We propose an acoustic vision substitute system to transfer environmental information with high spatial resolution.

In advanced countries, heart disease is one of the main causes of death. For example, it is the second biggest cause of death in Japan. In order to improve the medical diagnosis of heart disease, 3-D volumetric high-resolution acoustic images are currently in high

demand. In this study, therefore, we investigate volumetric 3-D acoustic imaging systems as promising candidates for this purpose. We propose a novel acoustic 3-D imaging system to realize real-time high-resolution imaging.

1.2 Obstacle detection devices

Obstacle detection devices need to detect an obstacle by a certain means. The current main means for detecting an obstacle are as follows.

1) White cane.

2) Acoustic mobility aid devices.

3) Laser sensing devices.

1.2.1 White cane

A white cane is the most famous instrument used to detect obstacles. A white cane consists of a grip, shaft, and tip, as shown in Fig. 1.1. Their usage, originally contrived by R. Hoover, is generally uniform across many countries [1]. The user holds the white cane out in front of, and centered with, the body, shaking it right and left to discern the surrounding physical context. The tip of the cane detects obstacles located up to two paces in front of the user. It is important that each step taken and each touch of the tip of the cane on the ground occur at once.

This usage of a white cane as a type of mobility aid device is called the " touch technique " [2]. In the touch technique, it is necessary to note the following points. First, the white cane needs to be long enough to detect obstacles at locations as far as two steps in front of the user. Therefore, cane length is often adjusted to accommodate for each user 's body size, arm length, walking pace, walking speed, and reaction time. Second, the user shakes the cane to the right and left in order to scan in an arc-shape with the tip of the cane. The arc width is a little wider than the shoulders. Next, the user swings the cane rhythmically such that each walking step coincides with each touch of the tip on the ground. A light touch of the tip on the ground is desirable. Furthermore, the user interprets the tactile and auditory sensations caused by the swing of the cane, allowing for perception of the environment.

However, white canes are not without its problems. First, as they pass geometrical planes through the scanning motion, swells in the planes can be detected. However, as the tips of canes only pass through arcs, users are therefore only able to detect pits located within the arc. Second, canes only scan the area lower than the user 's chest, and thus they can not detect obstacles located higher than the chest. Next, canes can only detect

obstacles within a range of two steps. The ability to detect obstacles farther than two steps away is necessary for safe and comfortable walking. Moreover, canes can not be used in places where there are crowds of people. In addition, the utilization of a white cane requires arm movement, and thus users become tired after prolonged use. Lastly, a long period of training time is needed in order to become able to walk alone with a cane.

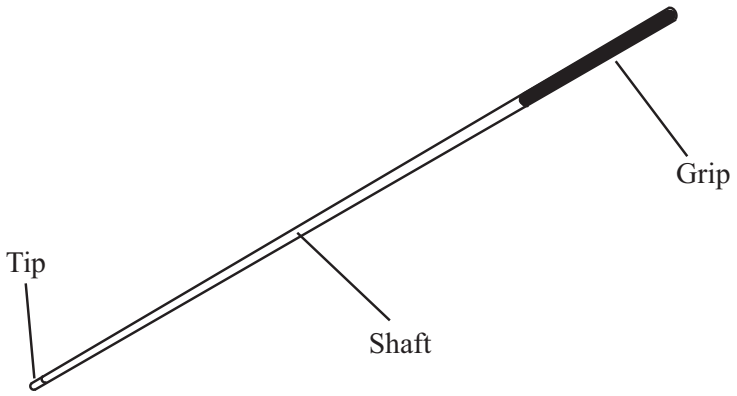

Figure 1.1: Schematic view of a white cane.

1.2.2 Acoustic mobility aid devices

High frequency sound above the audible range is generally referred to as ultrasound. An ultrasound wave is defined as a sound wave or elastic vibration with a frequency of more than 20 kHz. An ultrasound wave has directivity, and thus it can be radiated to a particular measurement field. Echoes from obstacles in a measurement field can then be received, allowing the obstacles to be detected.

For the determination of the target range, there are two possible methods. One employs pulse waves, and the other swept-frequency ultrasound. Fig. 1.2 shows a schematic view of the propagation route of a transmit wave. A pulse wave, radiated from a transmit element, is scattered by a target and then received on a receive element. This causes a time delay Δt between the transmit time and the receive time, as shown in Fig. 1.3. The target range is given by

$$r = c\Delta t/2, \tag{1.1}$$

where c is the sound velocity in the air.

Fig. 1.4 shows the frequencies of transmit and receive waves when a device radiates swept-frequency ultrasound, where the center frequency is f_0. In this method there is a certain frequency difference f_d between the transmit wave and the receive wave during most of the measurement time, as shown in Fig. 1.4. The target range is obtained by

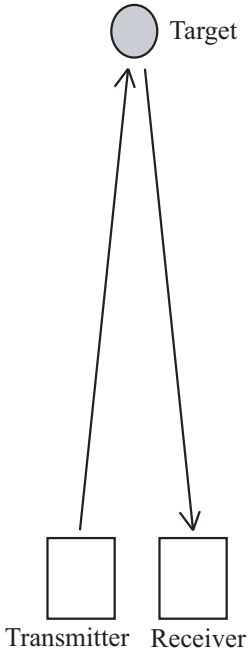

Figure 1.2: Schematic view of wave propagation.

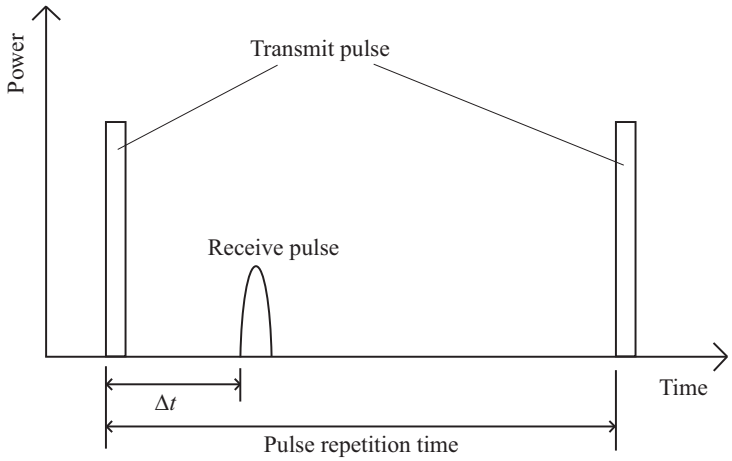

Figure 1.3: Transmit and receive time when pulse waves are radiated.

$$r = cf_{\mathrm{d}}T/(2\Delta f), \tag{1.2}$$

where T is the modulation repetition time, and Δf is the maximum modulation frequency.

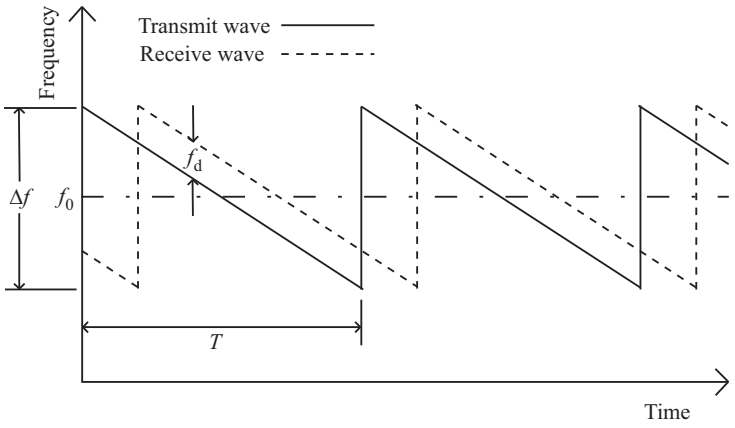

Figure 1.4: Frequency modulation of transmit and receive waves for target range detection.

A simple method to determine the target direction is to measure one direction in a transmit and receive event. A user directs a device of this type to a measurement direction and then checks for the existence of an obstacle in that direction. The user scans the device in the entire measurement field.

Another strategy to determine the target direction utilizes plural receive elements. Fig. 1.5 shows a schematic view of a device having one transmitter and two receivers. In this case the target direction is given by

$$\phi = \mathrm{asin}\left(\frac{{r_{\mathrm{R}}}^2 - {r_{\mathrm{L}}}^2}{2\sqrt{2}d\sqrt{{r_{\mathrm{R}}}^2 + {r_{\mathrm{L}}}^2 - 2d^2}}\right), \tag{1.3}$$

where r_{R} and r_{L} are the distances of the right and left receivers from the target, respectively, and d is the baseline interval of the transmitter and receiver. When $(r_{\mathrm{R}} - r_{\mathrm{L}})^2 - 4d^2 \ll (r_{\mathrm{R}} + r_{\mathrm{L}})^2$, the target direction is obtained by

$$\phi \simeq \mathrm{asin}\left(\frac{r_{\mathrm{R}} - r_{\mathrm{L}}}{2d}\right). \tag{1.4}$$

A mobility aid device measuring one direction in a transmit and receive event is called a clear path indicator. Devices of this type are designed to indicate paths without obstacles. N. Pressey [4] proposed the Mowat sensor, a hand-held device radiating acoustic pulses 15 degrees long and 30 degrees wide. It can detect within a range of 4 m. In cases where an obstacle exists in the measurement field, the Mowat sensor alerts the user and reports the range of the obstacle. L. Russel proposed the Pathsounder [5], a device worn on the

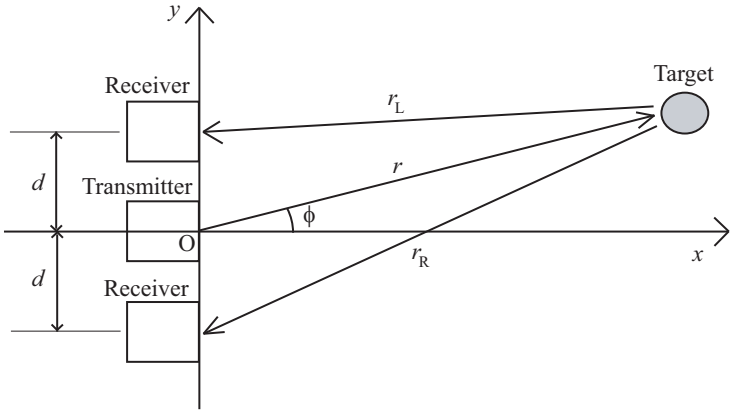

Figure 1.5: Schematic view of the detection of the target direction with two receive elements.

chest. It radiates an acoustic beam 15 degrees wide and can detect within a range of 1.8 m. These devices, therefore, require either manual scanning or chest movement in order to measure all of the target field, resulting in low time resolution.

L. Kay proposed another ultrasonic obstacle detector called Sonicguide [6]. The measurement field of this detector is 3 m wide within a range of 5 m. A transmitter radiates frequency modulation ultrasound continuously to the entire measurement field. One receiver is put at each of the right and left sides of the transmitter. Since the range of an obstacle corresponds to the difference between the transmit and receive frequencies, the device detects the distances of obstacles from the two receivers. In addition, the device can evaluate the direction of an obstacle from its respective distances from the two receivers. The device then presents this environmental information separately to the right and left ears. Since there is a difference between the strengths of the signals presented at to each ear corresponding to the different environmental information regarding the target direction, a user can therefore perceive the target direction based on this difference. For example, if the presented power at the right ear is larger than that at the left ear, then the target direction is to the right. The problems associated with the use of the Sonicguide are as follows. 1) Since it presents complex sounds continuously, it is greatly influenced by environmental noise. 2) Despite a required, long training period before use, still only a portion of potential users become accustomed to using it.

S. Shoval *et al.* presented the Navbelt, an instrument intended as a travel aid [7]. It consists of a portable computer, ultrasonic sensors, and stereophonic headphones. The acoustic signals are transmitted as discrete beeps or continuous sound. The device can detect the existence of obstacles, but its spatial resolution is insufficient for distinguishing plural obstacles.

1.2.3 Laser sensing devices

Laser sensing devices have been available commercially for more than thirty years. J. M. Benjuamine *et al.* [3] proposed the Laser Cane using GaAs laser pulses. From the top of this cane three pulses are radiated in three directions: upward, forward, and downward. The measurement fields are, respectively, at head-height, in front of the user within a range of 3.5 m, and at the foot of the user. The device is a clear path indicator, meaning that it informs the user only of the existence of obstacles in a path. The problems associated with the use of the Laser Cane are as follows. 1) Since it is heavier than a normal white cane (the latest version of the Laser Cane, C-5, weighs 453 g), users can easily become fatigued. 2) The manipulation of the Laser Cane is complex. 3) It has low range resolution. 4) Scattered light, and in particular that of solar light, can cause the device to falsely detect obstacles that are not present.

For high range resolution, laser triangulation systems have been proposed. A schematic view of such a system is shown in Fig. 1.6. The target range r is given by

$$r = \frac{B(f\sin\alpha - d\cos\alpha)}{f\cos\alpha + d\sin\alpha}, \tag{1.5}$$

where B is the baseline between the laser and the center of the lens, f is the focal distance of the lens, d is the location of the laser spot, and α is the slope of the element array to the laser line.

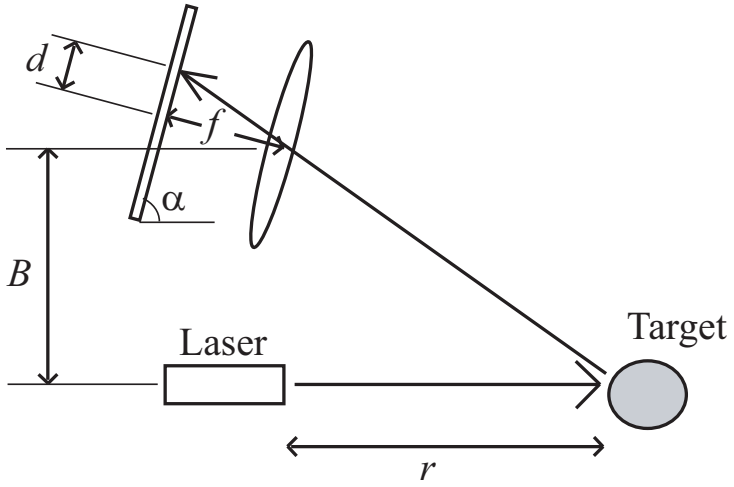

Figure 1.6: Schematic view of a laser triangulation system.

R. Farcy *et al.* proposed such a device for detecting obstacles [9]. It consists of a triangulating laser telemeter, electric parts, and auditory feedback devices close to the ear. D. Yuan *et al.* investigated another hand-held mobility aid device using active

triangulation [10]. The range information is presented to a user through a haptic interface. Since a device of this type needs hand movement scanning for measuring all of the target field, its time resolution is low.

1.3 Vision substitute systems for environmental information

Studies on vision substitute systems are generally conducted for one of two purposes: to inform users of visual information or to read books. As a reading aid for the blind, J. G. Linvil and J. C. Bliss proposed the Optacon [8]. This instrument has a 6 x 24 stimulator matrix, and each stimulator 's intensity is controlled by the received power at each photo-transistor of a camera. A user holds the camera in the right hand and uses it to scan a page of a book. The stimulator matrix is 2 cm wide and 5 cm long, and each stimulator presents 230 Hz vibrotactile stimulations. The user touches the matrix by fingertip and recognizes letters. In cases where a time of 2.4 seconds is used to read a Japanese Katakana character, the possibility of making a correct response is 83 %. S. Saida *et al.* investigated the function of 3 display modes using a vibrotactile display against the abdomen [11]. Y. Yanagida proposed another reading aid instrument with 3 x 3 vibrating motors on the back of a chair [12]. Using this instrument, a success rate of 87 % was obtained for letter reading.

In order to properly detect and distinguish obstacles, a vision substitute system to inform users of visual information is needed. G. Brindley and W. Lewin [13] produced a sensation of vision by electrical stimulation of the visual cortex. They implanted a 90-electrode matrix into each of the right and left visual cortexes. They confirmed that the electrical stimulation to the visual cortex allowed subjects to perceive phosphenes. M. S. Humayan [14] implanted electrodes at the retinal layers and then stimulated them electrically under local anesthesia. In a resolution test, a subject could resolve phosphenes at a 1.75 degree center-to-center distance. M. Mahadevappa *et al.* [15] investigated perceptual thresholds and electrode impedance with respect to the electrical stimulation of the retinal layers. All of the abovementioned methods, however, have the following problems. 1) Since they require the implantation of electrodes into users, they are strongly invasive. 2) Technological advances of these methods are slow because they require implantation in human subjects. L. Hesse *et al.* [16] evaluated the effectiveness of the implantation of retina stimulation electrodes using cats. In their experiment, they investigated responses in the visual cortexes of cats. However, as the chief purpose of vision substitute systems is not to make responses in the visual cortex but to inform the user of visual information, studies using animals are easy to conduct but difficult to be put to practical use.

C. C. Collins [17], P. Bach-y-Rita [18], C. C. Collins and P. Bach-y-Rita [19] proposed a tactile vision substitute system called TVSS. An image taken by a television-type camera is transformed to either vibrotactile or electrotactile stimulations on the skin of a user.

Each stimulation intensity corresponds to the intensity of each pixel of the image. They confirmed that users can distinguish vertical, horizontal, and diagonal lines. In addition, the TVSS can inform users of the rough form and size of objects [20]. In spite of these capabilities, however, the TVSS is not useful for informing users of the spatial information of plural objects. More specifically, the following problems associated with the TVSS are caused by its insufficient spatial resolution for the informing of complicated visual information. 1) Since the spatial resolution of the TVSS is much poorer than that of the eyes, a user can not identify each object when plural objects exist in the sight. 2) A user cannot perceive the range of an object without identifying the object.

Another strategy for the presentation of visual information to the blind involves the employment of auditory sensations. J. Coffey [21] and G. Smith *et al.* [22] created letter reading assistance systems using auditory sensations. In these systems, each letter corresponds to a sound of a particular frequency, with the output comprising multiple sounds. R. Fish [23] presented a vision substitute system using sound localization. The problem with such systems, however, is that in order for users to be able to grasping the actual environmental situation from auditory sensations, they must first have some previous knowledge of the environment.

1.4 Information transfer method for sensory substitute system

A 2-D tactile stimulator array can present spatial information to the skin in a way similar to the way visual information is presented to the retina. However, such an array has insufficient spatial resolution and dynamic range compared with visual information. Because of the lack of transfer information presented with a tactile stimulator array, it is therefore not useful when plural targets exist in the measurement field, that is, in daily life. Thus, many researchers have investigated the limitations of spatial information presented through tactile stimulation.

Sensory substitution systems employ either vibrotactile or electrotactile displays. K. A. Kaczmarek *et al.* [24] and C. A. Perez *et al.* [25] compared electrotactile and vibrotactile stimulations. According to their findings, the characteristics of eletcrotactile stimulation are as follows. 1) Since the stimulator is an electrode, the structure of a stimulator array is simple. 2) While the constant current stimulation provides stable sensations to users, regardless of the connection condition of the electrode to the skin, users will often burn themselves at the stimulation point with a bad connection to an electrode. 3) In a state of constant voltage stimulation, although a user will not be injured even if the connection to an electrode is bad, the current is not constant, and thus the sensation will not be stable. As for the characteristics of vibrotactile stimulation, they are as follows. 1) Piezo-electric transducers are miniature, consume low power, have low stimulation power, and can employ high stimulation frequency. Therefore they are mainly used for fingertip

stimulation. 2) While solenoids can not select high stimulation frequency, they can still stimulate in high power.

Vision substitution methods using tactile sensation have been reported from the early 1970s. As mentioned above, the TVSS employed tactile stimulations, but the lack of presented visual information and power consumption issues became problematic. Therefore many researchers have investigated ways to improve its stimulus quality and reduce power consumption. K. A. Kaczmarek *et al.* investigated the optimum pulse repetition rate, the number of pulses per burst, and the burst frequency for maximizing the dynamic range of electrotactile stimulation [26][27]. C. J. Poletto *et al.* designed a high-voltage constant current stimulator for exact electrotactile stimulation at the fingertip [28]. Since constant current stimulation is often painful, they examined a method for elevating the pain threshold for electrotactile stimulation [29]. C. A. Perez *et al.* investigated the optimum vibrotactile waveform for maximizing tactile sensitivity and decreasing power consumption [25][30]. Furthermore, they investigated the stimulation power required to reach tactile thresholds in electromechanical and piezo-electric transducers. Although several stimulation waveforms have been reported, the information presented by a tactile stimulator array is not sufficient for a vision substitute system to detect and distinguish obstacles.

1.5 Filtered back projection

To analyze an object by X-ray scanning, the line integral data should be inverted to retrieve the absorption coefficient distribution of the target field. J. Radon [31] solved this problem, and A. M. Cormack [32] gave a solution for X-ray scanning. Numerical reconstruction methods can be classified into two groups: Fourier reconstruction and filtered back-projection methods. It has been shown that both of these groups of methods are theoretically equivalent [33].

The Fourier reconstruction method is based on the projection-slice theorem [refnum1990]. Fourier transform and inverse Fourier transform are given, respectively, by

$$L(\alpha) = \int_{-\infty}^{\infty} l(x) e^{-j\alpha x} dx, \tag{1.6}$$

$$l(x) = \frac{1}{2\pi} \int_{-\infty}^{\infty} L(\alpha) e^{-j\alpha x} d\alpha. \tag{1.7}$$

The projection function onto the x' axis is given by

$$\begin{aligned} g(x', \theta) &= \int_{-\infty}^{\infty} f(x, y) dy' \\ &= \int_{-\infty}^{\infty} \int_{-\infty}^{\infty} f(x, y) \delta(x\cos\theta + y\sin\theta - x') dx dy, \end{aligned} \tag{1.8}$$

where $f(x, y)$ is the absorption coefficient, and θ is the direction of the x' axis from the x axis, as shown in Fig. 1.7. The set of projection functions for all directions is equivalent

to the Radon transform. The Fourier transform of $f(x, y)$ is given by

$$F(X, Y) = \int_{-\infty}^{\infty} \int_{-\infty}^{\infty} f(x, y) e^{-j(xX+yY)} dxdy. \tag{1.9}$$

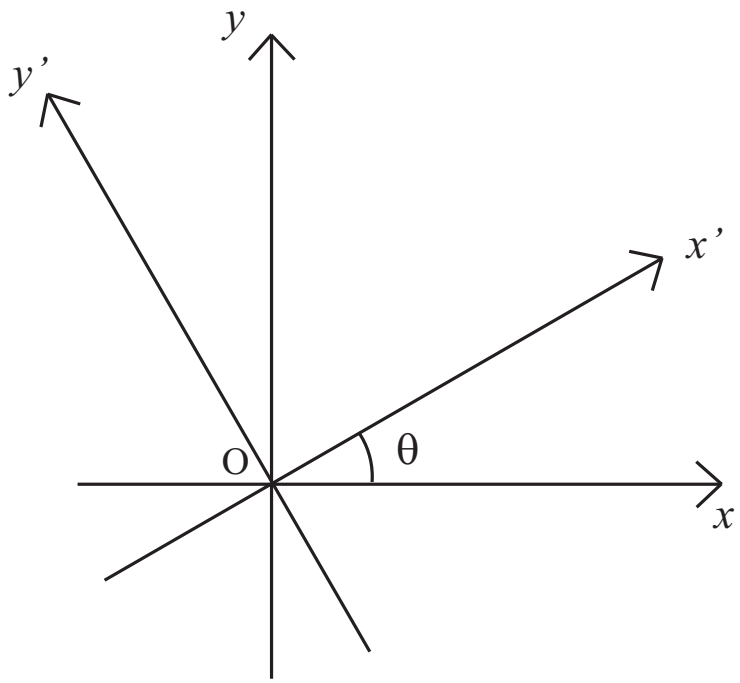

Figure 1.7: Coordinate systems used for Radon transform.

The 1-D Fourier transform of g is given by

$$\begin{aligned} G(r, \theta) &= \int_{-\infty}^{\infty} g(x', \theta) e^{-jrx'} dx' \\ &= \int_{-\infty}^{\infty} \int_{-\infty}^{\infty} \int_{-\infty}^{\infty} f(x, y) \delta(x\cos\theta + y\sin\theta - x') e^{-jrx'} dxdydx' \\ &= \int_{-\infty}^{\infty} \int_{-\infty}^{\infty} f(x, y) e^{-jr(x\cos\theta + y\sin\theta)} dxdy. \end{aligned} \tag{1.10}$$

Since $X = r\cos\theta$ and $Y = r\sin\theta$, $G(r, \theta)$ is equivalent to $F(X, Y)$. $f(x, y)$ is therefore solved from $G(r, \theta)$ using an inverse 2-D Fourier transform.

The Fourier reconstruction is sensitive to errors of calculation in Fourier space. Such errors influence the whole image, and of these, phase errors have the most serious effects. R. N. Bracewell *et al.* [34] found a way to avoid numerical Fourier transforms. After an equivalent correction is applied to all of the projection functions, the absorption coefficient distribution is reconstructed from the modified functions using back-projection.

Back-projection of g is given by

$$\begin{aligned} B(x,y) &= \int_0^{\pi} g(x',\theta)d\theta \\ &= \int_0^{\pi} g(x\cos\theta + y\sin\theta, \theta)d\theta. \end{aligned} \tag{1.11}$$

From Eq.1.9 and 1.10, $f(x,y)$ is obtained by

$$\begin{aligned} f(x,y) &= \frac{1}{4\pi^2}\int_{-\infty}^{\infty}\int_{-\infty}^{\infty} F(X,Y)e^{j(xX+yY)}dXdY \\ &= \frac{1}{4\pi^2}\int_0^{\pi}\int_{-\infty}^{\infty} G(r,\theta)e^{jr(x\cos\theta+y\sin\theta)}|r|drd\theta. \end{aligned} \tag{1.12}$$

To compensate for the difference between $f(x,y)$ and $B(x,y)$, a ramp filter $|r|$ is utilized. When no noise exists, the image can be acquired. However, a ramp filter is one of the high-path filters, and thus high-frequency noise is amplified. Therefore in this case some kind of low-path filter must be used. Back-projection after a particular kind of filtering is called filtered back-projection.

1.6 Medical acoustic 2-D imaging system

Medical acoustic imagers, having high value for medical diagnoses, are low cost and non-hazardous to human body. They are thus widely used for medical diagnoses. Most radiate ultrasound pulses to the human body. The pulses are scattered at the inhomogeneity of the medium, and then the echo is received at the transducers of the imagers. Most such imagers measure one direction in a transmit and receive event.

There are two types of images constructed from the measurement of one direction in the body. One is called the A mode image and the other is known as the M mode image. An acoustic probe of an A-mode imager is fixed and measures one direction in the body. The longitudinal and lateral axes of the A-mode image show the amplitude of the echo and the range of the reflection point, respectively. An acoustic probe of a M-mode imager also measures one direction in the body. However, the longitudinal and lateral axes of the image show the range of the reflection point and the measurement time, respectively. The echo power is converted to the brightness in the M-mode image. An M-mode imager is used for the measurement of fast moving organs, such as the heart.

B-mode imaging, on the other hand, was designed to measure one section of a human body. An acoustic probe of a B-mode imager scans transmit and receive beams either electronically or mechanically in a measurement plane in the body. The echo power is converted to the brightness, and a 2-D image is constructed from the data of all measurement directions. Several scan types of B-mode imagers are currently used for medical diagnoses. Fig. 1.8 shows a schematic view of these types. Although these imagers are useful, for the further improvement of medical diagnoses, a high-resolution acoustic 3-D imager has become necessary.

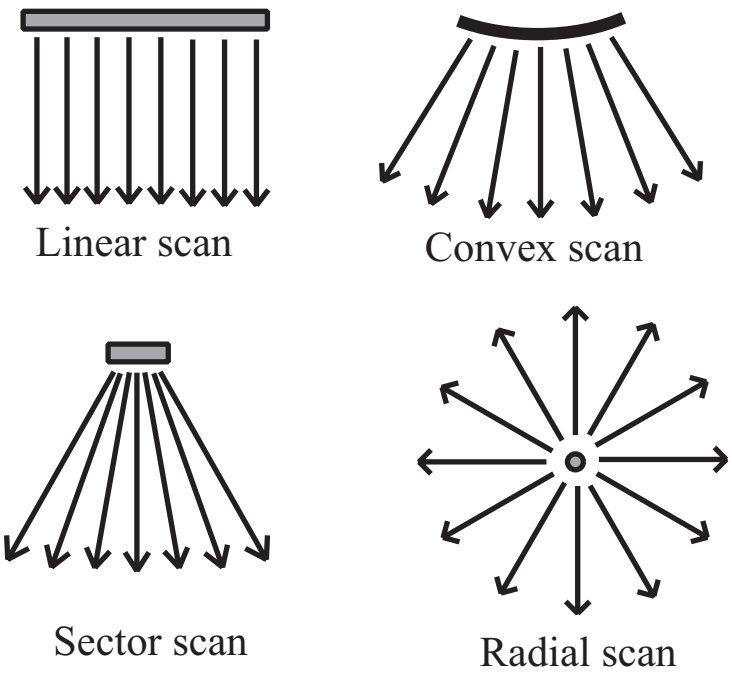

Figure 1.8: Scan types employed by B-mode imagers.

1.6.1 Mechanical scanning

A probe of this type measures one direction in a transmit and receive event, and the measurement direction is changed mechanically. Probes of two types are employed for mechanical scan imagers. One is a single element probe, and the other is an annular array probe. The structure of a single element probe is simple, and thus the probe has a low cost. However, the focal distance is fixed due to either its use of an acoustic lens or the element shape. This causes a limitation in the range of measurement.

An annular array probe is employed to measure a wide range. The probe consists of plural elements, as shown in Fig. 1.9. An annular array probe can change focal distance using electronic focusing, and thus the measurement range can become wider than that of a single element probe.

Three types of mechanical scanning are utilized for 2-D imaging. In linear scanning, a probe moves along a line and measures in a rectangular field. In sector scanning, a probe is swung and a sector measurement field is acquired. Finally, in radial scanning, a radial scan imager is used, e.g., for endoscopes. Fig. 1.10 shows an endoscope with a radial scan imager. Ultrasound pulses radiated from a transducer are reflected by a mirror and then transmitted to the measurement field. Rotation of the mirror causes the beam scan.

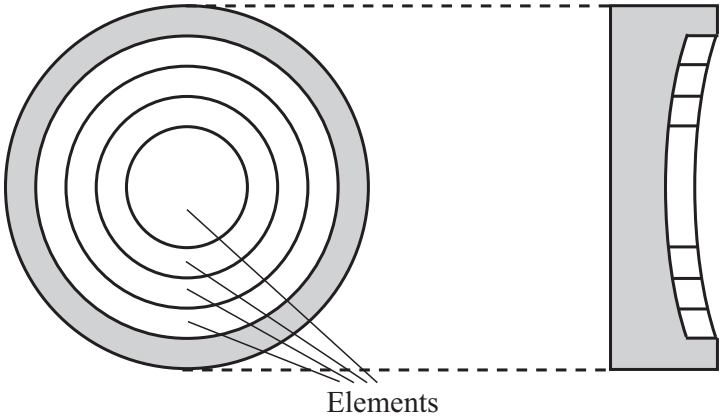

Figure 1.9: Schematic view of an annular array probe.

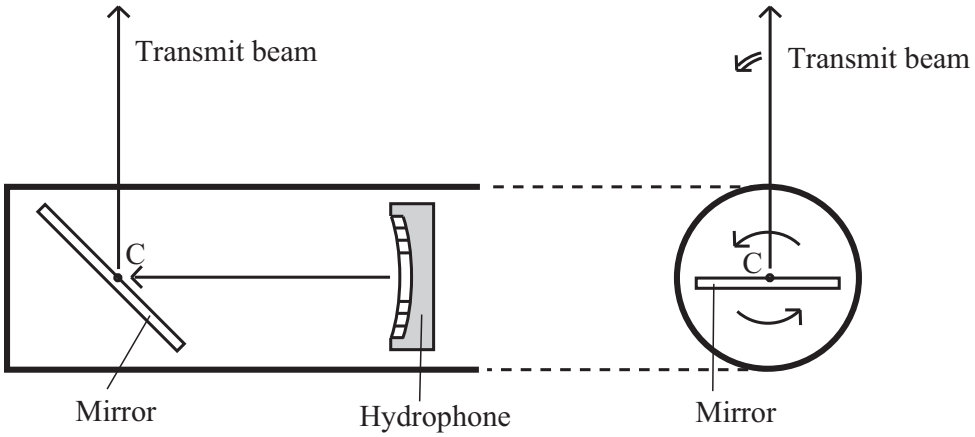

Figure 1.10: Schematic view of an endoscope with a radial scan imager. The left and right parts of the figure are the longitudinal and cross sections of the endoscope, respectively.

1.6.2 Electronic scanning

Linear and sector scanning are the main scanning methods of electronic scanning. A linear scan probe has dozens of elements placed in a row, and a change in the activated elements causes the beam scan, as shown in Fig. 1.11.

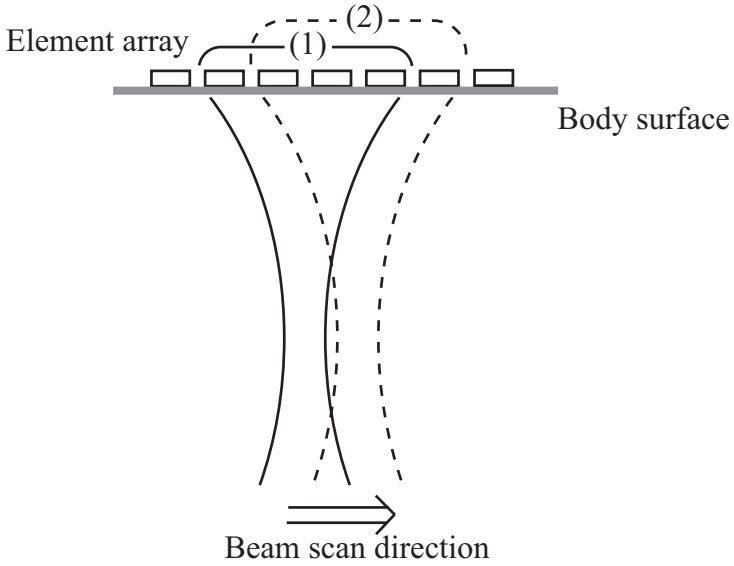

Figure 1.11: Beam scanning caused by a change in the activated elements. The change in activated elements from (1) to (2) causes the beam to scan in the right direction.

The operational basis of a convex scan imager is similar to that of a linear scan imager, with the main difference being that through the use of a convex scan probe, the elements are placed along a curved surface. A convex probe scans radially, and thus the long range measurement field is wider than that of a linear probe.

A sector electronic scan probe has narrow elements placed in a row. Beam formation is caused by the radiation of ultrasound pulses from the elements with proper time delays, as shown in Fig. 1.12. The time delay T_{D} employed by an element is given by

$$T_{\mathrm{D}} = \left\{ -\sqrt{(F\tan\theta + d_{\mathrm{E}})^2 + F^2} + F/\cos\theta \right\} /c, \tag{1.13}$$

where F is the range of the focus, θ is the angle of the focus from the center, c is the sound velocity, and d_{E} is the distance between the element employing the time delay T_{D} and the center of the array. When $F\tan\theta \gg d$, the time delay T_{D} is obtained from Eq. 1.13 by

$$T_{\mathrm{D}} \simeq d\sin\theta/c. \tag{1.14}$$

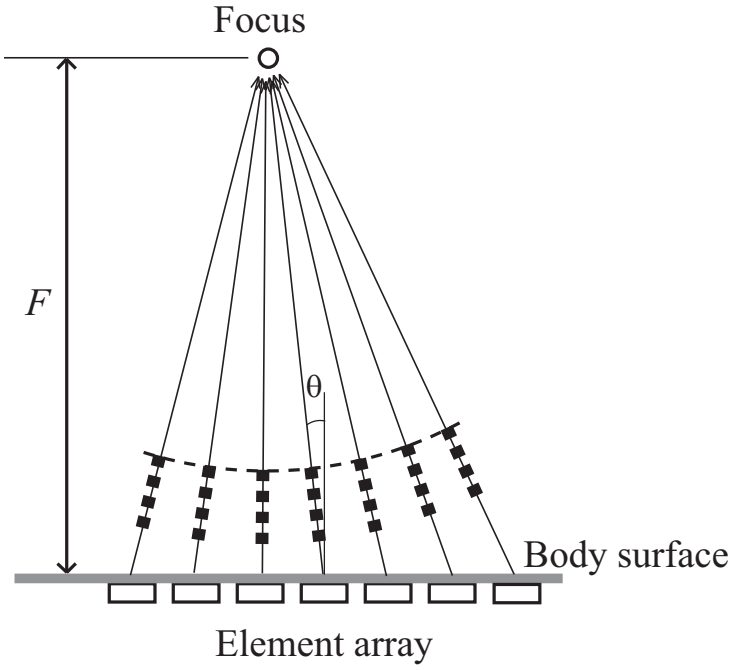

Figure 1.12: Schematic view of the beam formation employed by a sector scan probe.

In some conditions of the element intervals, a lobe other than the main lobe appears in the measurement field. This lobe is called as a grating lobe, and is shown in Fig. 1.13. When grating lobes appear, the received signal is influenced by the echo caused by the directions of the grating lobes, and thus a correct image is not acquired. Since it is necessary to prevent unwanted grating lobes, the element interval of a electronic sector scan probe I_{E} must satisfy the following equation.

$$I_{\mathrm{E}} < \frac{\lambda}{1 + \sin\theta_{\mathrm{M}}}, \tag{1.15}$$

where θ_{M} is the maximum scan angle, and λ is the wavelength employed by the probe.

1.6.3 Dynamic beam focusing

The spatial resolution of an imager utilizing beam focus deteriorates in front of and behind the focus. To improve spatial resolution, therefore, an imager with an element array probe utilizes the following methods. In the multi-stage electronic focusing method, transmit beams with various focal length are radiated for each measurement direction. Only the information around the focus is employed, and then an image in one measurement direction is constructed from multiple transmit and receive events. The problem with this

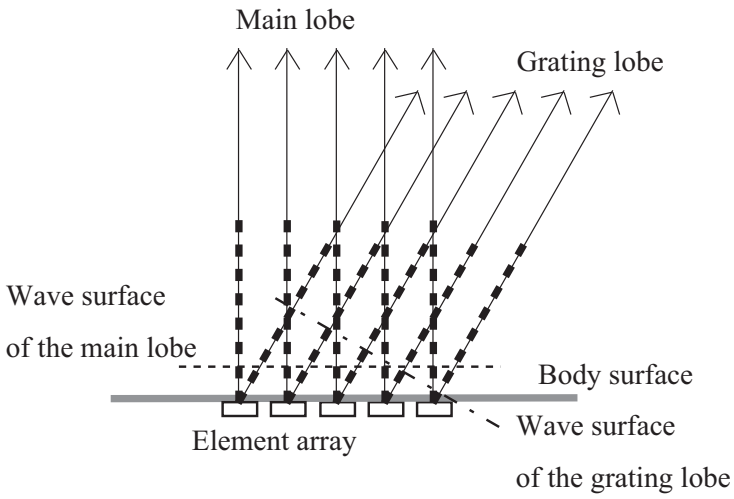

Figure 1.13: Grating lobe appearance in the measurement field. An unwanted lobe appears in a certain condition of the element interval.

method is the low time resolution caused by the construction of one image line from plural transmit and receive events.

In the dynamic focusing method, on the other hand, a single transmit beam is radiated for one measurement direction. In the receive phase, the element array employs various sets of time delays to acquire a narrow receive beam at each measurement range, as shown in Fig. 1.14. Dynamic focusing is a kind of signal processing to the receive signal, and thus an image in one measurement direction is constructed in a transmit and receive event. Therefore the time resolution of an imager with dynamic focusing does not deteriorate.

1.7 Medical acoustic 3-D imaging system

For the improvement of medical diagnoses, volumetric 3-D high-resolution acoustic images are in high demand. A 3-D acoustic imager employs one of the following methods according to the particular intended purpose.

1) Mechanical scan of a single element probe

2) Manual or auto-scan of a 1-D array with position tracking

3) Mechanical scan of a 1-D array

4) Electronic scan of a 2-D array

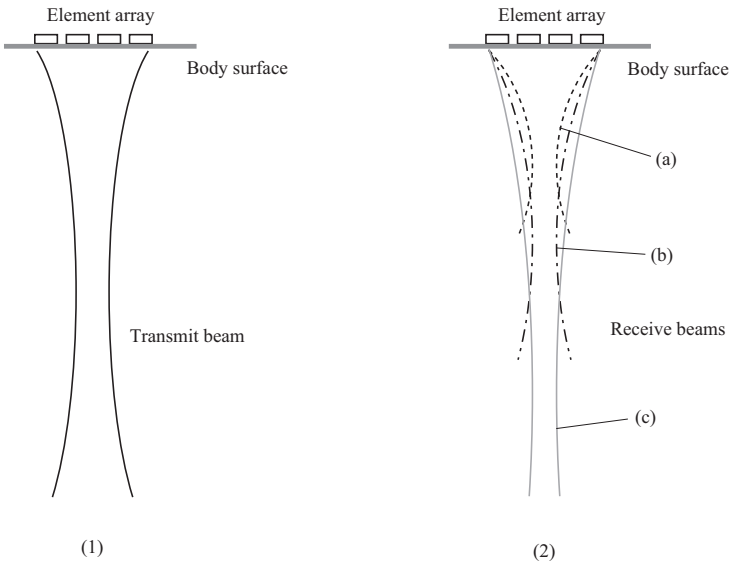

Figure 1.14: Schematic view of the dynamic beam focusing method. (1) A single transmit beam is radiated for one measurement direction. (2) In the receive phase, the element array employs various sets of time delays to acquire a narrow receive beam at each measurement range. The receive beams (a), (b), and (c) are formed for short, middle, and long range measurement, respectively.

A mechanical scan of a single element probe can utilize high transmit frequency, and thus there is the possibility that it can be useful for short range measurement. A manual or auto-scan of a 1-D array is employed to acquire a large measurement field in a static organ, such as the breast of a woman. An acoustic imager with a mechanical scan of a 1-D array has a large measurement field and high spatial resolution with adequate time resolution. Finally, the electronic scan technique using a 2-D array has improved speed. It is therefore used when high time and spatial resolution are necessary.

1.7.1 Mechanical scan of a single element probe

A single element probe with a fixed focus, caused by either an acoustic lens or the element shape, measures one direction in a transmit and receive event. Thus a 3-D image is acquired from a 2-D scan of a single element probe. The problem with this method, however, is its low lateral resolution in front of and behind the focus.

Since the 1960s, numerical image reconstruction using synthetic aperture techniques has been proposed [35][36]. Numerical image reconstruction utilizing the mechanical scan of a single element is the simplest of these techniques [37][38]. A monostatic data

acquisition scheme can reconstruct images with adequate spatial resolution. However, an imager using this method has insufficient time resolution for practical clinical application.

1.7.2 Manual or auto scan of a 1-D array with position tracking

Since a 1-D element array measures in the plane parallel to the longitudinal axis of the array, a 3-D image is acquired from a 1-D scan perpendicular to the longitudinal axis of the array. A 3-D imager of this type utilizes either freehand or mechanical scans. A position sensor is attached to the acoustic probe to track the position of the probe, and thus the position of the measurement plane in the body is located. A 1-D scan of this type causes the 3-D imager to have low time resolution. Therefore this type of scanning is employed for the measurement of static organs.

1.7.3 Mechanical scan of a 1-D array

Similar to the auto scan method described above, a 1-D element array probe can be swung or rotated to acquire a 3-D image, as shown in Fig 1.15. A conventional 1-D element array probe measures one direction in a transmit and receive event. It is necessary for a 3-D imager to measure many more directions than is necessary for a 2-D imager. Thus a 3-D imager with a 1-D array probe has much lower time resolution than a 2-D imager. When a 3-D imager measures a field of $60^\circ \times 60^\circ \times 10$ cm, the time resolution of the imager becomes 2.2 volumes/s, where we assume the beam spacing to be 1 degree and the sound velocity to be 1550 m/s. For the improvement of the time resolution of such 3-D imagers, multi-line imaging and digital beam-forming methods have been studied. Moreover, a synthetic aperture technique has been introduced for higher spatial resolution. Finally, to improve the signal-to-noise ratio, a defocusing method has been proposed.

Fig. 1.16 shows a schematic view of multi-line imaging [39]-[41]. In this method, the transmit beam is sufficiently wide to include multiple narrow receive beams. The multiple receive beams are formed in parallel using multiple sets of receiver delay lines. Therefore in this method multiple image scan lines are acquired in a transmit and receive event.

A synthetic aperture imager with a 1-D element array [42][43] transmits a wide beam of single element response to the entire measurement plane, as shown in Fig. 1.17. All elements on the array receive the echo, and then all the image lines in the measurement plane are formed in parallel. In the next transmit event, a transmit beam is radiated from the next transmit point. After all the transmit points radiate once, the final image is constructed from the sum of all the received signal beams formed at the measurement point. In this method the effective aperture of the imager is synthesized from multiple transmit and receive events, as shown in Fig. 1.18. Coherent integration utilizing the synthetic aperture technique realizes a spatial resolution equivalent to that of an aperture given by the convolution of the transmit points and the receive aperture, and thus a synthetic aperture imager with multiple transmit and receive events has high spatial

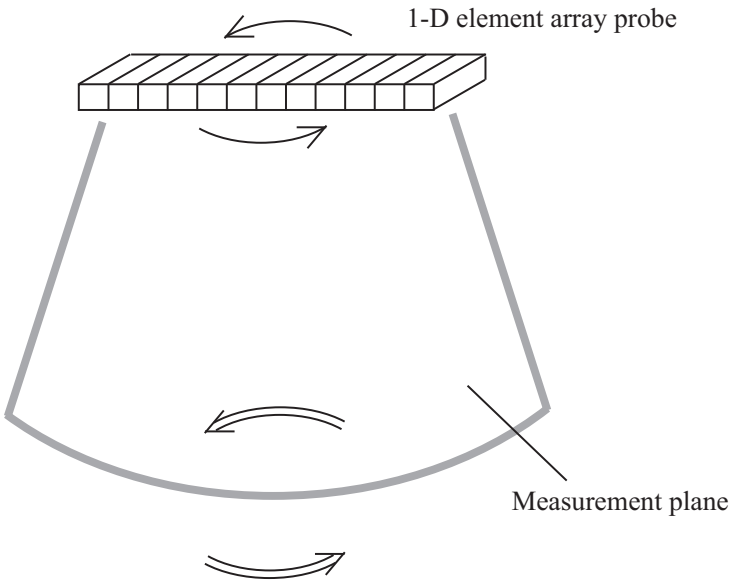

Figure 1.15: Schematic view of a mechanical scan of a 1-D element array probe. A 3-D image is constructed from multiple 2-D images acquired by the rotation of a 1-D probe.

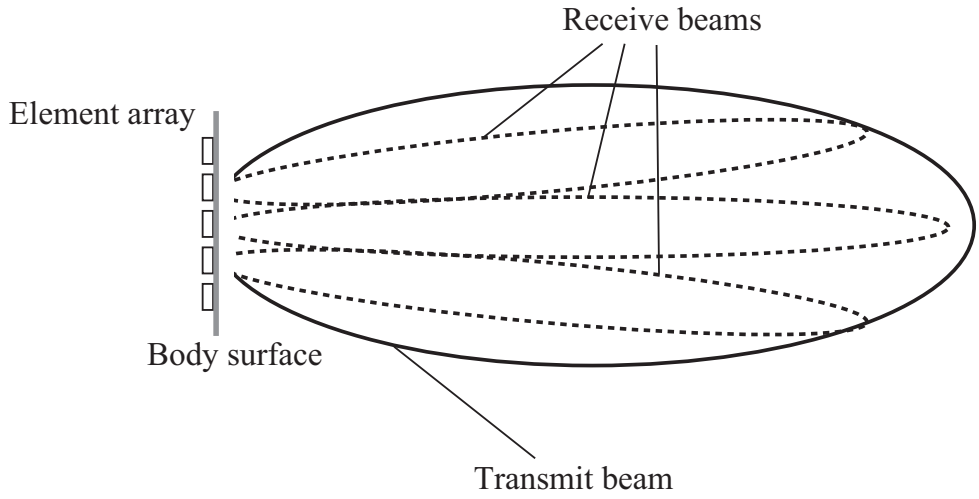

Figure 1.16: Schematic view of multi-line imaging. A transmit beam is wider than a receive beam. The receive beam is formed in parallel, and thus plural image lines are acquired in a transmit and receive event. Therefore this type of multi-line imager has adequate time resolution.

resolution. The time resolution of a synthetic aperture imager is not determined by the number of image lines, but by the number of transmit points. Therefore an imager of this type trades spatial resolution for time resolution.

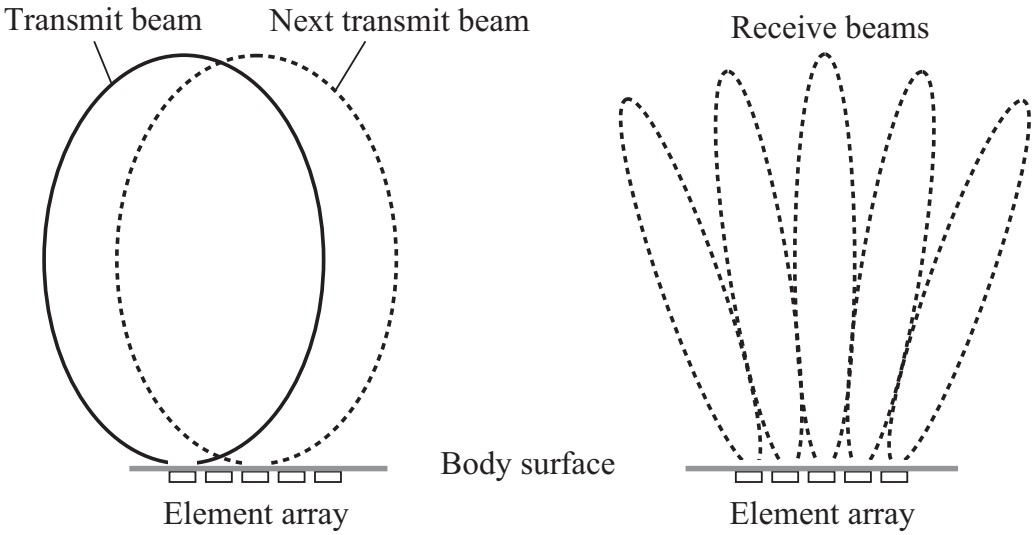

Figure 1.17: Transmit and receive schemes of a synthetic aperture imager. A wide transmit beam is radiated to the entire measurement plane. Then all the image lines in the measurement plane are formed in parallel. In the next transmit event, a transmit beam is radiated from the next transmit point.

The acoustic power radiated from a single element limits the signal-to-noise ratio (SNR) of a synthetic aperture imager. To improve the SNR of imagers, therefore, multiple elements can be used to radiate ultrasound pulses with either apodization or a set of time delays, as shown in Fig. 1.19 [42]. When multiple elements radiate ultrasound pulses simultaneously with apodization, a wide transmit beam is formed. However, in this case the acoustic power capacity of each element is not fully used. When multiple elements radiate defocused ultrasound pulses with a set of time delays, on the other hand, the acoustic power capacity of each element can be fully utilized in addition to the synthesis a single element response.

1.7.4 Electronic scan of a 2-D array

Volumetric 3-D high-resolution acoustic images are in high demand for medical diagnoses. A conventional phased array imager excites all array elements to form a transmit beam and then uses all of those elements to form a receive beam [44]. Although only the receive beam is dynamically focused, imaging under this condition results in a high electronic SNR as well as good spatial and contrast resolution. However, this configuration also has

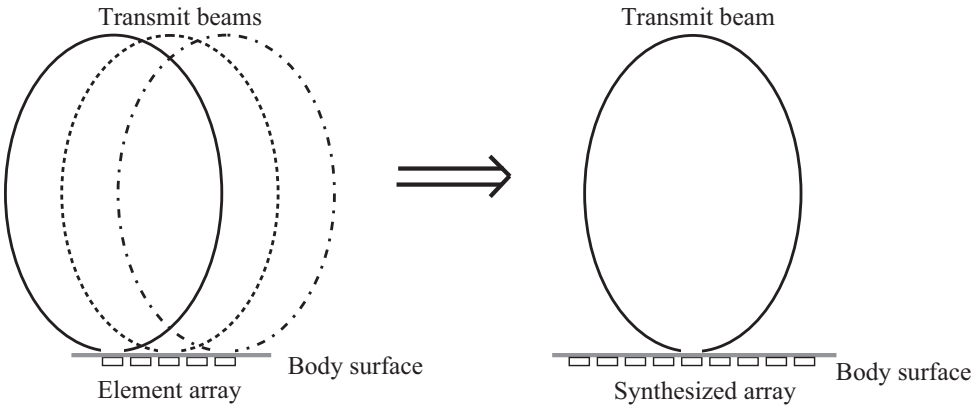

Figure 1.18: The effective aperture of the imager synthesized from multiple transmit and receive events. Coherent integration utilizing the synthetic aperture technique realizes a spatial resolution equivalent to that of an aperture given by the convolution of the transmit points and the receive aperture.

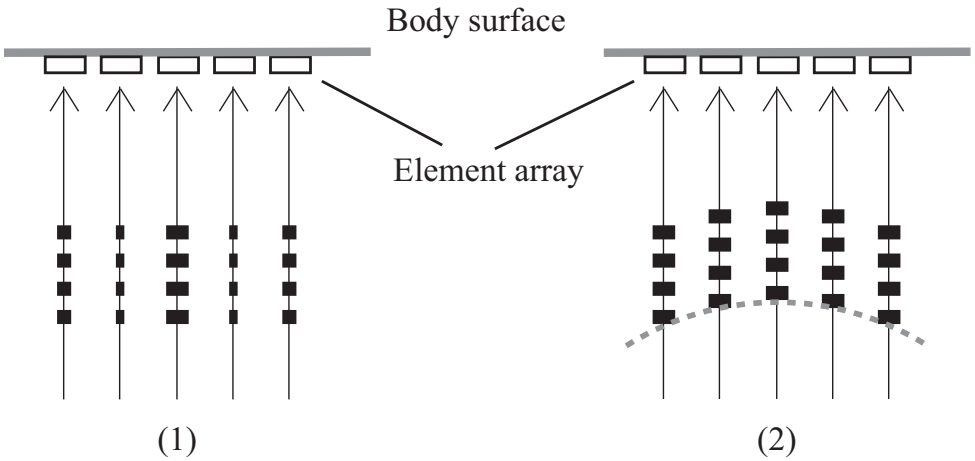

Figure 1.19: Transmit schemes using multiple elements to synthesize a single element response. Multiple elements are excited (1) simultaneously with apodization, and (2) with a set of time delays to form defocused ultrasound pulses.

two major problems. First, the number of elements becomes enormous for a 2-D array of a 3-D phased array imager. Second, it has low time resolution due to the enormous number of image lines in the 3-D measurement field.

One strategy for decreasing the number of elements, at a cost of the loss of some lateral resolution and SNR, is to utilize a 2-D sparse array with an element spacing of more than one-half of a wavelength. D. H. Turnbull *et al.* [45] investigated the arrangement of such a sparse random 2-D array. Since the 2-D random array has no periodicity, the problem of grating lobes can be avoided. In addition, T. S. Sumanaweera *et al.* investigated 2-D spiral arrays [46].

S. W. Smith *et al.* [47] proposed the idea of using different transmit and receive geometries, as shown in Fig. 1.20. Since a transmit beam and a receive beam have different radiation patterns, the directions of grating lobes become different. As a result, the grating lobe levels can be suppressed. This idea was developed by Lockwood *et al.* [48][49]. A. Austeng *et al.* [50] investigated and made a comparative study of sparse arrays. Although several designs of sparse arrays have been reported, it is difficult to reduce the number of elements to less than half of that of dense arrays. Furthermore, a 3-D imager of this type has low time resolution.

One strategy for improving time resolution is a multi-line imaging technique applied to an acoustic imager with a 2-D array [51]. In this method, multiple image lines are acquired in a single transmit and receive event at the cost of some loss of lateral resolution, similar to a multi-line imager with a 1-D array.

The technique of digital beamforming [52] is mainly used for radar systems. Since the echo received on an element array is digitized, an imager utilizing this technique has high flexibility through the formation of multiple beams in parallel. This results in significantly improved time resolution and the employment of proper aperture apodization to suppress sidelobe levels. However, an enormous number of elements are needed to acquire a 3-D image with sufficient spatial resolution.

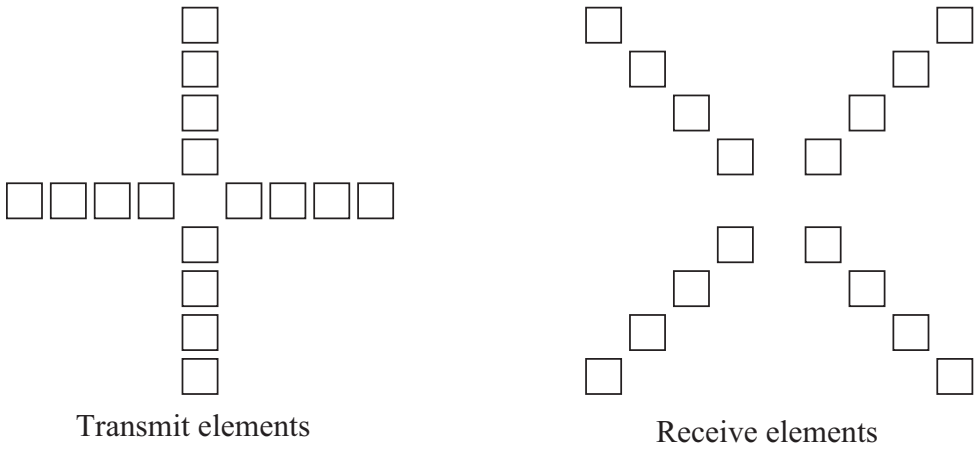

Figure 1.20: A 2-D element array design using different transmit and receive geometries. Since a transmit beam and a receive beam have different radiation patterns, the directions of grating lobes become different. Grating lobe levels can therefore be suppressed.

c

Chapter 2

A Hybrid Method and Sensor for a High-Resolution Ultrasound Vision Substitute System for the Visually Impaired

2.1 Introduction

A white cane is widely used as a vision assistance device for the blind; however, such a device has difficulty detecting an obstacle at chest height. Other instruments, such as a hand held laser telemeter and an eyeglass configured sonar-type device, only inform of the existence of an obstacle. Since they have insufficient spatial resolution, they are not useful as navigation systems under conditions with plural targets such as are encountered in daily life.

A vision substitute system for blind needs two capabilities. One is high time resolution for real-time operation. The other is high spatial resolution to individually recognize and to identify plural target positions. This study is directed to propose a vision substitute system for use in daily life. Thus the system needs to recognize objects on a table and to find the direction where a wall breaks off, that is, where an exit is. Stereo method utilizing CCD cameras has high angular resolution; however, the angular resolution is needless because the spatial information presented by tactile stimulation is limited. A stereo imaging system can not detect target range sufficiently. Especially it can not measure the range of the monotone region of a target. Acoustic sonar systems, having low angular resolution, can detect target range accurately. In addition, an acoustic imager is robust. Thus many studies have focused on acoustic through-air sensors [53]-[55]. However, so far there has been insufficient spatial and time resolutions for a proposed vision substitute system to be of practical use.

In the field of the electromagnetic waves, phased array and digital beamforming meth-

ods are often used to acquire high spatial resolution images. A phased array imager measures one direction in a transmit and receive event and so it is difficult to scan a 3-D target field in a short time. Utilizing parallel scanning with plural sensors improves time resolution of a phased array imager [56][57]; however, it has still insufficient time resolution because of the velocity of sound in air.

A digital beamforming imager measures the entire target field in a transmit and receive event and therefore has high time resolution. However, the number of elements on the array becomes enormous to achieve sufficient spatial resolution. Another strategy to improve time resolution and decrease the number of elements, at the cost of the loss of some lateral resolution and signal-to-noise ratio, is a digital beam forming imager with a 2-D sparse array with element spacing of more than one-half of a wavelength [41][47][50]. This method uses a wide transmit beam and multiple receive beams formed simultaneously. Although several designs for arrays have been reported, it is difficult to reduce the number of elements to less than half of a dense array.

In this paper we propose a system based on a hybrid array-reflector configuration. In this system a wide transmit beam is radiated to the entire measurement field. The echo from a target is gathered by a reflector and received on a 2-D element array. Since the proposed imager measures the entire target field in a single transmit and receive event, it is suitable for real-time operation. In addition, most of the echo arrived at the reflector mirror is received on the array and thus the spatial resolution and signal-to-noise ratio is improved from a digital beamforming imager with a same size 2-D array.

In section 2, we outline the framework on the proposed hybrid imager. Section 3 provides some necessary wave equations and parameters to evaluate the spatial resolution of the proposed imager. In section 4, we propose the off-focus method. In this method, a reflector and a 2-D array are fixed. Images are reconstructed from the received signal on the array by numerical back projection. Section 4 optimizes the reflector shape. Section 6 evaluates the spatial resolution of the proposed imager using physical optics. We propose a method for real-time signal processing in section 7. Finally, we draw conclusions in section 8.

2.2 Principle of the hybrid 3-D imaging system with a 2-D array and a reflector

Fig. 2.1 shows a schematic view of the proposed vision substitute system. It consists of a transmitter, a concave reflector, a 2-D element array, and a stimulating device. The transmitter radiates ultrasound pulses to the entire measurement field. Elements on the array are spaced at intervals of one-half of the wavelength. Images are reconstructed from the received signal on the array. Since the human forehead has a low two-point discrimination threshold and a wide stimulating area, we propose that the stimulating device is placed on the forehead. The proposed vision substitute system stimulates this location

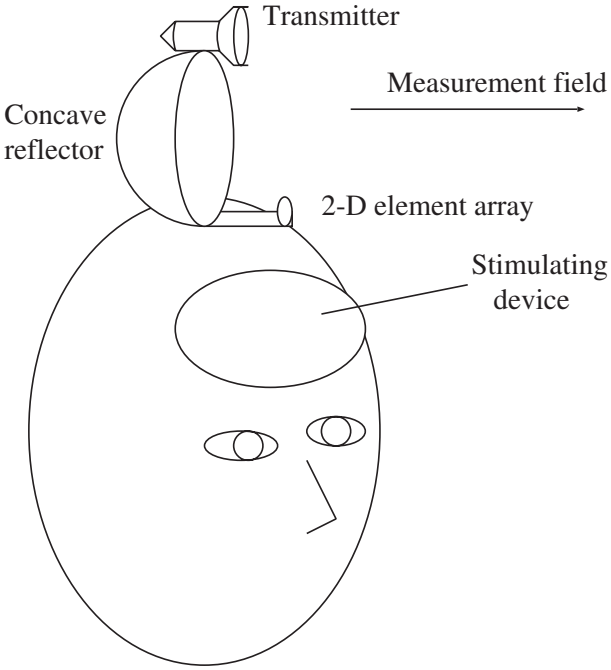

Figure 2.1: Schematic view of the proposed vision substitute system.

on the forehead. The target direction corresponds to the location of the stimulating point on the forehead. In this way a user can recognize the target direction.

The proposed imager measures the entire measurement field in a transmit and receive event. Thus the time resolution of the proposed imager is improved significantly from that of a phased array imager. Since most of the echo reflected by the mirror is gathered and received on the array, the proposed imager has higher spatial resolution than a digital beamforming imager with a same size array. Therefore, the number of elements can be reduced to about 1/8 of a dense 2-D array having the same spatial and time resolution but using a digital beamforming method, as is shown later.

The echo from a peripheral direction, far from the center, is not received on the array. This restricts the measurement field of the proposed imager to forward area. Thus the proposed imager can measure accurately without regard to the existence of scatterer in a peripheral direction.

2.3 Acoustic propagation calculations

In this section we explain the wave equations to evaluate the angular resolution of the proposed imager. Fig. 2.2 is the coordinates system used in this calculation. The z axis is directed to the measurement field. Generality is not lost when the proposed imager is

symmetrical in the x-z plane. We set the center and a normal vector of a 2-D array as $(x_\mathrm{s}, 0, z_\mathrm{s})$ and $(-\sin\theta_\mathrm{s}, 0, \cos\theta_\mathrm{s})$, respectively. Where θ_s is the angle between the normal vector of the array and the z axis, as shown in Fig. 2.2. We assume the reflection ratio of the mirror as 1.

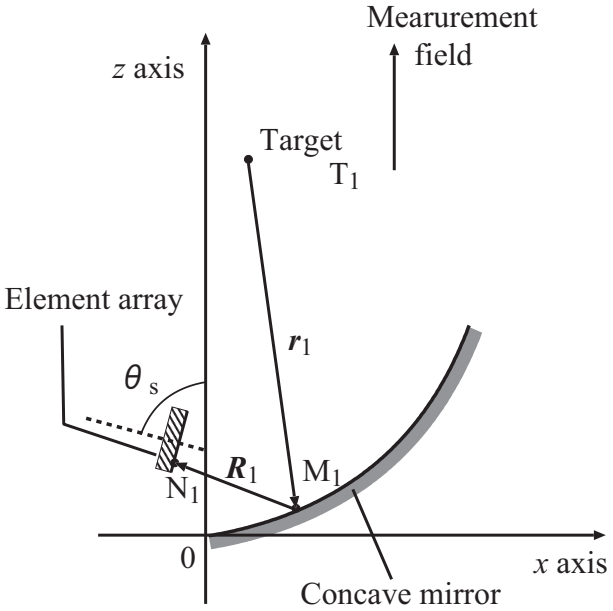

Figure 2.2: Arrangement of the sensor array and mirror.

When a target exists at $\mathrm{T}_1(x, y)$, the particle velocity of the transmit wave at T_1 is given by

$$v_{\mathrm{T}_1 0} = \sqrt{\frac{W}{2\pi k\rho\omega}} G_\mathrm{r} R_\mathrm{r}(x, y, z) \frac{1 + jkr}{r^2} \cdot e^{-(\alpha + jk)r}, \tag{2.1}$$

where α is the attenuation coefficient of the air, W is the radiation power from a transmitter, G_r is the gain of the transmitter, $\boldsymbol{r}$ is the vector from the transmitter to T_1, $r = |\boldsymbol{r}|$, k is the wave number, ω is the angular frequency, ρ is the density of the medium, $R_\mathrm{r}(x, y, z)$ is the directivity function of the transmit element satisfying the condition $0 \leq R_\mathrm{r}(x, y, z) \leq 1$. We assume the transmitter as a point source. Eq. 2.1 is correct under the condition that ${l_t}^2 \ll r^2$ when an imager employs a circular transmit element of $2l_t$ in diameter.

The echo scattered at T_1 is reflected on the mirror at M_1, and received by an element at N_1. The volume velocity of a small area around T_1 is given by $v_{\mathrm{T}_1 0} \Delta S' \frac{\boldsymbol{n}_0 \cdot \boldsymbol{r}}{n_0 r}$, where $\Delta S'$ is the square measure of the small area around T_1, $\boldsymbol{n}_0$ is the normal vector of the

target surface at T_1, $n_0 = |\boldsymbol{n}_0|$. Then the velocity potential and pressure variation at M_1 are given, respectively, by

$$\phi_{\mathrm{M}_1} = A(x,y)\frac{v_{\mathrm{T}_1 0}}{2\pi r_1}\frac{\boldsymbol{n}_0\cdot\boldsymbol{r}}{n_0 r}e^{-\alpha r_1 - jkr_1}\Delta S', \tag{2.2}$$

$$v_{\mathrm{M}_1} = \frac{1+jkr_1}{r_1}\phi_{\mathrm{M}_1}, \tag{2.3}$$

where the reflection ratio of the amplitude at the target surface is $A(x,y)$, $\boldsymbol{r}_1 = \overrightarrow{\mathrm{T}_1\mathrm{M}_1}$, $r_1 = |\boldsymbol{r}_1|$. The volume velocity of the small area around M_1 is given by $v_{\mathrm{M}_1}\Delta S(\frac{\boldsymbol{n}_1\cdot\boldsymbol{r}_1}{n_1 r_1})$, where ΔS is the square measure of the small area around M_1, $\boldsymbol{n}_1$ is the normal vector of the mirror at $\mathrm{M}_1, n_1 = \boldsymbol{n}_1$. We assume a spherical wave is radiated from M_1 and thus the velocity potential at N_1 is given by

$$\begin{aligned}\phi_1 &= \int_{S'}\int_S \frac{v_{\mathrm{M}_1}}{2\pi R_1}(\frac{\boldsymbol{n_1}\cdot\boldsymbol{r_1}}{n_1 r_1})e^{-\alpha R_1 - jkR_1}dSdS' \\ &= \int_{S'}\int_S \frac{jkA(x,y)v_{\mathrm{T}_1 0}(1+jkr_1)}{4\pi^2 {r_1}^2 R_1}(\frac{\boldsymbol{n_0}\cdot\boldsymbol{r}}{n_0 r}) \\ &\quad\cdot(\frac{\boldsymbol{n_1}\cdot\boldsymbol{r_1}}{n_1 r_1})e^{-(jk+\alpha)(r_1+R_1)}dSdS',\end{aligned} \tag{2.4}$$

where $\boldsymbol{R}_1 = \overrightarrow{\mathrm{M}_1\mathrm{N}_1}$, $R_1 = |\boldsymbol{R}_1|$.

The particle velocity along the x and y axes are obtained by $v_{1x} = -\frac{\partial\phi_1}{\partial x}$ and $v_{1z} = -\frac{\partial\phi_1}{\partial z}$, respectively, and thus the particle velocity perpendicular to the element array is given by

$$v_1 = -v_{1x}\sin\theta_{\mathrm{s}} + v_{1z}\cos\theta_{\mathrm{s}}. \tag{2.5}$$

Since the pressure variety is given by $p_1 = \rho\frac{\partial\phi_1}{\partial t} = j\rho\omega\phi_1$, the echo power at N_1 is given by $I_1 \simeq I_{1\mathrm{m}} = \frac{1}{2}p_1 v_1^*$, when the phase of p_1 is the same as that of v_1.

p_1 and v_1 have almost the same phase under the condition that $kR_1 \gg 1$. When $R_1 > 3$ cm and the sound velocity $c = 340$ m/s, the condition is satisfied when the transmit frequency $f \gg 1.8$ kHz. Therefore, the condition is satisfied when ultrasound is transmitted. In this study $f = 170$ kHz, and so $I_1 = 0.99994\ I_{1\mathrm{m}}$. We thus assume $I_1 = I_{1\mathrm{m}}$. Since the receive power is given by

$$W_{\mathrm{R}} = I_1 D, \tag{2.6}$$

where D is the square measure of the effective aperture of a receive element. The ratio of the receive power to the transmit one is then given by

$$W_{\mathrm{R}}/W = I_1 D/W. \tag{2.7}$$

In this paper we introduce the assumption that the transmit and receive elements have no directivity.

2.4 Off-focus method for image reconstruction

To detect target locations from the images received on the array it is necessary to adjust the distance between an element array and the reflector mirror for the purpose to focus on the array, as shown in Fig. 2.3. We call this the auto-focus method. This method needs a device to mechanically adjust the distance, and thus an imaging system based on an auto-focus method becomes complex.

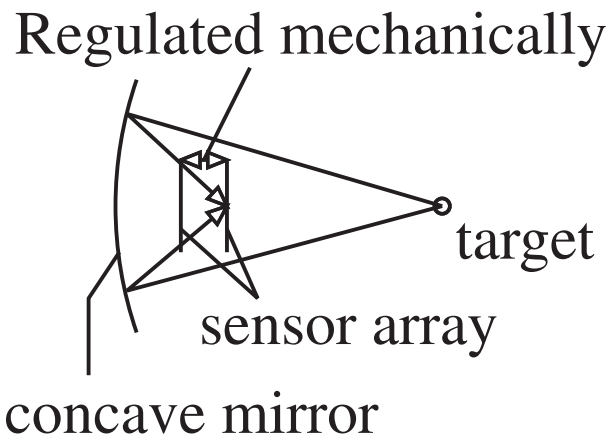

Figure 2.3: Schematic view of the auto-focus method.

We propose a method in which images are reconstructed from the distributed images received on the element array by numerical back projection. We call this the off-focus method, as shown in Fig. 2.4. For image reconstruction by numerical back projection, it is necessary to draw the estimated power in the measurement field. Image reconstruction based on numerical back projection is processed as follows. The phase of the received signal is reversed before being projected backward from the receive element U at N_2. The waves projected backward are reflected by the mirror at M_2 and then focused at the target locations.

The estimated velocity potential at T_2, caused by the element U, is obtained by

$$\begin{aligned} \phi_{2U} &= \frac{{A_U}^*}{2\pi}\int_S \frac{1+jkR_2}{{R_2}^2 r_2}\frac{\boldsymbol{n_2}\cdot\boldsymbol{R_2}}{n_2 R_2} \\ &\quad \cdot e^{-(jk+\alpha)(r_2+R_2)}dS, \end{aligned} \tag{2.8}$$

where the amplitude received by the element U is A_U, $\boldsymbol{R}_2 = \overrightarrow{\mathrm{N_2M_2}}$, $\boldsymbol{r}_2 = \overrightarrow{\mathrm{M_2T_2}}$, $\boldsymbol{n}_2$ is the normal vector of the mirror at M_2, $R_2 = |\boldsymbol{R}_2|, r_2 = |\boldsymbol{r}_2|, n_2 = |\boldsymbol{n}_2|$. The estimated velocity potential at T_2 is given by

$$\phi_2 = \sum_U \phi_{2U}. \tag{2.9}$$

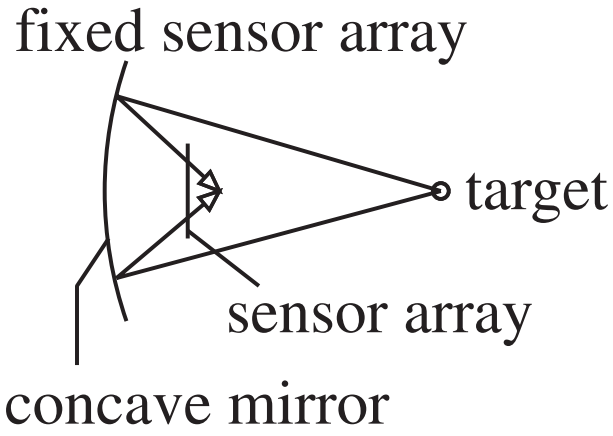

Figure 2.4: Schematic view of the off-focus method.

In the off-focus method images are reconstructed from the signal received on the array by numerical back projection; therefore, it is not necessary to focus on the array. To evaluate the correctness of the off-focus method we compare the spatial resolution of different array positions. In this section, for the simplicity of calculation, we employ a rotationally symmetric parabolic mirror and assume that the blocking due to the array over the mirror can be neglected.

The parameters used in this evaluation are; a square array 4 cm in width is set on a plane parallel to the x-y plane for a depth of $z = z_{\mathrm{s}}$, the center of the array is on the z axis, the shape function of the mirror, 10 cm in width, is $z = (x^2 + y^2)/12$. The square measure of the effective aperture of an element is 0.01 cm^2, the transmit frequency $f = 170$ kHz, attenuation coefficient $\alpha = 3 \times 10^{-8} f$ neper/cm. In this paper we assume that the echo scattered backward from a target is a spherical wave. We investigate the image of a point target to evaluate the spatial resolution of a proposed imager.

The received power on the array when $z_{\mathrm{s}} = 3.1$ and 2.5 cm are shown in Fig. 2.5 and 2.6, respectively, where the focal length of the reflector mirror is 3.1 cm. A point target is located at the center for a 100 cm depth.

The spatial resolution of the proposed imager is shown in Fig. 2.7. The responses in the two cases correspond with each other in the field of high estimated power; that is, the shapes of the main lobe, and the first and second sidelobes are the same in the both cases. This indicates that the distance between the element array and the mirror has just a trifling effect on the spatial resolution. Since adjustment of the element array is not necessary with the off-focus method, we employ the proposed off-focus method for both its simplicity of the structure for the imaging system and the decrease in weight it brings.

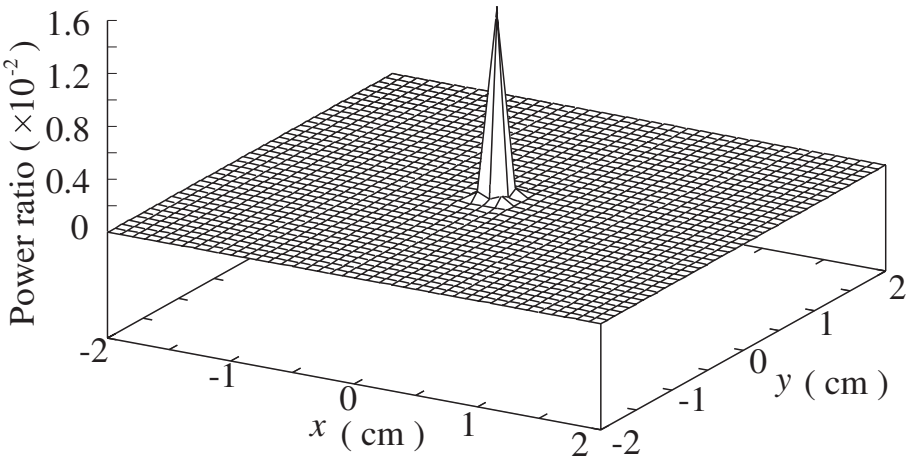

Figure 2.5: Received power distribution map on an element array. The distance between the array and the bottom of the mirror is 3.1 cm. A point target exists at the center for a 100 cm depth.

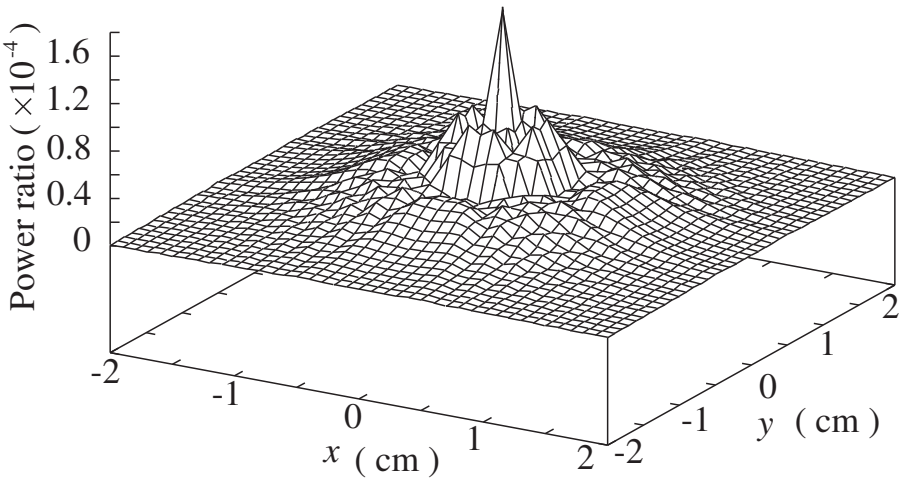

Figure 2.6: Received power distribution map on an element array. The distance between the array and the bottom of the mirror is 2.5 cm. A point target exists at the center for a 100 cm depth.

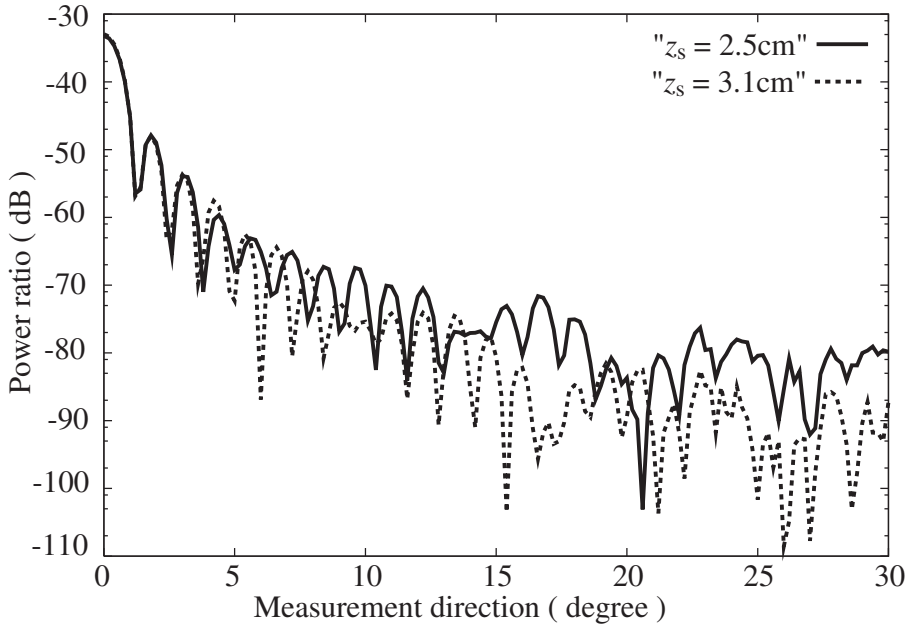

Figure 2.7: Estimated power of an imager based on the off-focus method. A point target exists at the center for a 100 cm depth.

2.5 Optimization of the mirror shape

In section 4, we employ a rotationally symmetric parabolic mirror. It is not necessary for an imager based on the off-focus method to focus on the array and thus there is a probability that a reflector mirror with no focus is optimal for the off-focus imager. For a wide measurement field it is desired that the imager has high spatial resolution and sensitivity in the peripheral direction, as well as in the center. In this section we investigate the optimum shape of the reflector mirror for an imager based on the off-focus method.

2.5.1 Coordinate system used in the optimization of the mirror shape

We arrange a 2-D element array and a reflector mirror offset to prevent the array from blocking the echoes arriving at the mirror, as shown in Fig 2.8. The center of the measurement field is in the x-z plane and the angle between the center and the z axis is 15 degrees, where the center is in the field of $x > 0$. We determine the parameters for the optimization of the mirror shape as follows; the visual angle of the measurement field is 30 degrees vertically and 60 degrees horizontally, the imager employs an elliptical array 3

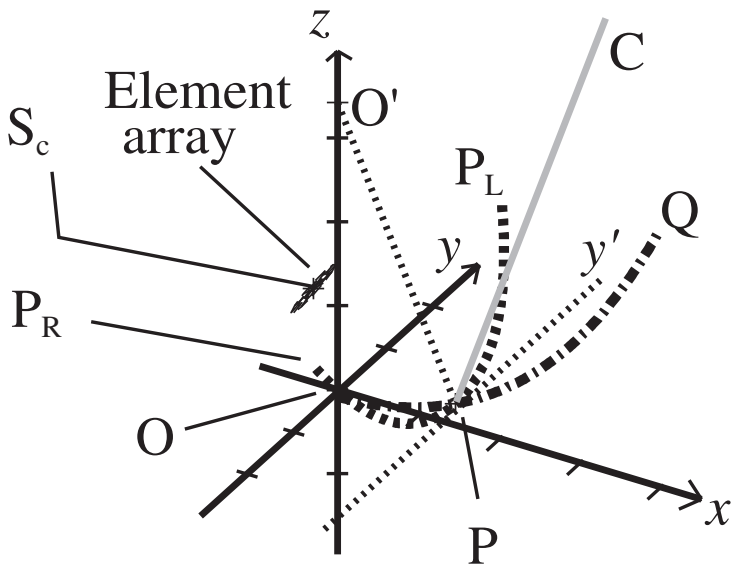

Figure 2.8: Coordinate system used for optimization of the mirror shape.

cm long and 4 cm wide, and the reflector mirror is 20 cm in width for both x and y axis directions. The imager is symmetrical in the x-z plane, and the center of the array exists at $\mathrm{S_c}$. The section of the mirror in the x-z plane is OQ. P is on the curved line OQ, where $\angle \mathrm{OS_cP} = \angle \mathrm{PS_cQ}$. The x' axis is the tangent of the curved line OQ at P in the x-z plane. The y' axis is parallel to the y axis, and P is on the y' axis. $\overrightarrow{\mathrm{O'P}}$ is the normal vector of the mirror at P, and $\overrightarrow{\mathrm{PC}}$ corresponds to the center of the measurement field. The z' axis corresponds to the line PO′.

We optimize the mirror shape using geometric optics [60] for effectively gathering the echo to the array. First, we optimize the curvature of the curved line OQ, and then optimize that of $\mathrm{P_LP_R}$, where the curved line $\mathrm{P_LP_R}$ is the section of the mirror in the O′P-y' plane. Finally we determine the shape of the reflector mirror by interpolating between the two curved lines.

2.5.2 Optimization of the mirror shape in the vertical section

In this study we assume that the reflector mirror is symmetrical in the x-z plane, and we set the center of the element array $\mathrm{S_c}$ at $(-1.5\ \mathrm{cm}, 0, z_\mathrm{s})$. We then determine the mirror shape and the slope of the array as follows. We define $I_{1\nu}$ and $I_{\mathrm{DBF}1\nu}$ as the summation received on the array with and without, respectively, a reflector for gathering the echo on the array, where ν is the angle between the line PC and the target direction in the x-z plane. The ratio of $I_{1\nu}$ to $I_{\mathrm{DBF}1\nu}$ shows the efficiency of the proposed method in a target

direction in a vertical plane. We then maximize the evaluation function

$$V_{\rm ver} = \prod_{\nu=-15}^{15} {E_{1\nu}}^{1+2*(15-|\nu|)/15}, \tag{2.10}$$

$$E_{1\nu} = I_{1\nu}/I_{{\rm DBF}1\nu}. \tag{2.11}$$

We employ a geometric exponential function for the evaluation for two reasons. First, the function gives a low evaluation value when the proposed imager has one and more directions of low efficiency. Second, the center of the measurement field requires high efficiency for high spatial resolution, as with the visual information. The optimized shapes of the mirror are the same when the values of the weight over the efficiency at the center are in the range of the square and the fifth power. Thus we set the weight as the cube.

We assume the shape function of the mirror in the x-z section as a quartic function in the xyz coordinate system. We optimize the shape function of the mirror, $\theta_{\rm s}$ and $z_{\rm s}$, where $\theta_{\rm s}$ is the angle between the x axis and the array, and $z_{\rm s}$ is the height of the array center at at $\rm S_c$ from the bottom of the mirror at O. Fig. 2.9 shows the efficiency of the proposed imager with the optimized mirror in each measurement direction in the x-z plane when $4 \leq z_{\rm s} \leq 9$.

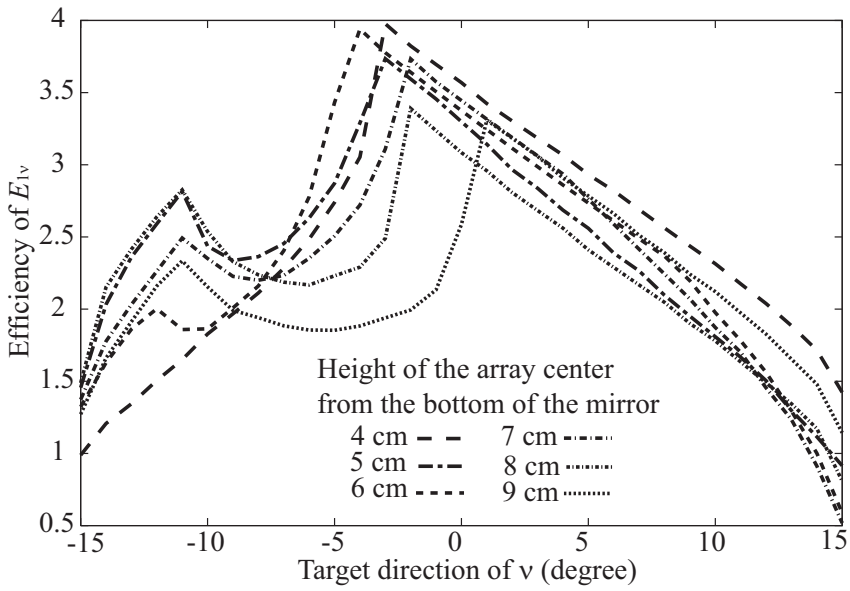

Figure 2.9: Angular characteristics of the efficiency of the proposed imager in a vertical section.

2.5.3 Optimization of the mirror shape in a horizontal section

In this study we assumed that the imager was symmetric in the x-z plane and thus the horizontal section of the array would be parallel to the y axis. Since the horizontal section of the mirror is also symmetrical in the x-z plane, we set the shape function of the section of the mirror as a polynominal function of degree 8 in the $x'y'z'$ coordinate system. We also define $I_{2\nu}$ and $I_{\mathrm{DBF}2\nu}$ as the summation received on the array with and without, respectively, a reflector for gathering the echo on the array, where ν is the angle between the line PC and the target direction in the CP-y' plane. The ratio of $I_{2\nu}$ to $I_{\mathrm{DBF}2\nu}$ shows the efficiency of the proposed method in a target direction in a horizontal plane. We then maximize an evaluation function

$$V_{\mathrm{hor}} = \prod_{\nu=0}^{30} {E_{2\nu}}^{1+2*(30-\nu)/30}, \tag{2.12}$$

$$E_{2\nu} = I_{2\nu}/I_{\mathrm{DBF}2\nu}. \tag{2.13}$$

Fig. 2.10 shows the efficiency of the proposed imager with the optimized mirror in each measurement direction in the CP-y' plane when $4 \leq z_{\mathrm{s}} \leq 9$.

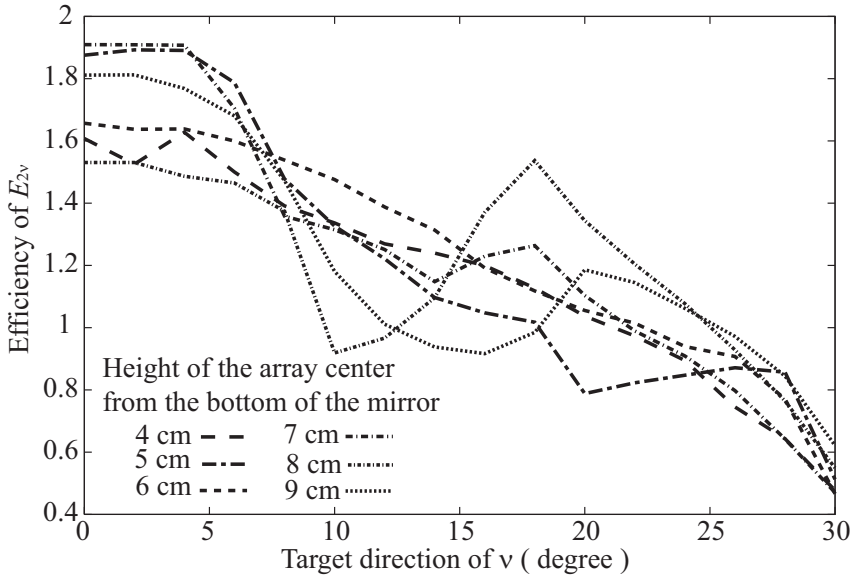

Figure 2.10: Angular characteristics of the efficiency of the proposed imager in a horizontal section.

2.5.4 Optimization of the 3-D reflector mirror

We determine the optimum of θ_{s} and the shape functions in the vertical and horizontal plane from the product of two evaluation functions, V_{ver} and V_{hor}. We then interpolate

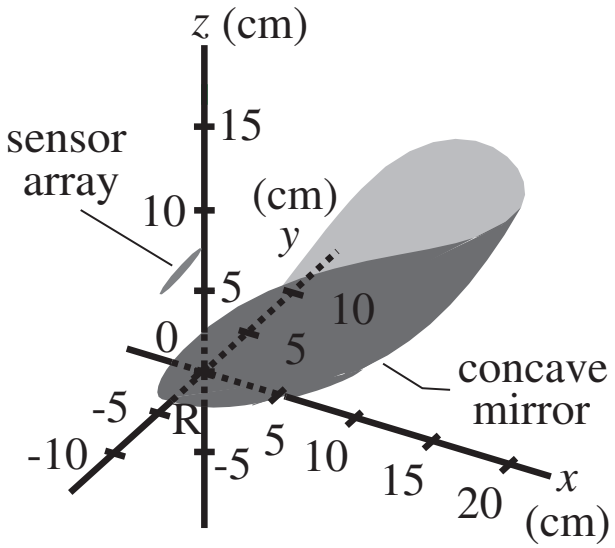

Figure 2.11: Schematic view of the constructed 3-D mirror using interpolation.

to construct a 3-D reflector mirror from the shape functions, as shown in Fig. 2.11. Fig. 2.12 shows the angular characteristics of the efficiency of the proposed imager with the interpolated mirror.

For the optimization of a 3-D mirror shape it is necessary to ascertain the optimization of $z_{\rm s}$, $\theta_{\rm s}$ and the shape functions of the mirror with a 3-D problem. Therefore, we set the interpolated mirror as the initial value, and then we optimize a 3-D mirror using geometric optics as follows.

In the proposed imager, most of the echoes are reflected by the mirror and received on the array. We call the region of the mirror as the used area. When the used area consists of plural parts, a division of the main lobe is caused from interference of the parts. Therefore, it is necessary to set an evaluation function to prevent the used area from being divided into several parts. Minimizing the second moment of the used area about its center of gravity ensures that the used area consists of just one part; however, the used area also becomes small. Then we set functions

$$V_\nu = \sum \quad W_\nu(x'_{\rm m}, y'_{\rm m}) I_{{\rm m}\nu}(x'_{\rm m}, y'_{\rm m}), \tag{2.14}$$

$$d_\nu(x'_{\rm m}, y'_{\rm m})^2 = (x'_{\rm m} - x'_{{\rm G}\nu})^2 + (y'_{\rm m} - y'_{{\rm G}\nu})^2 + (z'_{\rm m} - z'_{{\rm G}\nu})^2, \tag{2.15}$$

$$W_\nu(x'_{\rm m}, y'_{\rm m}) = S_\nu - d_\nu(x'_{\rm m}, y'_{\rm m})^2, \tag{2.16}$$

where ν is the angle between the target direction and the line PC, $I_{{\rm m}\nu}(x_{\rm m}', y_{\rm m}')$ is the

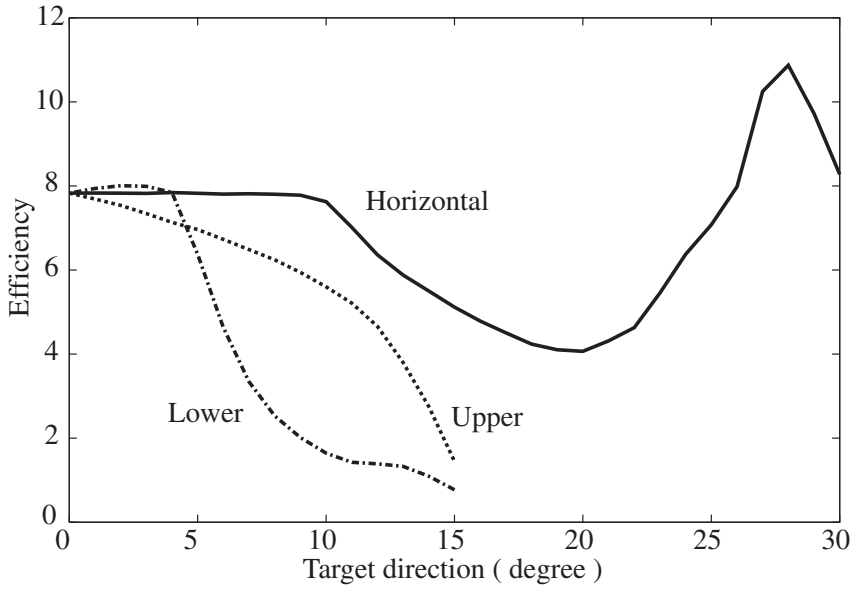

Figure 2.12: Angular characteristics of the efficiency of the proposed imager.

echo power received on the array and reflected at the small area of the square measure as $\Delta S(x_{\mathrm{m}}', y_{\mathrm{m}}')$ around $\mathrm{M}'(x_{\mathrm{m}}', y_{\mathrm{m}}', z_{\mathrm{m}}')$ on the mirror, $\mathrm{G}_\nu(x_{\mathrm{G}_\nu}', y_{\mathrm{G}_\nu}', z_{\mathrm{G}_\nu}')$ is the center of gravity of the used area, and S_ν is the square measure of the used area. Since the measurement field is 30 degrees vertically and 60 degrees horizontally, we set the evaluation function $V_{3\mathrm{D}}$ as the geometric function of V_ν when the target exists in the x-z and CP-y' planes.

$$V_{3\mathrm{D}} = \prod_{\nu_1=-15}^{15} V_{\nu_1}^{1+2*(15-|\nu_1|)/15} \cdot \prod_{\nu_2=0}^{30} V_{\nu_2}^{1+2*(30-\nu_2)/30}, \tag{2.17}$$

where ν_1 and ν_2 are the angles between the target direction and the line PC in the x-z and CP-y' planes, respectively.

In the next section we evaluate the spatial resolution of the optimized mirror.

2.6 Evaluation of the spatial resolution of the proposed imager in physical optics

In the optimization of the mirror shape we utilize geometric optics to simplify the optimization and so decrease the calculation time. We can use geometric optics when the

mirror size is sufficiently larger than the wave length λ, because it neglects the effect of interference at the edge of the mirror. In this section we more exactly evaluate the spatial resolution of the proposed imager utilizing physical optics [61], where the sound pressure variation on the reflector mirror is integrated numerically to consider the effect of the interference at the rim of the mirror.

Fig. 2.13 and 2.14 shows the angular resolution of the proposed imager from physical optics. The -3 dB lateral resolution of the proposed imager is; 2.52, 1.16 and 1.88 degrees in the target directions of $-10, 0$ and 10 degrees from the center in the vertical plane, and 1.20, 0.98 and 1.78 degrees in the target directions of 0, 10 and 20 degrees in the horizontal plane, where the transmit frequency f is 170 kHz. Fig. 2.15 shows the used area on the mirror from geometric optics, where a point target exists at the center for a 100 cm depth. The lateral resolution calculated using physical optics is consistent with that estimated from the used area on the mirror from geometric optics.

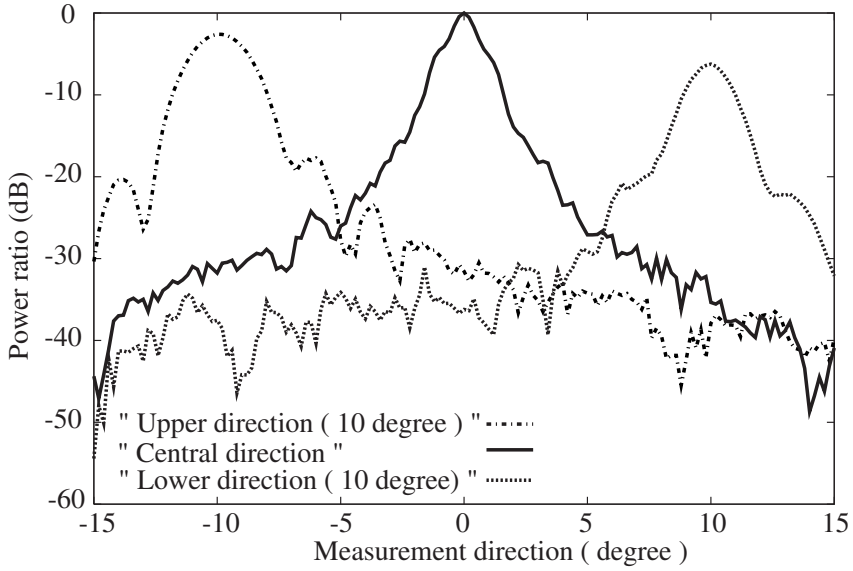

Figure 2.13: Lateral resolution of the proposed imager in a vertical plane.

In Fig. 2.16 we compare the efficiency of the proposed imager with an optimized 3-D imager using physical optics from a geometric one when a point target exists in the horizontal plane for a 100 cm depth. The angle between the target direction and the center is less than 30 degrees. We define the efficiency as the power ratio received on the array with or without a reflector mirror. The two efficiencies correspond with each other when a target exists in a field that is less than 15 degrees away from the center. There is some distance when a target exists in the direction that is more than 15 degrees away from the center; however, the fluctuation tendency of the efficiencies is the same. Fig. 2.17 shows the used area on the mirror when a point target exists in a direction of 30 degrees

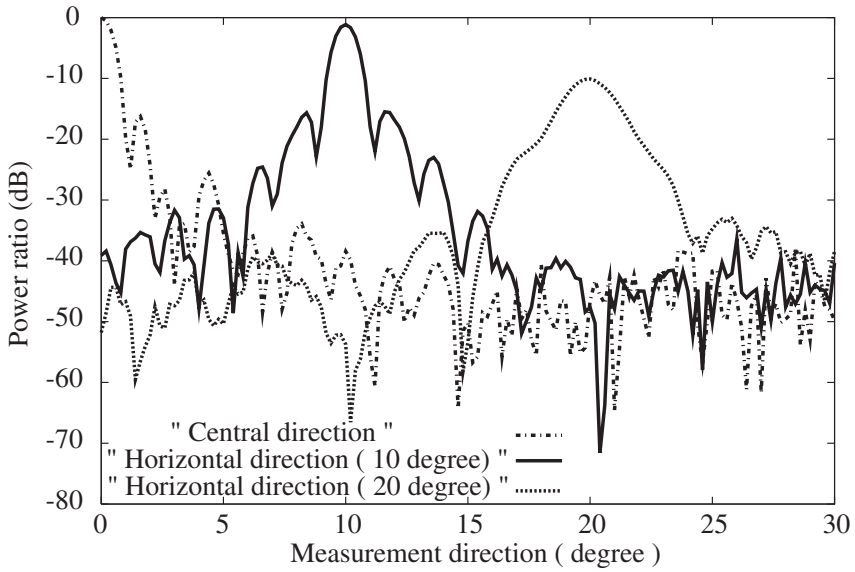

Figure 2.14: Lateral resolution of the proposed imager in a horizontal plane.

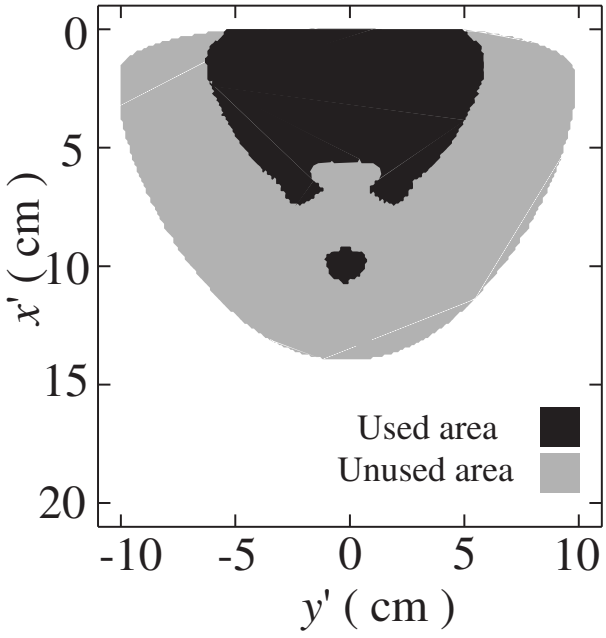

Figure 2.15: Used area on the mirror when a target exists at the center.

away from the center. This indicates that the echo from a peripheral direction is reflected at the peripheral region of the mirror and then received on the array. Since the calculation using geometric optics assumes that a mirror exists with the width of the Fresnel zone around a reflection point, the receive power on the array is estimated as larger than the true value. We assume that this causes the difference between the efficiencies estimated using the two methods. The difference is a simple function of the target direction; thus, it can be easily corrected using Fig. 2.16. In this way the validity of the optimization of the mirror shape using geometric optics is demonstrated.

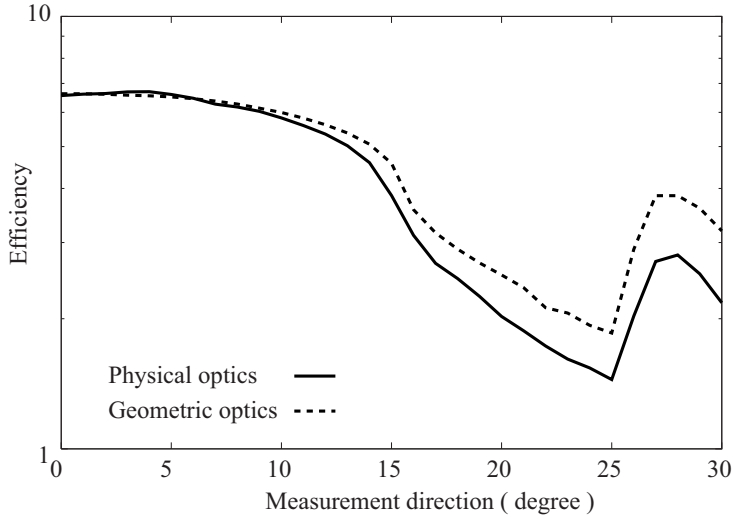

Figure 2.16: Receive power efficiency of the proposed imager in a horizontal plane.

The efficiency at the center is 6.62 and 6.56 in geometric and physical optics, respectively. The -3 dB lateral resolution at the center is 1.16 and 1.20 degrees in the vertical and horizontal planes, respectively. A digital beamforming imager with a circular 2-D element array has -3 dB lateral resolution

$$\theta_{1/2} = 58.4\lambda/D_1, \tag{2.18}$$

where D_1 is the diameter of the array. Therefore, the spatial resolution of the proposed imager is the same as that of a digital beamforming imager with an elliptical array 10.07 cm long and 9.73 cm wide. The proposed imager has a elliptical array 3 cm long and 4 cm wide and thus the square measure of the array is 1/8.17 of that used in a digital beamforming imager having the same lateral resolution. This indicates the number of elements on the array can be reduced to about 1/8 of a dense 2-D array of a digital beamforming imager. The proposed imager has -3 dB lateral resolution that is better than 2 degrees in a measurement field of 15 degrees long and 30 degrees wide. This demonstrates that the proposed imager can satisfactorily be used as a vision substitute system.

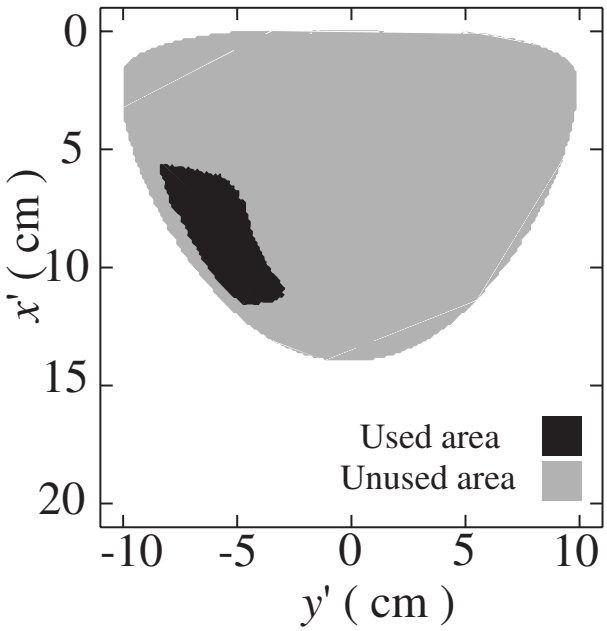

Figure 2.17: Used area on the mirror when a point target exists in a direction 30 degrees away from the center.

2.7 Real-time signal processing

For real-time signal processing, we calculate in advance the part of Eq. 2.8

$$L_{U\mathrm{T}_2} = \frac{1}{2\pi}\int_S \frac{1+jkR_2}{{R_2}^2 r_2}\frac{\boldsymbol{n_2}\cdot\boldsymbol{R_2}}{n_2 R_2} \cdot e^{-(jk+\alpha)(r_2+R_2)} dS. \tag{2.19}$$

The estimated velocity vector is given by

$$\phi_{2U} = \sum_U {A_U}^* L_{U\mathrm{T}_2}, \tag{2.20}$$

where we prepare a set of the values $L_{U\mathrm{T}_2}$ in a dictionary and calculate the vector from received signals with the aid of a dictionary look-up algorithm.

The data quantity used for a dictionary is estimated as follows. A dictionary has a set of the values $L_{U\mathrm{T}_2}$ at all the measurement points. The number of elements used on the array is 942 when the elements are placed on an elliptical array 3 cm long and 4 cm wide at intervals of 0.1 cm. The number of measurement directions is about 430 where the measurement direction intervals are 1 and 3 degrees at the center and a direction 30 degrees away from the center in a measurement field 30 degrees vertically and 60 degrees

horizontally, respectively. The number of sampled in the range from 15 cm and 4.5 m is 29 when the intervals of those sampled range between 1 cm and 30 cm for 1.5 cm and 4.5 m depths, respectively. Therefore the data number in a dictionary is 12 million.

A dictionary needs a memory device of about 90 MB when each datum is a single precision complex floating point number. All the data in the dictionary can be read to a memory device at one time; thus this system needs a suitably short data access time but without using a hard disc drive.

The calculation time of the estimated power of all the measurement points is about 0.07 seconds when we use an Xeon Pentium4 of 2.8 GHz. Since the sampling rate is 14μs when the imager transmits a acoustic pulse wave of 2 cm in pulse length and samples 4 times for each range, the sampling process is realized using an analog-digital converter with a 64 MHz sampling rate when the number of elements is 942. The sample and hold time is 14μs, which can be neglected compared to the propagation time. Hence the proposed imager can sample and receive signals at one time. The signal processing time containing the propagation time is about 0.1 second, and thus the proposed system can realize real-time imaging of 3-D environmental information.

2.8 Conclusion

We propose a hybrid imager with a concave mirror and a 2-D element array that uses an off-focus method, where images are reconstructed numerically from the received signals, as a low cost vision substitute system with high time and spatial resolution. Using a hybrid method a wide transmit beam is radiated to the entire measurement field. Since most of the echo from a target is reflected on the mirror and gathered on the array, the spatial resolution of the proposed imager is improved from that of a digital beamforming imager with a same size array. Using an off-focus method the distance between the reflector mirror and the array is fixed, and images of targets are reconstructed from the received signals by numerical back-projection. We optimize the mirror shape by utilizing geometric optics, and then evaluate the spatial resolution of the proposed imager using physical optics. The measurement field of the proposed imager is 30 degrees vertically and 60 degrees horizontally. The -3 dB lateral resolution is about 1 degree at the center, where the transmit frequency is 170 kHz, the concave mirror is 20 cm in width, and the elliptical array is 3 cm long and 4 cm wide. This means that the number of elements can be reduced to about 1/8 of that for a dense 2-D array of a digital beamforming imager. We also investigated a real-time signal processing system for the proposed imager.

Chapter 3

Human Interface and Transmit Frequency Control for the Through-Air Acoustic Real-Time High Resolution Vision Substitute System

3.1 Introduction

Intensive studies have been made on human-machine information transfer through tactile excitation for vision substitution. A two-dimensional matrix of stimulators can display spatial information to the skin, and previous works have been directed to change visual image to vibrotactile or electrotactile stimulation [62][63]. In this method intensity of each stimulator corresponds to the light intensity of visual image and does not indicate the range of the target. Vision substitute system needs high time resolution to present dynamic change of spatial resolution and high spatial resolution to recognize many targets individually. Although various tactile vision substitution systems have been proposed, they are not useful as navigation systems for visually handicapped due to limited spatial and time resolution [24][64][65]. We proposed a high resolution real-time vision substitute system [66]. In this method we transmit ultrasonic pulse wave and receive the echoes by an element array with a reflector mirror. In this study we further propose a spatial information transfer method to present the range, direction and surface topography of the target through tactile excitation on the forehead, and a technique to control transmit frequency.

3.2 Summary of high resolution vision substitute system

Phased array imagers and digital beam forming imagers have been proposed for high-resolution 3-D imaging system. Phased array imagers measure one direction by a transmit and receive event, and do not have sufficient time resolution. Digital beam forming imagers with 2-D dense array measure entire the target area by a transmit and receive event, but need enormous elements on the array. Though digital beam forming imagers with sparse array have been reported, it is difficult to reduce the number of elements to less than half of the dense array [49][50].

We proposed an acoustic 3-D imaging system based on a hybrid array-reflector configuration which realizes high time and spatial resolutions with modest computional load. Fig. 3.1 shows the schematic view of the proposed vision substitute system. In this system a broad transmit beam is radiated over the entire measuring area. The reflected echo is first focused by a concave reflector, and then received by the array. Reconstruction of widely distributed images on the array is based on numerical back projection. We call this hybrid method.

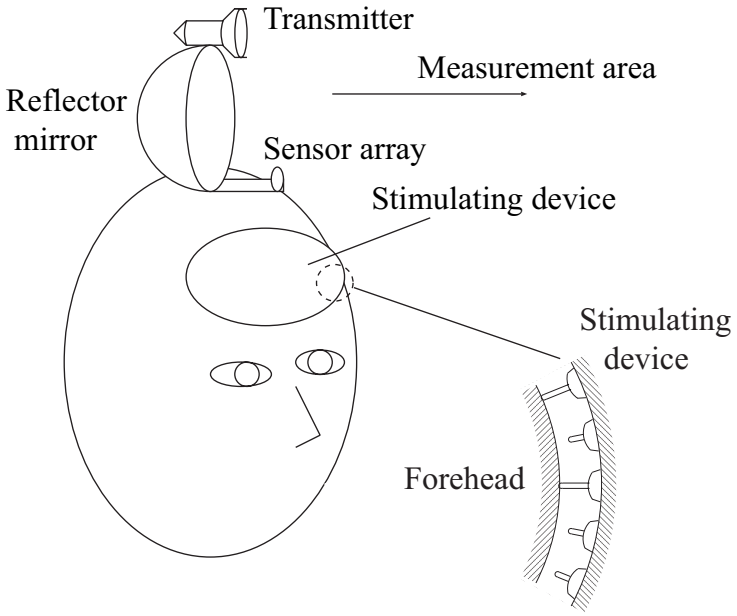

Figure 3.1: Schematic view of the system.

Fig. 3.2 shows the spatial resolution of the hybrid method in the case of the reflection mirror width of 20 cm, the elliptic dense 2-D array with 4cm major axis and 3cm minor axis, and the transmit frequency of 170 kHz. Its angle of view is ±15 degrees and ±30

degrees in the vertical and horizontal section, respectively. As evaluated by physical optics, the angular resolution at the center direction is 1.16 degree in the vertical section, and 1.20 degree in the horizontal section. Only 1/8 times as many elements are needed compared to the digital beam forming method. With the aid of dictionary look-up algorithm, the image reconstruction based on numerical back projection takes less than 0.1 second, which is sufficiently short for a real-time operation.

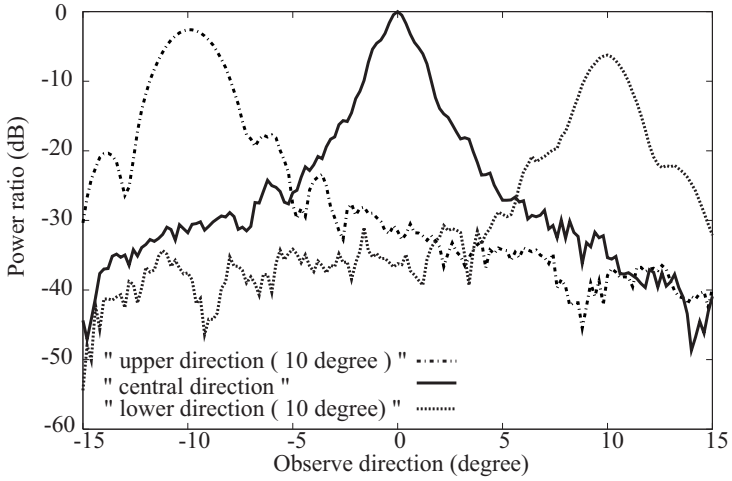

Figure 3.2: Angular characteristics of imaging calculated by physical optics in the vertical section.

3.3 Transmit frequency control

In the previous section, spatial resolution is investigated for the case that transmit frequency is 170 kHz and measuring range is 1 m. The signal to noise ratio of the echo from long distance deteriorates when we radiate pulses of high transmit frequency like 170 kHz due to strong attenuation. In this section we propose a scheme to select the optimum transmit frequency versus range.

Absorption attenuation of the echo power is proportional to $e^{-4\alpha l}$, where l is the target range and α is the absorption coefficient. Fig. 3.3 shows frequency characteristics of the received echo power versus range. We set the absorption coefficient $\alpha = 1.0 \times 10^{-8} f$ neper/cm, where f is the transmit pulse frequency. Received power is normalized by that of measuring range 1 m and transmit pulse frequency 20 kHz. Echo power attenuation of a high frequency pulse is limited at a short range, but significant at a long range. This means that a low frequency pulse should be radiated for a long range detection. The angular resolution of digital beam forming imager with 2-D circular array

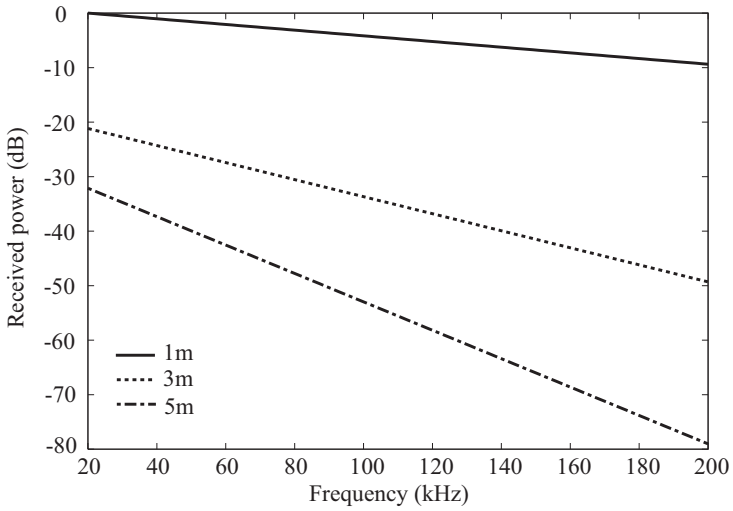

Figure 3.3: Frequency characteristics of the received signal power at various range.

is c/fD rad, where c is the propagation velocity of sound and D is the array size. We transmit low frequency pulses for long range detection to increase the echo power and high frequency pulses for short range detection to improve angular resolution. Repetition of transmit and receive events causes range aliasing. Echo power from another range over that from measuring range is given by

$$P_n = e^{-4\alpha(n-1)l}/n^4, \tag{3.1}$$

where nl is the range which causes range aliasing. We set constant lf to make P_n and l independent of each other by controlling the transmitting frequency. In the case of $lf = 170$ m $\cdot$ kHz, $P_2 = -20.9$ dB and $P_3 = -36.8$ dB. This means the influence of range aliasing is negligible. Fig. 3.4 shows signal to noise ratio of received echo versus range. Solid line is signal to noise ratio of proposed method, and broken line is that of constant transmit frequency of 170 kHz. Improvement of SNR becomes larger at longer range detection, which increases to 40 dB at the measuring range of 5 m.

Acoustic imaging systems are useful to measure in the body for medical diagnoses. When the measurement range is 10 cm, the center frequency of transmit pulses is 5 MHz. Thus the pass length is about 630 times the wave length. The sound velocities in a liver, a heart, and fat are 1585, 1580, and 1420 m/s, respectively. Therefore the variation of sound velocity is about 10 %. As for the proposed through air acoustic imaging system, the pass length is 1000 times the wave length without regard to target range. When the variation of the temperature is 20 degrees, the variation of sound velocity is about 3 %. Therefore the effect of the aberration to the proposed imager is weaker than that to an acoustic medical imager.

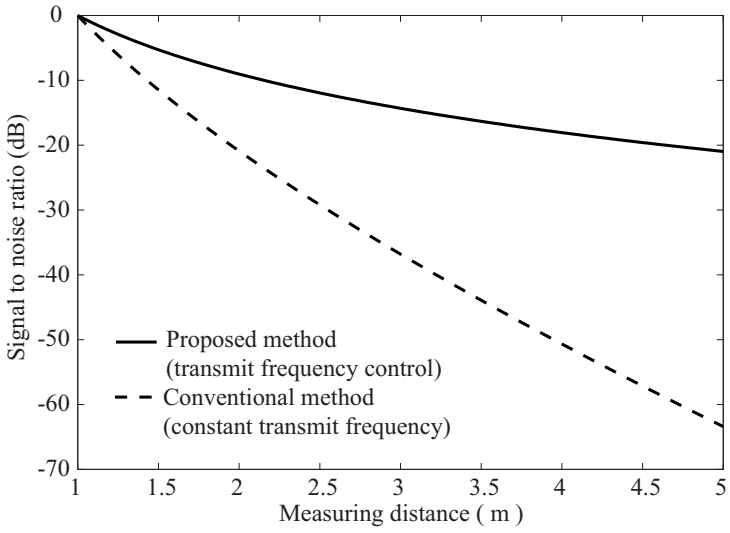

Figure 3.4: Signal to noise ratio versus range.

3.4 Spatial information transfer by tactile display

3.4.1 Setting of stimulation points and measuring direction

We assume to stimulate vibrotactile excitation at the location corresponding to the target direction. As the forehead has wide area for stimulation and keen sense of touch, it is suitable for stimulation region. Since the spatial resolution against stimulation at the forehead is about 5 mm, we set stimulator pitch 5mm. Fig. 3.5 shows the alignment of the stimulating points on the forehead in the case of the stimulating area of 6 cm long and 10 cm wide. The stimulator array consists of 13×21 elements.

Vision has wide angle of view and high angular resolution at the center. We set the angle of view of the vision substitute system ± 15 degrees in the vertical section, ± 30 degrees in the horizontal section, and the sampling interval of measuring direction 1 degree at the center. We set measuring directions as follows.

First, we arrange measuring directions on the horizontal and vertical lines at irregular spacing. We set hyperbolas which go through the measuring points on the lines, and we define their intersections as the measuring directions. Fig. 3.6 shows measuring directions in the target area. The sampling interval of measuring directions on the lines follow quadratic function. Stimulating points on the forehead of Fig. 3.5 and measuring directions of Fig. 3.6 correspond one to one.

In the case of arranging 21 measuring directions on the horizontal line of ± 30 degrees at a regular spacing, the sampling interval is 3 degree. In the proposed layout, the interval is 1 degree at the center and 4 degree at the peripheral directions.

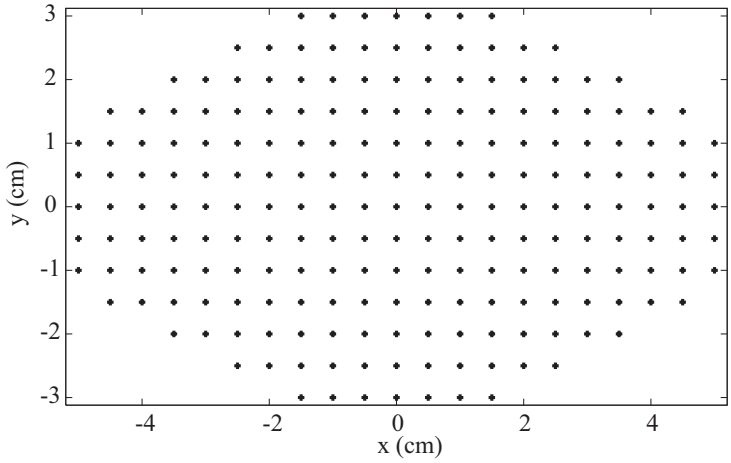

Figure 3.5: Stimulating points on the forehead.

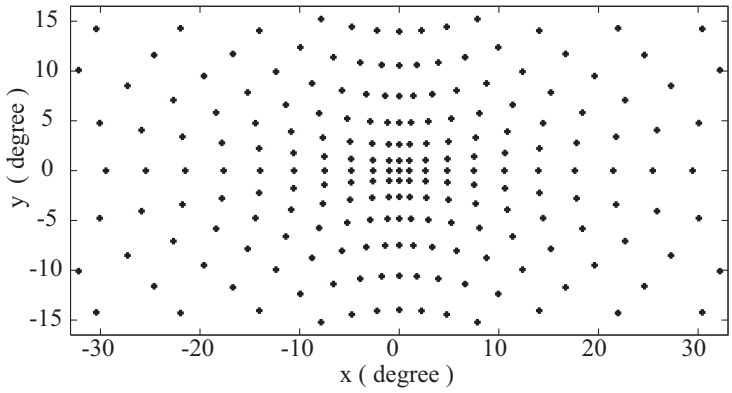

Figure 3.6: Measuring directions in the target area. Intervals follow quadratic function.

3.4.2 Spatial information transfer

To distinguish multiple targets, we need to present targets' direction, range and echo power related to their surface topography. The proposed system presents the direction of a target by stimulating location, and their echo power by vibrotactile excitation intensity. The subject can recognize target range as follows.

Fig. 3.7 shows schematic view of targets in the measuring area. Color depth of targets is related to their echo power. Fig. 3.8 is the projection image of targets to the measuring area. Neighboring target is displayed in the case of plural targets existing in the same direction. The range of target A, B, C is less than d1, and that of D, E, F is between d_1 and d_2.

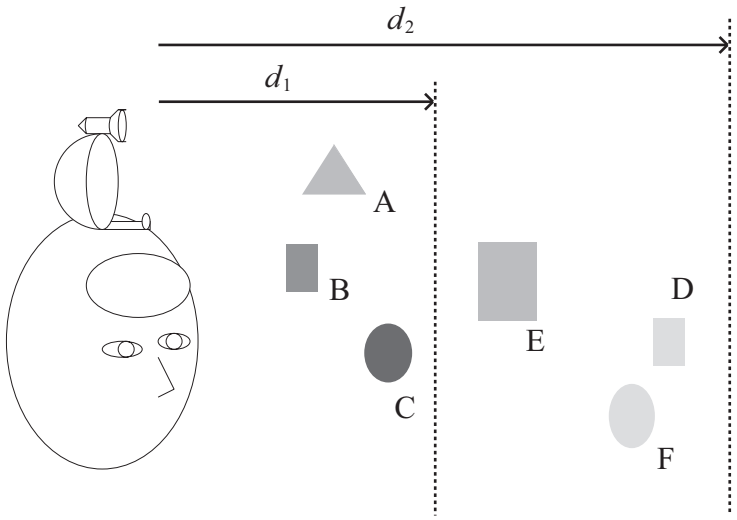

Figure 3.7: Schematic view of targets in the measuring area. Color depth is related to echo power.

First, the subject determines measuring range of d_1 and instruct it to the vision substitute system. We suppose the instruction is given by biting force of a switch. The pulse frequency and interval are made suitable to the range d_1 and the system present direction and echo power of target A, B, C by vibrotactile excitation on the forehead. Fig. 3.9 shows stimulating points matched with targets in the case of measuring range of d_1. Size of each symbol indicates the stimulation pressure related to the echo power. The system presents the echo power by stimulating pressure and the subject can recognize not only the size and direction of targets but also its surface topography. Second, he/she instructs the system the measuring range of d_2, and the system presents the directions and the echo power of target A, B, C, D, E, F. Fig. 3.10 shows stimulating points matched with targets in the case of measuring range d_2.

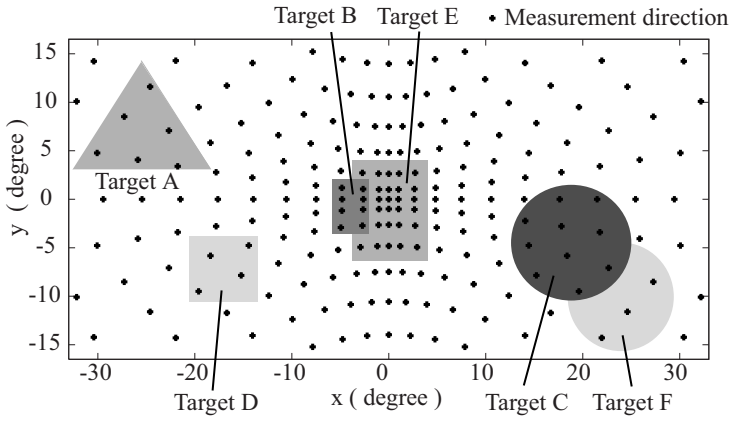

Figure 3.8: Targets' directions in the measuring area. Color depth is related to echo power.

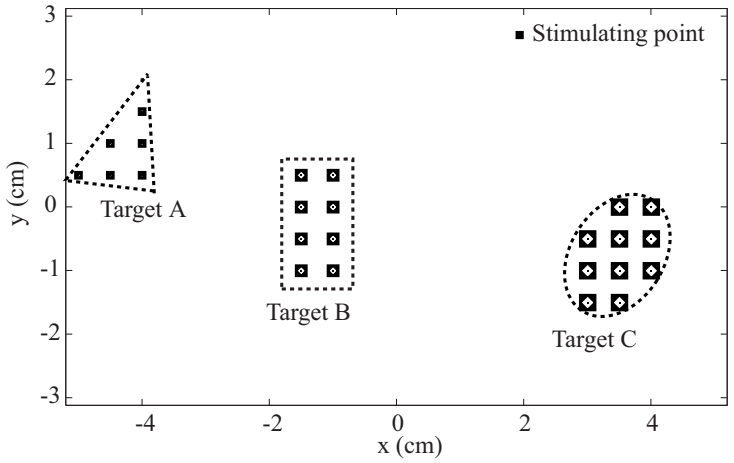

Figure 3.9: Stimulating points matched with targets in the case of measuring distance is d_1. Size indicates stimulating pressure related to echo power.

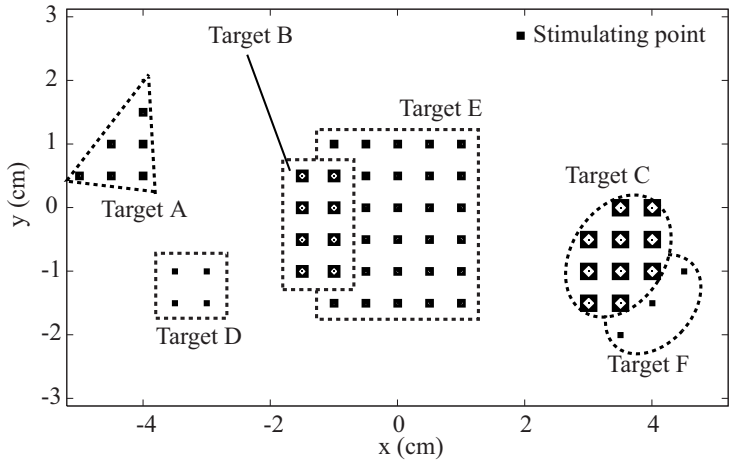

Figure 3.10: Stimulating points matched with targets in the case of measuring distance is d_2. Size indicates stimulating pressure related to echo power.

From the change of displayed information the subject recognizes the range of target D, E, F is between d_1 and d_2. He/she can also find the boundary of target B and E (also C and F) from stimulating pressure difference. Targets at shorter range is more important and vision detects only the nearest target in each direction. For safety of subjects and similarity with vision we propose to present the nearest target in the case of plural targets existing in the same direction. By measuring from short range to long range, we get spatial information of the whole target area. The time resolution of the system is about 0.1 second, which can deal with movement of pedestrians.

3.5 Conclusion

For the wide range detection of the acoustic vision substitute system, we proposed a transmit frequency control method. In this method, we transmit low frequency pulses for long range detection to receive sufficient echo power and high frequency pulses for short range detection to improve angular resolution. In the case of product of transmit frequency and measuring range is $lf = 170$ m $\cdot$ kHz, the effect of range aliasing is reduced to less than -20 dB. We also proposed a human-machine information transfer method to present the target area of ± 15 degrees long and ± 30 degrees wide by the sampling interval of 1 degree at the center. The vibrotactile stimulator array consists of 13×21 arrangement on the forehead of 6 cm $\times$ 10 cm size. The subject instructs measuring range to the vision substitute system, and it presents direction and echo power of targets existing within the instructed range. The direction and echo power of the target is presented by stimulating location on the forehead and excitation intensity, respectively. In this method, he/she

can distinguish multiple targets of the same range. The time resolution of 0.1 sec per 1 image is sufficiently high for the use of pedestrians.

Chapter 4

Transfer Information Enhancement with a 2-D Tactile Stimulator Array for an Acoustic Vision Substitute System

4.1 Introduction

Many researchers have investigated human machine information transfer methods through tactile excitation. Often, a 2-D stimulator array is used in a vision substitute system [63][64][24][27][67]. Previous research has been directed to converting visual images to vibrotactile or electrotactile excitation, and thus excitation intensity does not correspond to the range of the target in these methods. For target range detection, a user needs to memorize the shape of the target. Then the user identifies the target and compares the presented information with the memorized shape. Therefore, it is difficult to recognize the location of plural targets with different ranges, because of the difficulty for memory of the plural target shapes and identification of them.

It is expected that early blind have a quite different recognition way of spatial information from late blind, and thus it is difficult to design a vision substitute system for both early and late blind. In recent years Japan rapidly turns into aging society and the occurrence of diabetes increases. Therefore the number of late blind will increase because of senile macular degeneration and diabetic retinopathy. Hence, we direct to a vision substitute system for late totally blind. For acquiring information from visual environments with plural targets, existing vision substitute systems need to improve their angular and range resolutions. The goal of this study is to develop an efficient system for presenting environmental information. To provide environmental information with a portable instrument, we have proposed an acoustic vision substitute system based on a hybrid array-reflector configuration that realizes high time and spatial resolutions with

just a modest computational load [66]. Fig. 4.1 shows the schematic view of our vision substitute system in which a broad transmit beam is radiated over the entire measurement area. The reflected echo is first focused by a concave reflector, and then received by the 2-D sensor array. Images are reconstructed from the widely distributed signals received on the array by numerical back projection. With this method, one transmit and receive event can make a 3-D image of the whole measurement area. This system realizes 34 images/s in the case that the measurement range is 5 m.

We propose that spatial information, measured by the acoustic sensor, is presented by a 2-D tactile display placed on the forehead. Auditory sense is one of the most important information for the blind. Mounting a stimulating device on a hand or an arm prevents a user from moving freely. Of all body regions on which we could mount a stimulating instrument without an obstruction, the forehead has a low two-point discrimination threshold and wide stimulating area. Thus we determined the stimulation region should be the forehead. As well, the forward direction of the face corresponds to the center direction of the measurement area. Therefore, for late totally blind, recognizing target directions is relatively easy.

This paper has two purposes. The first is the angular resolution improvement of transfer information to provide sufficient environmental information. The second is to transfer the target ranges exactly for the distinction of plural targets at different ranges. So that each stimulator individually transfers different information, the stimulators in the array are spaced at intervals of the two-point discrimination threshold [68]-[70]. This restricts the number of stimulators that transfer information through a certain area. In this paper we propose two methods to improve angular resolution and transfer target range. The methods employ a 2-D stimulator array having stimulators spaced at intervals of less than the length of the simultaneous two-point discrimination threshold to increase the number of stimulators. Since two stimulators adjoined to each other work with a certain stimulus onset asynchrony (SOA), they can separately transfer different information. Furthermore a user selects the measurement range and the system proposes targets within the range to the user. By selecting from a short range to a long range, the user can acquire spatial information of the entire target area. Since the user knows the measurement range, the range of the targets can be accurately recognized. Here, we investigate these methods experimentally, and confirm their effectiveness.

In section 2, we propose two methods, an alternating stimulation method and a voluntary range selection method. We then explain the instrument used in the experiment and the content of the experiment. In section 3, we evaluate the experimental results. Finally, conclusions are drawn in section 4.

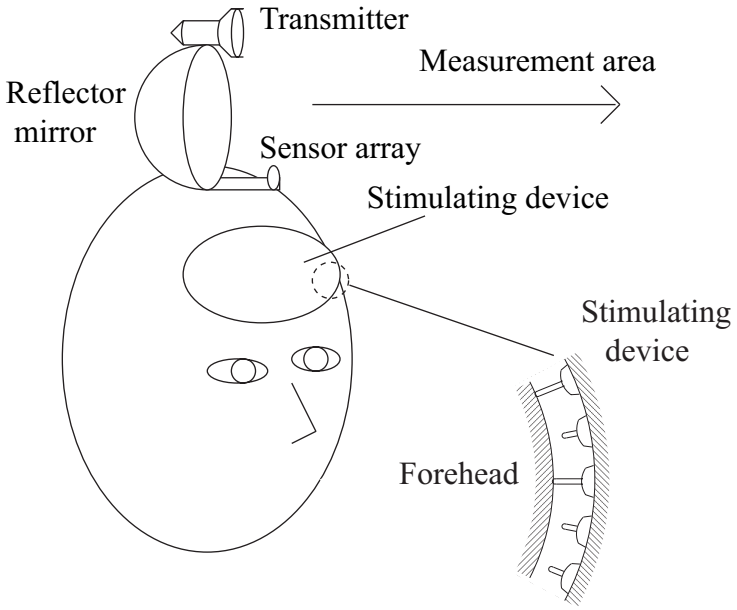

Figure 4.1: Schematic view of the acoustic vision substitute system.

4.2 Methods

4.2.1 Alternating stimulation method

This system uses a 2-D stimulator array as a stimulating device. The stimulator spacing should be more than the two-point discrimination threshold so that each stimulator transfers different information to the user. Since this restricts the number of stimulators constituting a 2-D stimulator array, it is difficult to transfer enough information to a user for the vision substitute system. We propose an alternating stimulation method to gain transfer information by increasing the number of stimulators. In this method stimulators in a 2-D array are divided into several groups. Fig. 4.2 shows examples of the stimulators divided into two and four groups. Stimulators that belong to a group move synchronously and each stimulator group is activated alternately. Stimulators within a group are spaced at intervals of the two-point discrimination threshold. However, the interval of two stimulators that adjoin each other is less than the interval of the two-point discrimination threshold. Since they belong to different groups, there is a SOA between two stimulations. In this case, the two stimulations are perceived individually under the condition that the stimulator spacing is about 1/3 of the two-point discrimination threshold [69]. In the case of the two examples shown in Fig. 4.2, the intervals of the stimulators adjoining each other are respectively 0.71 and 0.5 of the two-point discrimination threshold. Therefore, if the stimulator spacing of the same group is set to the two-point discrimination

threshold, stimulations can individually transfer different information. This means that the number of stimulators can be increased to 2 or 4 times that in a 2-D array spaced at an interval of the two-point discrimination threshold. Thus the spatial information presented in this method is improved to 2 or 4 times that in the simultaneous stimulation one.

4.2.2 Voluntary range selection

To distinguish multiple targets, we need to present the direction and range of targets. The proposed system presents the direction of a target by stimulating the location on the forehead. The subject can then recognize the range of targets as follows.

Fig. 4.3 shows a schematic view of targets in the measurement area. Fig. 4.4 is the projection image of targets to the measurement area. The range of targets A, B is less than d_1, and that of C, D is between d_1 and d_2. Since a target with a shorter range is more important, the target of the shortest range is displayed in the case where plural targets exist in the same direction.

First, a user determines the measurement range of d_1 and gives instructions to the vision substitute system. We suppose the instruction is given by a brain switch [71], a biting force switch, a voice switch, or a kind of contact switch. In future we will examine these various switch types and select the best. The system presents directions of targets A, B by vibrotactile excitation on the forehead. Fig. 4.5 shows stimulating points matched with targets in the case of the measurement range of d_1. From the stimulating position presented by this system, the user can recognize the size and direction of the targets.

Second, the user gives the instruction regarding the measurement range of d_2 to the system, and it presents the directions of targets A, B, C, D. Fig. 4.6 shows stimulating points matched with targets when the measurement range is d_2. From the changes in the information displayed the user recognizes that the range of targets C, D is between d_1 and d_2. By measuring from a short to a long range, the user acquires spatial information of the entire target area.

For identifying objects on a table, there is no need to measure targets with a long range; therefore, a user fixes the measurement range as a short one. Then the interval of each radiation time becomes shorter in the case that a transmitter radiates after the echo from the longest range is received. This allows an improvement in the time resolution. For long range detection, the user can memorize the range of targets from a single detection of the whole measurement area. Then the user can fix the measurement range as a long one, after measuring from the short range to a long one. When the measurement range is 5 m, the time resolution of the system is about 0.03 second, which means that it can deal with pedestrian movement.

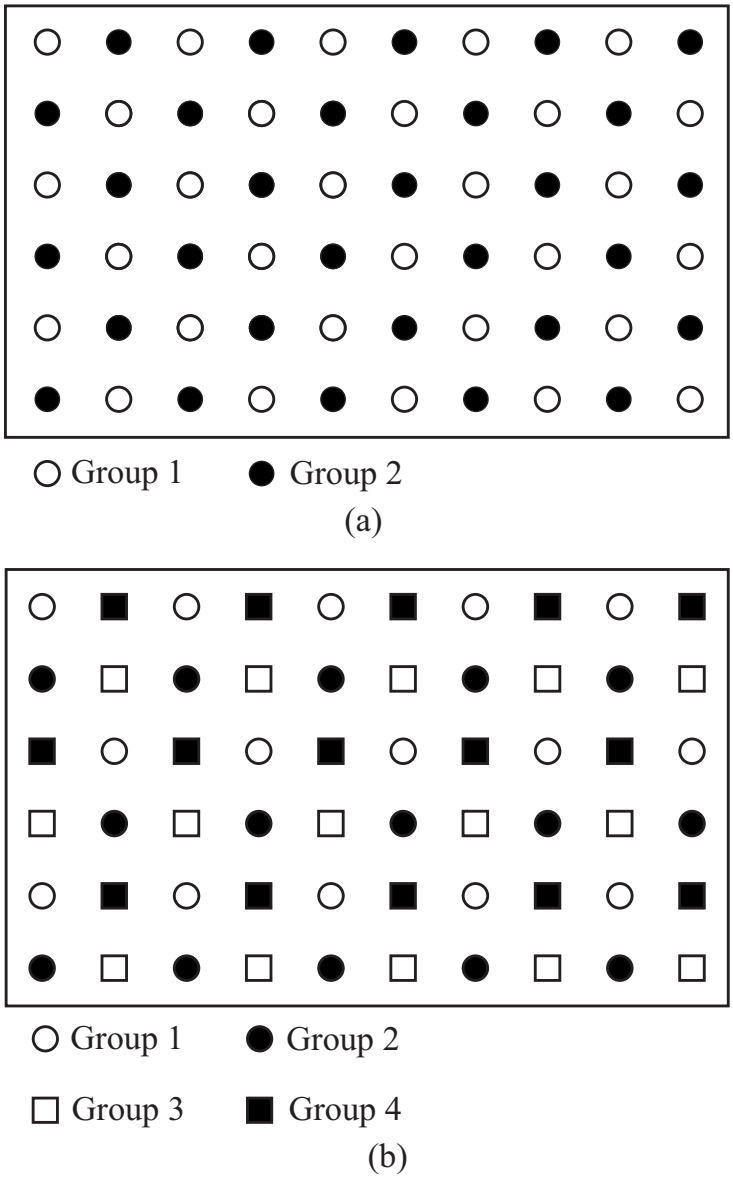

Figure 4.2: Division of stimulators that are components of a 2-D array stimulating device placed on the forehead. Stimulators are divided into (a) two and (b) four groups. Stimulators that belong to a group move synchronously and stimulator groups are activated alternately.

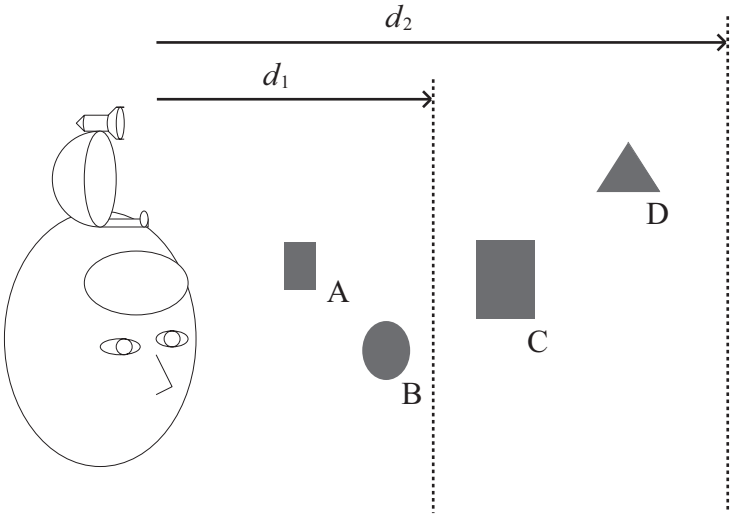

Figure 4.3: Schematic view of targets in the measurement area.

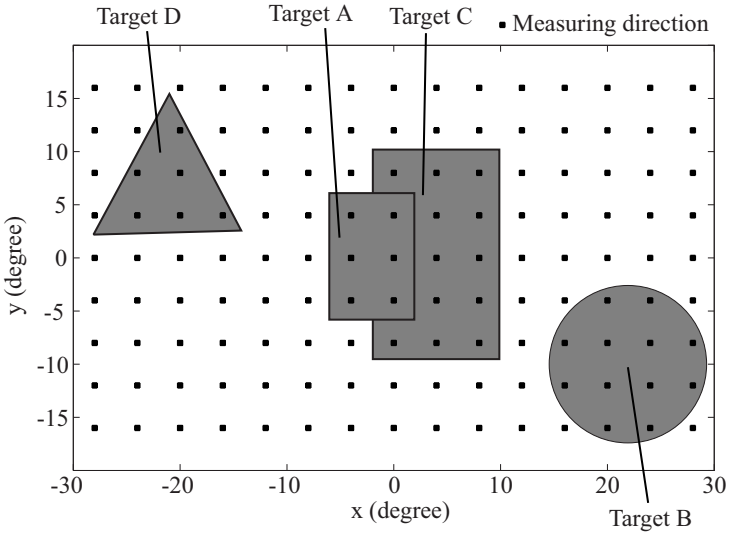

Figure 4.4: Directions of targets in the measurement area.

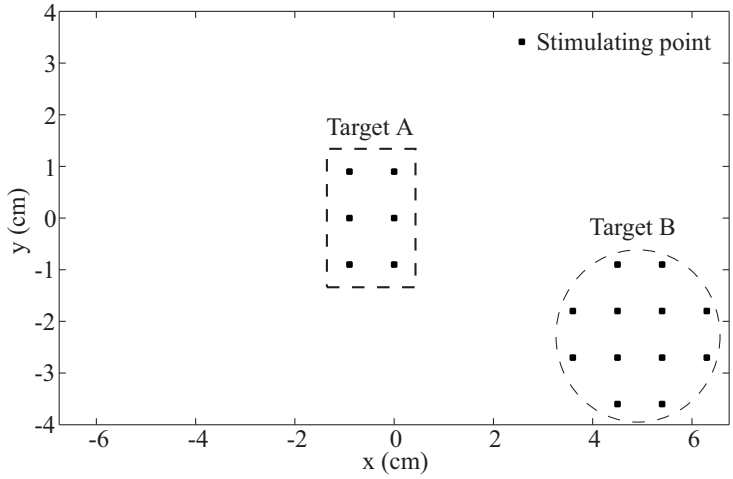

Figure 4.5: Stimulating points matched with targets when the measuring range is d_1.

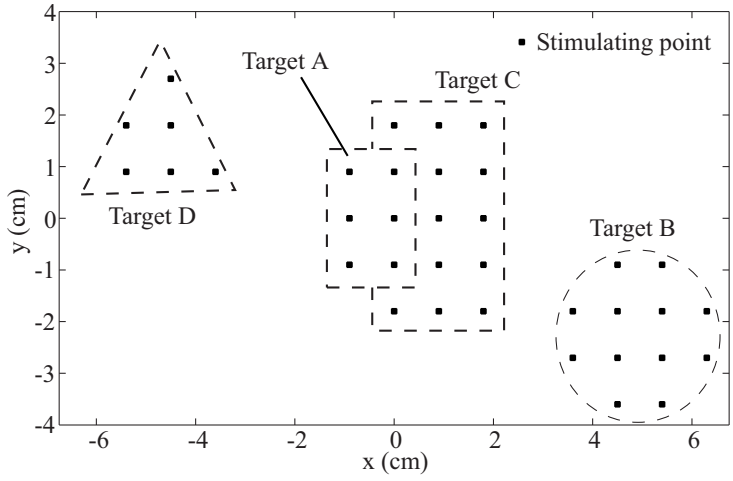

Figure 4.6: Stimulating points matched with targets when the measurement range is d_2.

4.2.3 Overview of the experiment

We examine the alternating stimulation and the voluntary range selection methods experimentally using a 2-D solenoid array consisting of a 2 $\times$ 4 arrangement with two dummy solenoids placed at the left and right side of the array, as shown in Fig. 4.7. The two solenoids placed at both sides always generate sound and vibration, to prevent participants distinguishing tactile patterns by sound. The protuberances, placed at both edges of the array, restrain the stimulation rods from pushing hard against the forehead. When employing the simultaneous stimulation method, the active stimulators work synchronously. When employing the alternating stimulation method, the stimulators in the 2-D array are divided into two groups, as shown in Fig. 4.8. Each stimulation group is activated alternately. With this proposed stimulation method, a couple of stimulation sets present single spatial information. To correspond the power consumption of the dummy solenoids between the two stimulation methods, the left side dummy solenoid belongs to group 1 and the right side to group 2. We first compare the perceived stimulus quality of the alternating stimulation to that of simultaneous stimulation. We then investigate the exactitude of transferring range information of targets using a voluntary range selection method. We suppose that the user gives instructions to the system for a short to a long range. Since the target with a longer range is presented later, the stimulation points increase within a stimulation set.

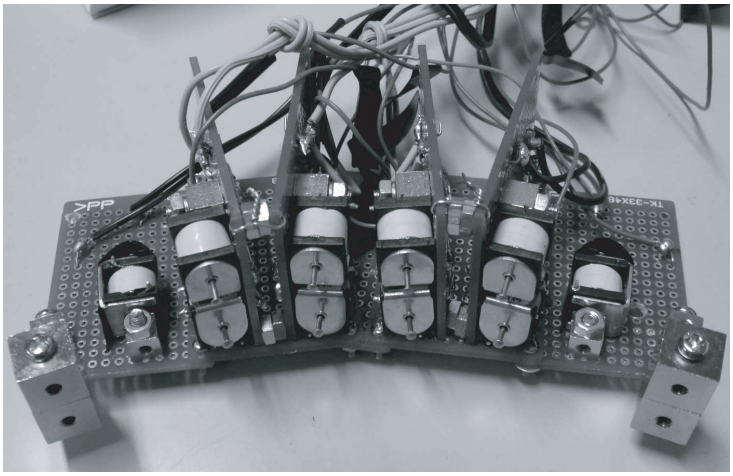

Figure 4.7: Solenoid array placed on participants ’foreheads. The 2 $\times$ 4 solenoids placed at the center of the array are the stimulators. The two solenoids placed at the sides always generate sound and vibration to prevent participants from distinguishing tactile patterns by sound.

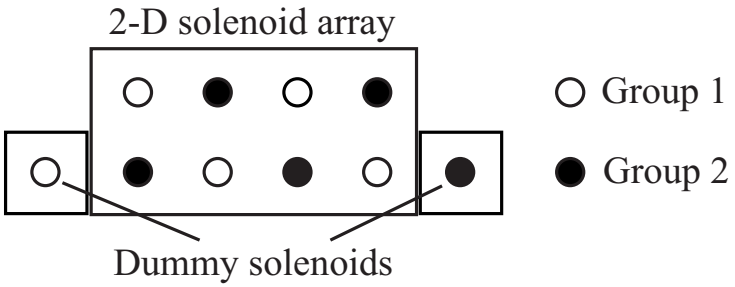

Figure 4.8: An arrangement of stimulators divided into two groups when employing the alternating stimulation method.

4.2.4 Vibrotactile stimuli

In this study, we use a solenoid array as the stimulating device. Each solenoid has a round-topped vibrating rod, as shown in Fig. 4.9. As shown in [70], the two-point discrimination threshold at the forehead is 0.9 cm to 1.5 cm. It is assumed from the Loomis 's study [72], that the localization error at the forehead is about 1/4 of the two-point discrimination threshold. Since we assume that the stimulator spacing is about two-point discrimination threshold for transferring information accurately, the tops of the vibrating rods are spaced at intervals of 1.3 cm vertically and 1.5 cm horizontally. A participant places the array on his forehead and responds to the tactile pattern presented by the array. Rectangular pulses are delivered to activate solenoids, which contain two dummy solenoids. The voltage delivered to a solenoid is 3 V. Its pressure, dependent on the stroke of the stimulation rod, is 1 to 2.5 gf.

To provide fine spatial information, it is necessary to stimulate the skin tactile receptors with high spatial resolution. The skin deform threshold of the receptor should be low for the stimulators to have a low power consumption. Since a Meissner 's corpuscle has both high spatial resolution and low skin deform threshold [24], we decided to activate Meissner 's corpuscles. Their most sensitive frequency is 20 to 40 Hz; so we set the stimulating frequency at 30 Hz. Fig. 4.10 shows the waveforms used in this experiment. The interval of pulse onsets is 33.3 ms (pulse repetition rate is 30 Hz) and pulse width is half of the interval. We follow Y. Shimizu [73], and set the duration of the stimulation and SOA at 200 and 800 ms, respectively; that is, the burst onset is separated by 800 ms and each burst contains 6 pulses.

A phantom sensation occurs under certain conditions of SOA, stimulator spacing and stimulation pressure. Such as when two stimulators that adjoin each other can not individually transfer different information. To prevent a phantom sensation, in the alternating stimulation trials we set the SOA and the duration of stimulation as 400 ms and 200 ms, respectively. We also set both types of trials to have the same power consumption as follows.

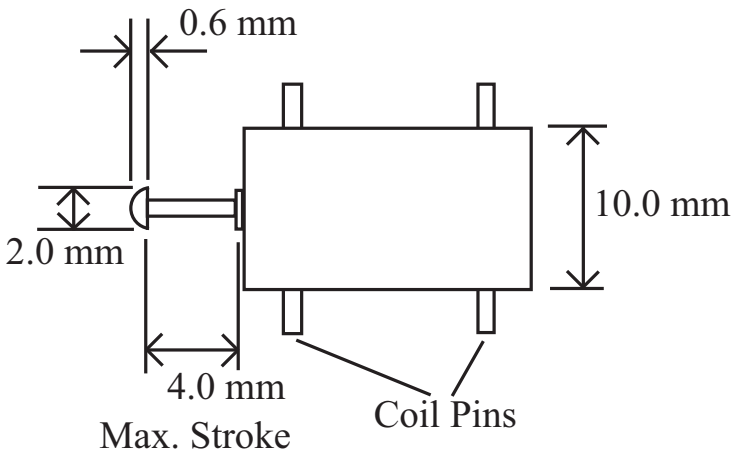

Figure 4.9: Schema of a solenoid component in the 2-D stimulator array placed on the forehead.

In the simultaneous stimulation trials, the waveform in Fig. 4.10 is delivered to all active solenoids. The tactile patterns used in these trials are 1-point stimulations and 4-point square stimulations, as shown in Fig. 4.11. The 1-point stimulations are presented at one of the 8 positions. The 4-point stimulations are presented simultaneously at one of three positions; left, middle, and right. In the alternating stimulation trials, the waveforms in Fig. 4.12 -(1) and 4.12 -(2) are delivered to the active solenoids of groups 1 and 2, respectively. The tactile patterns used in these trials are the same as those in the simultaneous trials. Each 4-point square stimulation is presented by two pairs of stimulators that are activated alternately, as shown in Fig. 4.13. A 1-point stimulation is presented in the same way as that in the simultaneous stimulation trials, except for the activation of the dummy solenoids.

In the alternating stimulation method experiment, the presentation time of each pattern is 5 s, which contains 6 bursts of voltage delivered to the solenoids. Since the receptive field of a Meissner 's corpuscle is 12.6 mm^2 [24], the influence of an individual stimulation over an adjacent stimulation point is neglectable. Both trials in this experiment have the same SOA, and therefore there is no difference between any influences from the adaptation in the two trials. This indicates that in the comparison between the simultaneous and alternating stimulation trials it is not necessary to evaluate the influence of the adaptation. The interval between two presentation times is 5 s, and at that time a participant responds to the presented pattern.

In the voluntary range selection method experiment, we assume that the measurement range has 5 phases. Two targets represented as 4-point square stimulations exist at the right and left in different ranges, and a user measures from a short to a long range. Here, these targets are presented one after the other, as shown in Fig. 4.14. The presentation

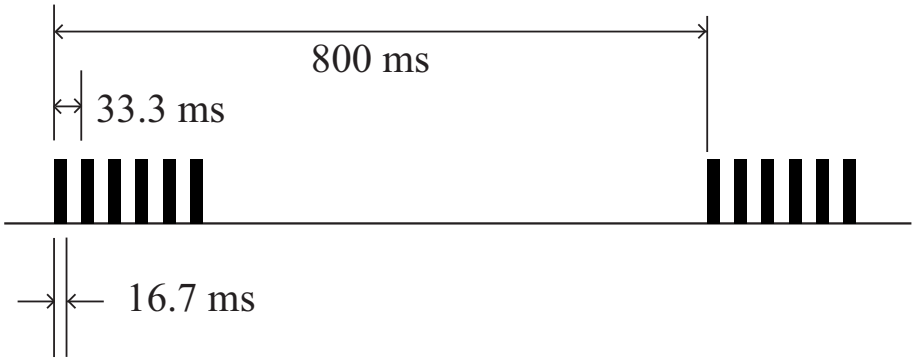

Figure 4.10: Stimulus waveform in the simultaneous stimulation trials. Pulse repetition rate is 30 Hz and pulse width is half of the pulse onset interval. Each burst has 6 pulses and burst onset interval is 800 ms.

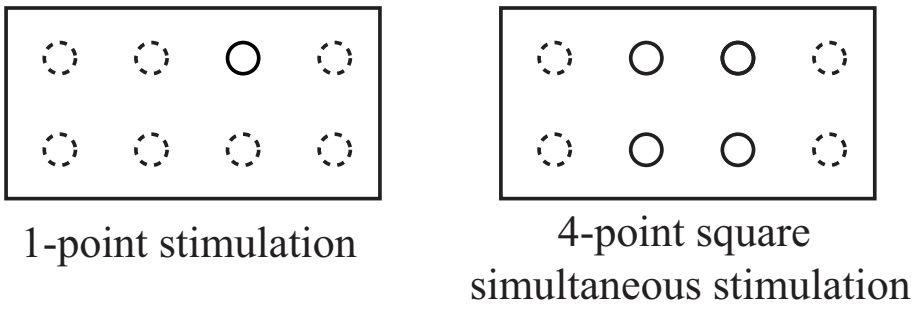

Figure 4.11: Tactile patterns in the simultaneous stimulation trials. The 1-point stimulations are presented at one of the 8 positions. The 4-point stimulations are presented simultaneously at one of the three positions; left, middle, and right.

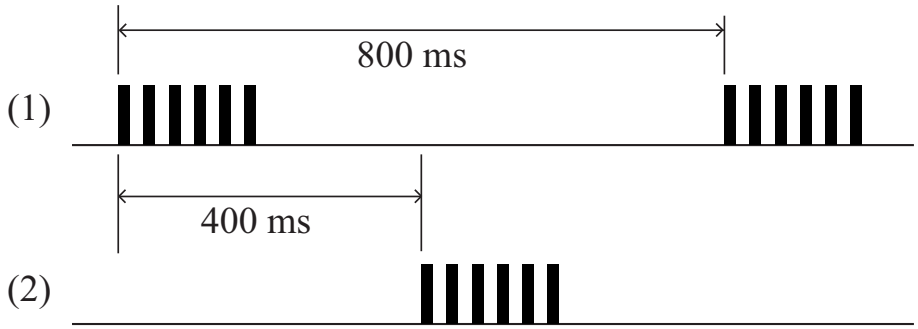

Figure 4.12: Stimulus waveform in the alternating stimulation trials. Waveforms (1) and (2) are delivered to the active solenoids of groups 1 and 2, respectively. Stimulus onset asynchrony between the two groups is 400ms.

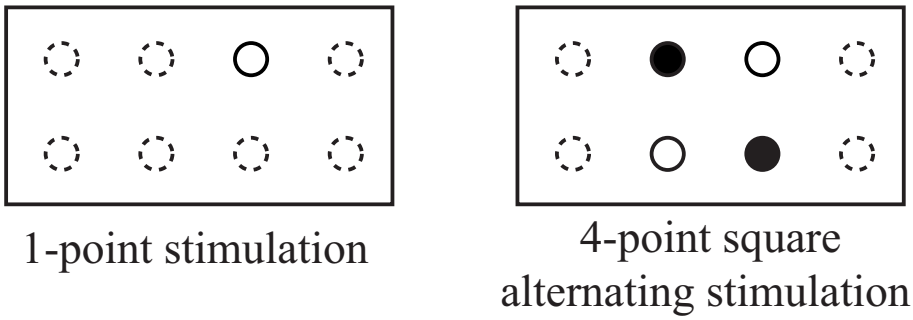

Figure 4.13: Tactile patterns in the alternating stimulation trials. The 4-point stimulations consist of two stimulation groups.

time for each stimulation set is 25 s, and contains 5 stimulation patterns. In this experiment, we use the alternating stimulation method and set the interval between the two presentation times as 5 s.

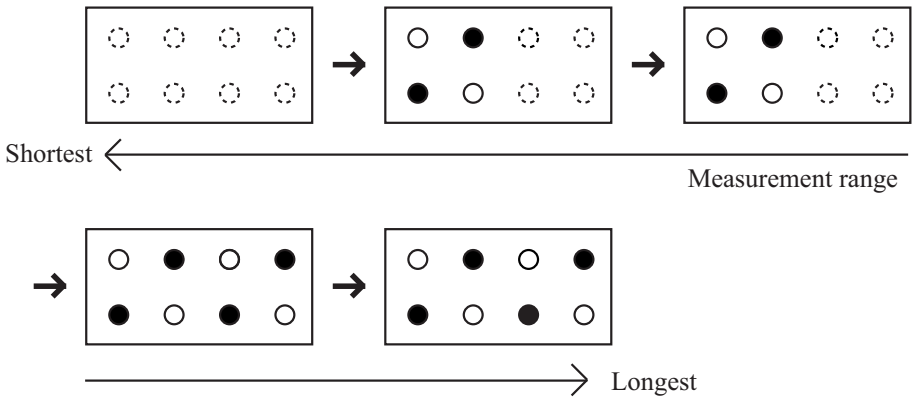

Figure 4.14: Tactile patterns in the voluntary range selection trials. Two targets, represented as 4-point square stimulations, are presented one after the other.

4.2.5 Participants

Six healthy males (21-28 years old) participated in this experiment. Participants provided informed consent and wiped their forehead before the start of the experiment. In the experiments, participants opened their eyes and inserted earplugs. We checked the contact between stimulation rods and the forehead before and after each experiment. All participants underwent the experimental procedures.

4.2.6 Main experiment

We number the solenoids from 1 to 8, as shown in Fig. 4.15. A 1-point stimulation is presented by activating one of the eight solenoids. A 4-point stimulation is presented at left, middle, or right position by four activated solenoids, as shown in Fig. 4.15. We call these stimulations as 1-8, left, middle, and right. A participant responds to the stimulations with the names, as shown in Table 4.1. If a participant perceives a 1-point pattern, he responds one of the 8 number; 1-8. If he perceives a 4-point pattern, he selects one of the three choices; left, middle, or right.

The alternating stimulation method experiment consists of two practical trials followed by two experimental ones. The first practical trial employs simultaneous stimulations, and the second alternating ones. In the practical trial, the stimulations of 1 to 8, left, middle and right are presented in that order. Participants are informed about the names

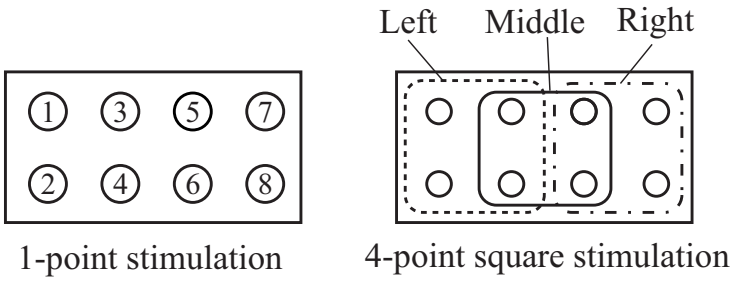

Figure 4.15: Solenoid numbers and activated solenoid groups of the 4-point stimulation. A 1-point stimulation is presented by activating one of the eight solenoids. A 4-point stimulation is presented at left, middle, or right position by four activated solenoids. Thus these stimulations are named 1-8, left, middle, and right.

Table 4.1: Variety of responses in the alternating stimulation method experiment. If a participant perceives a 1-point pattern, he responds with one of the 8 numbers; 1-8. If he perceives a 4-point pattern, he selects one of the three choices; left, middle, or right.

Perception	Response
1-point pattern	1 to 8
4-point pattern	Left, Middle, Right

of the stimulations presented and practice to become accustomed to the stimulations. This practice cycle is presented twice, and then each practical trial consists of 16 1-point stimulations and 6 4-point stimulations. Each experimental trial consists of 12 1-point stimulations and 12 4-point stimulations. The arrangement on the array and the order of these tactile patterns are random. In the experimental trials, participants respond to the stimulations with the names, as shown in Table 4.1. The first experimental trial employs simultaneous stimulations and the second alternating stimulations, similar to in the practical trials.

The voluntary range selection method experiment consists of one practical trial followed by an experimental one. The practical trial and the experimental one have 8 and 12 stimulation sets, respectively. The two 4-point stimulations of these 20 stimulation sets are presented randomly. Similarly to the alternating stimulation method experiment, in the practical trial participants are informed about the presented patterns and practice to become accustomed to these stimulation patterns. In the experimental trial they respond with the directions and the starting times of two 4-point stimulations. In this experiment we employ the alternating stimulation method.

4.3 Results

In the alternating stimulation method experiment, a participant responds with the pattern and position of the stimulation. There is a distance between the position of the stimulation and that of the response when the response to the stimulation pattern is correct. We evaluate the possibility that the distance, between the position of the stimulation and that of the response, is a certain distance when a 1-point stimulation is presented and the response being 1-point pattern. We define the possibility as the number of each distance over the total number of the responses being a 1-point pattern. The distance variation is 8 as follows; 0, 1.3, 1.5, 2.0, 2.6, 3.0, 3.9, and 4.2 cm. Therefore we define L_0 as the interval of the stimulation rods, and then classify the 8 distances to 4 grades; 0, L_0, $\sqrt{2}L_0$, and $2L_0$ or over. Table 4.2 shows the average and the standard deviation of the possibility. The possibility of the distance being 0 or L_0 is almost 1, and the possibility of the distance being $2L_0$ or over is almost nil. This indicates that we can neglect the probability of false positives.

Table 4.2: The average and the standard deviation of the possibility that the distance between the position of the stimulation and that of the response is each value when a 1-point stimulation is presented and the pattern of the response is correct. The average is written in the upper line of each cell, and the standard deviation with vinculum in the lower line.

Distance	0	L_0	$\sqrt{2}L_0$	$2\ L_0 \leq$
Simultaneous	0.437	0.469	0.0787	0.0152
stimulation	(0.117)	(0.173)	(0.091)	(0.034)
Alternating	0.518	0.408	0.0602	0.0139
stimulation	(0.305)	(0.278)	(0.065)	(0.031)

Table 4.3 shows the definitions of the variables used in the evaluation of the alternating stimulation method. Their values are the numbers of the responses in the experiment. Table 4.4 shows the average and the standard deviation of the possibilities that the response is correct or not correct when the response is a 4-point pattern. The possibilities for 4-point and 1-point stimulations are defined simply as $a_{22}/(a_{21} + a_{22} + a_{23})$ and $a_{12}/(a_{11} + a_{12} + a_{13})$, respectively. This result shows the effectiveness of the proposed alternating stimulation method for enhancing transfer of information with $p < 0.01$. We introduce the assumption that the possibility follows a normal distribution and use a t-examination.

Furthermore, the interpretation of a no signal response is as follows. Since the false positive probability can be neglected, a bad contact between a stimulator and the forehead causes a no signal response. For future work we need to improve the stimulation

Table 4.3: Definition of the variables used in the evaluation of the alternating stimulation method. Their values are the numbers of the sensation responded to in the experiment.

	Response		
	1-point pattern	4-point pattern	No pattern
1-point stimulation	a_{11}	a_{12}	a_{13}
4-point stimulation	a_{21}	a_{22}	a_{23}

Table 4.4: The average and the standard deviation of the possibilities that the response is correct or not correct when the response is a 4-point pattern, The possibilities for 4-point and 1-point stimulations are defined simply as $a_{22}/(a_{21}+a_{22}+a_{23})$ and $a_{12}/(a_{11}+a_{12}+a_{13})$, respectively.

	The possibility of a 4-point pattern response	
	4-point stimulation	1-point stimulation
Simultaneous stimulation	0.556 (0.190)	0.0278 (0.0393)
Alternating stimulation	0.861 (0.150)	0.0417 (0.0636)

instrument to prevent any bad contacts. The probability of a bad contact between a stimulator and the forehead, p_{BC}, satisfies

$$p_{\mathrm{BC}} = a_{13}/(a_{11} + a_{12} + a_{13}). \tag{4.1}$$

To revise the possibility that the response is correct when a tactile pattern is a 4-point square stimulation, we treat the result statistically. The number of 4-point square stimulations becoming 1-point stimulations because of a bad contact between stimulators and the forehead, b_1, satisfies

$$b_1 = 4(a_{21} + a_{22} + a_{23}){p_{\mathrm{BC}}}^3(1 - p_{\mathrm{BC}}). \tag{4.2}$$

In this interpretation, the possibility that a 4-point square stimulation becomes a no stimulation, ${p_{\mathrm{BC}}}^4$, is less than 0.2 %. This is consistent with the result that in all experimental trials $a_{23} = 0$. In this interpretation we define the correct response as a 4-point pattern response when a multiple-point stimulation is presented for a 4-point stimulation. The number of multiple-point stimulations presented is given by $a_{21}+a_{22}-b_1$. We remove the superficially correct occasion that the a participant mistakes and responds

with a 4-point pattern when a 1-point stimulation is presented because of a bad contact in the case of a 4-point stimulation. The number of occasions that this happens is given by

$$b_2 = b_1 a_{12}/(a_{11} + a_{12}). \tag{4.3}$$

Therefore the possibilities of a 4-point response when a 4-point stimulation and a 1-point stimulation are presented, p_{44} and p_{14}, satisfy

$$p_{44} = (a_{22} - b_2)/(a_{21} + a_{22} - b_1), \tag{4.4}$$
$$p_{14} = a_{12}/(a_{11} + a_{12}). \tag{4.5}$$

Fig. 4.16 shows the average of the possibilities, p_{44} and p_{14}, including the 2 standard deviation error bar. The result shows the effectiveness of the proposed alternating stimulation method for enhancing transfer of information with $p < 0.025$. We also introduce the assumption that the possibility follows a normal distribution and use a t-examination.

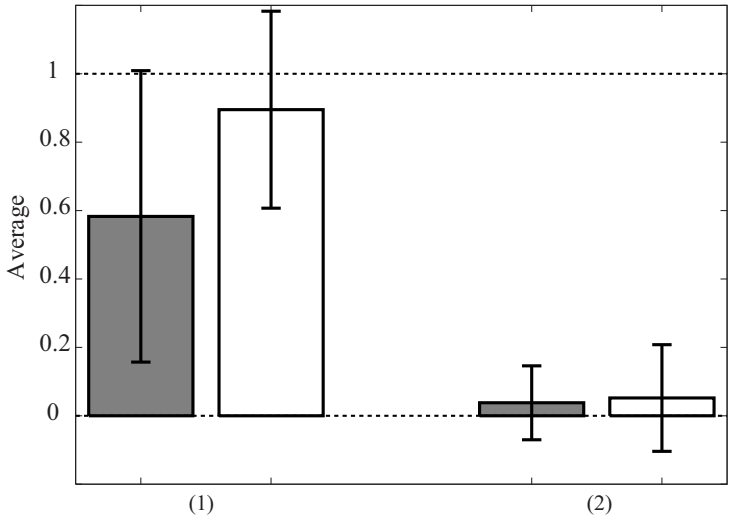

Figure 4.16: The average of the possibilities that (1) the response is correct or (2) not correct when the response is a 4-point pattern for the interpretation of the perception of no signal, including the 2 standard deviation error bar. Colored bars are those of the simultaneous stimulation; white bars are of the proposed alternating stimulation.

In this experiment we can reject cases in which a participant used auditory information caused by bone conduction, as follows. First, SOAs of the vibration sound are fixed at 800 and 400 ms in the simultaneous and alternating trials, respectively. It is then necessary

for a participant to distinguish the intensity of the vibration sound to make the correct response. In the simultaneous trials, 3 or 6 solenoids generate the vibration sound, and then the intensity variation of the sound is generated by 3 solenoids. In the alternating trials, 1, 2 or 3 solenoids generate the vibration sound, and then the maximum variation of the sound is generated by 2 solenoids. This indicates that if a participant utilizes auditory information, the participant distinguishes the two stimulation patterns in the simultaneous stimulation trials more easily than in the alternating stimulation trials. This is contradictory to the results of this experiment. Therefore, we reject the possibility that a participant used auditory information in this experiment.

Table 4.5 shows the average and the standard deviation of the possibilities that the response is correct in the voluntary range selection method experiment. The possibilities for direction and range are defined respectively as the numbers of the responses where target direction and range are correct over that of all responses. This result shows that range information is almost exactly transferred using the proposed method.

Table 4.5: The average and the standard deviation of the possibility that the response is correct when a tactile pattern is a 4-point square stimulation.

	Average	Standard deviation
Direction	0.958	4.05×10^{-3}
Range	0.979	1.01×10^{-3}

4.4 Conclusion

For the stimulating device to be utilized in our acoustic vision substitute system, we propose two information transfer methods that use a 2-D stimulator array. In the alternating stimulation method, stimulators are divided into several groups, and each stimulator group is activated alternately. Since two stimulators that adjoin each other belong to different groups, there is a certain SOA between two stimulations. In this case the two stimulations are perceived individually under the condition that the stimulator spacing is about 1/3 of the two-point discrimination threshold. When the stimulators are divided into two and four groups, the intervals of the stimulators adjoining each other are 0.71 and 0.5, respectively, of the two-point discrimination threshold. Therefore if the stimulator spacing of the same group is the two-point discrimination threshold, stimulations can individually transfer different information. This means that the number of stimulators can be increased to 2 or 4 times that in a 2-D array spaced at intervals of the two-point discrimination threshold. Then the spatial information presented in this method is improved to 2 or 4 times that of the simultaneous stimulation method. With the voluntary

range selection method, a user selects the measurement range and targets within the range are presented to the user. By selecting from a short to a long range the user acquires spatial information of the entire measurement area. Since the user knows the measurement range, the target ranges can be accurately recognized. We experimentally compare the alternate stimulation and the simultaneous stimulation methods and confirm that the former method is more useful to transfer information to a user. We also experimentally investigate the voluntary range selection method and show that a user can accurately recognize target ranges.

In future work we need to miniaturize this system to make a portable instrument. It will be necessary to reduce power consumption and select proper stimulation devices. To reduce power consumption we need to optimize the duration of the stimulation, SOA, the intensity of the stimulation, and the stimulation waveform. Here, we did not utilize intensity modulation of the stimulation for information presentation. The intensity modulation of stimulation can present other spatial information, such as the echo power from the target. This indicates that this method has the potential to clearly present environmental information.

Chapter 5

High-Resolution Real-Time 3-D Acoustic Imaging System with a Reflector

5.1 Introduction

Volumetric 3-D high-resolution acoustic images are in high demand for medical diagnoses. A conventional phased array imager excites all array elements to form a transmit beam, and uses all of them for receive beamforming [44]. Although only the receive beam is dynamically focused, imaging under this condition results in a high electronic signal-to-noise ratio (SNR) as well as good spatial and contrast resolution. The main problem of this configuration is that the number of elements becomes enormous for a 2-D array of a 3-D phased array imager.

One strategy to reduce the costs and complexity of a 3-D phased array imager is to use a linear or convex array that is moved mechanically [74]-[76]. In this method the number of elements can be reduced greatly by using a 1-D array. The lateral resolution in the measuring plane is high because a receive beam is focused dynamically. However, in the plane perpendicular to the longitudinal axis of the array, a transmit beam and a receive beam are focused on a fixed distance by acoustic lenses on elements. Thus, the lateral resolution is seriously deteriorated in front and behind the focus. Moreover, this type of 3-D phased array imager does not have satisfactory time resolution.

Another strategy to improve time resolution and decrease the number of elements, at the cost of the loss of some lateral resolution and SNR, is to use a digital beam forming technique with a 2-D sparse array, with an element spacing of more than one-half of a wavelength [45]-[50][77]-[80]. This method uses a wide transmit beam and multiple receive beams formed simultaneously. Although several designs of array have been reported, it is difficult to reduce the number of elements to less than half of the dense array.

Karaman *et al.* [42] proposed that a single-element spatial response with high acoustic

power can be synthesized by a defocused multi-element transmit subaperture. Lockwood *et al.* [43] applied this scheme to a 3-D synthetic aperture imager with a 1-D array. Although the SNR is improved, lateral resolution deteriorates in the section perpendicular to the array for the same reason as that of a phased array imager with a 1-D array.

In this study we propose a system based on a hybrid array-reflector configuration that realizes high time and spatial resolutions with modest computational load to resolve these problems. In this system all elements on a small dense array are excited with appropriate time delays to synthesize a spatial response similar to that of a single element. The echoes from targets are first gathered by a concave reflector, and then received by the array. The image of the target is reconstructed by numerical back projection [34] from the de-focused image distributed on the array.

In Materials and methods, we first outline the framework of the proposed 3-D acoustic imaging system. We provide some necessary wave equations and parameters to evaluate the spatial resolution of this method. Then we optimize the reflector shape and the array configuration for a wide measurement area with high spatial resolution. We propose a method to suppress the sidelobe level by employing a proper reflection coefficient of the mirror in the numerical back projection. The proposed method reconstructs images from received signals by numerical back projection, and thus the reflection ratio of the mirror can be set freely in the numerical back projection. We examine the spatial resolution of the proposed imager in Results. In Discussion, we compare the spatial resolution of the proposed imager with current 3-D imagers. Furthermore we evaluate improvements in the SNR with the proposed imager compared to conventional ones, such as digital beam forming and phased array imagers. Finally, we draw conclusions.

5.2 Materials and methods

5.2.1 Principle of the hybrid 3-D imaging system with a small dense array and a reflector

A digital beamforming imager transmits a wide beam to the whole measured area and receives echoes by a 2-D array. It then utilizes inverse Fourier transform to make all the images in the measurement area. Since this imager makes a 3-D image from one transmit and receive event, it has high time resolution. However, a large 2-D array with an enormous number of elements is required to obtain high spatial resolution, which thus is very costly. We propose a system to decrease the number of elements but having the same high time and spatial resolutions.

Fig. 5.1 shows a schematic view of the acoustic real-time 3-D imaging system based on a hybrid array-reflector configuration. In this method, all elements on a small dense array are excited with proper time delays so that all transmit pulses are focused at a single point after reflecting at the reflector mirror. Then the transmit pulses are synthesized

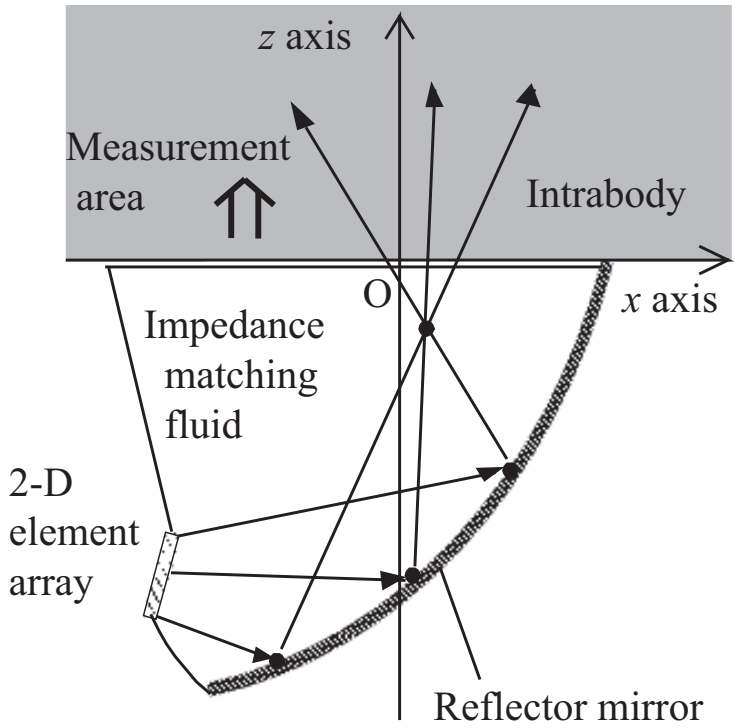

Figure 5.1: Schematic view of the system in the transmit phase.

to a broad beam similar to that of a single transmit element with high acoustic power. A transmit beam is radiated over the entire measuring field from this focal point. The reflected echoes are first gathered by a concave reflector, and then received by the array, as shown in Fig. 5.2. Since the reflector and the array are fixed, it is out of focus and so a de-focused image is distributed on the array. The image of the target is reconstructed from the received signal on the array by numerical back projection.

With this scheme, images of the whole area measured can be reconstructed from a single transmit and receive event, which enables real-time 3-D imaging. Assuming that the propagation velocity of sound is 1600 m/s, in the case that maximum measuring range is 0.16 m, it is theoretically possible to realize a frame rate of 5000 3-D images/s, when the SNR is sufficiently high.

5.2.2 Calculation of acoustic propagation

In this section, to evaluate spatial resolution of the proposed 3-D acoustic imager, we explain the wave equations to calculate signals received on the array and the estimated pressure at the measuring points.

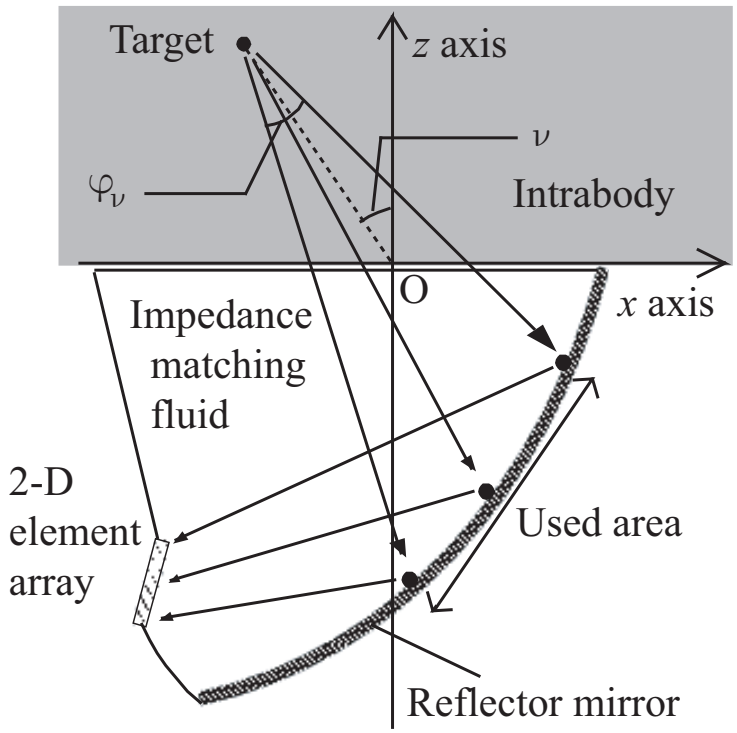

Figure 5.2: Schematic view of the system in the receive phase.

Calculation of received signals

The received signal is the scattered pressure field integrated over the element array. We calculate this signal in the frequency domain. Fig. 5.3 shows the coordinate system for the calculation.

All transmit pulses from elements with proper time delays are reflected on the mirror and focused at $\mathrm{T_r}$. A broad beam is then radiated from this point. The transmit beam is scattered at $\mathrm{T_a}$ by the inhomogeneity of the target. The backscattered echo is reflected on the mirror at M, and received by an element at $\mathrm{S_1}$. $\mathrm{U_1}$ and $\mathrm{U_2}$ are the intersections of lines $\mathrm{T_rT_a}$ and $\mathrm{T_aM}$, respectively, in the x-y plane. If the size of the target is sufficiently smaller than the wavelength, the pressure variation in the frequency domain at M is given by

$$\begin{aligned} p_{\mathrm{M}}(\omega) &= \left\{ \frac{\Delta c}{c_0} + (1 + \cos\theta_1) \frac{\Delta \rho}{2\rho_0} \right\} \\ &\quad (jk)^2 \frac{e^{-(\alpha_1 + jk)(r_{1\mathrm{a}} + r_{2\mathrm{a}}) - (\alpha_2 + jk)(r_{1\mathrm{b}} + r_{2\mathrm{b}})}}{4\pi^2 (r_{1\mathrm{a}} + r_{1\mathrm{b}})(r_{2\mathrm{a}} + r_{2\mathrm{b}})} A(\omega) \Delta V, \end{aligned} \tag{5.1}$$

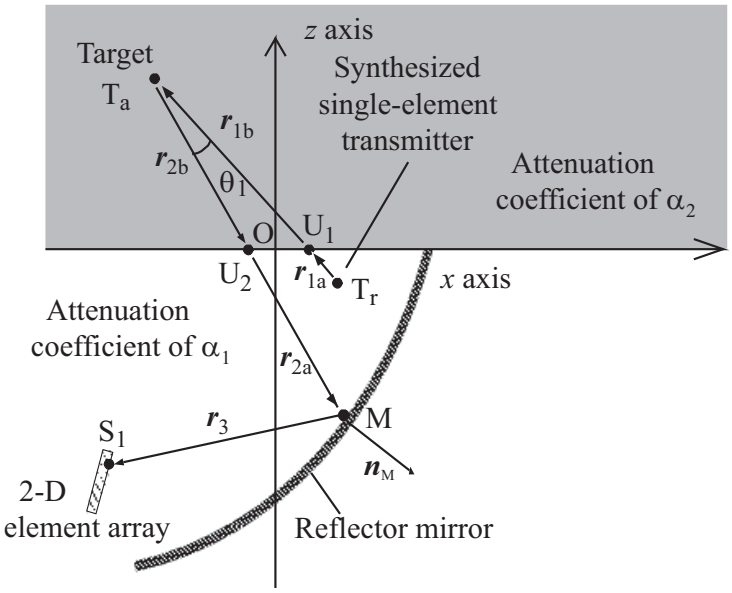

Figure 5.3: Arrangement of a 2-D element array and a mirror in a transmit and receive event.

where $\boldsymbol{r}_{1a} = \overrightarrow{T_rU_1}, \boldsymbol{r}_{1b} = \overrightarrow{U_1T_a}, \boldsymbol{r}_{2a} = \overrightarrow{U_2M}, \boldsymbol{r}_{2b} = \overrightarrow{T_aU_2}, r_{1a} = |\boldsymbol{r}_{1a}|, r_{1b} = |\boldsymbol{r}_{1b}|, r_{2a} = |\boldsymbol{r}_{2a}|, r_{2b} = |\boldsymbol{r}_{2b}|$, ω is the angular frequency, $k = \omega/c_0$ is the wave number, $\theta_1 = \angle T_rT_aM$, ρ_0 is the density of the undisturbed medium, c_0 is the mean propagation velocity, $\Delta\rho$ is the variation of the density, Δc is the variation of the propagation velocity, ΔV is the volume of a target, and $A(\omega)$ is the frequency spectrum of transmit beam radiated from T_r [82]. α_1 and α_2 are attenuation coefficients of the impedance matching fluid and the intrabody, respectively. $|\Delta c|/c_0$ and $|\Delta\rho|/\rho_0$ should satisfy

$$|\Delta c|/c_0 \ll 1, \tag{5.2}$$

$$|\Delta\rho|/\rho \ll 1. \tag{5.3}$$

We introduce the assumption that $r_{2a} + r_{2b}$ is much longer than the wavelength, in other words $k(r_{2a} + r_{2b}) \gg 1$, and then the particle velocity at M is given by

$$\nu_M(\omega) = p_M(\omega)/\rho_0 c_0. \tag{5.4}$$

The volume velocity of a small area around M is

$$V_M = \nu_M(\omega)\Delta S \frac{\boldsymbol{r}_{2a} \cdot \boldsymbol{n}_M}{r_{2a} n_M}, \tag{5.5}$$

where $\boldsymbol{n}_M$ is a vector perpendicular to the mirror at M, $n_M = |\boldsymbol{n}_M|$, and ΔS is the square measure of the small area on the mirror. Then the velocity potential and pressure variation at S_1 are obtained respectively by

$$\Phi_{S_1}(\omega) = \int_S \frac{V_M e^{-(\alpha_1+jk)r_3}}{2\pi r_3} dS, \tag{5.6}$$

$$\begin{aligned} p_{S_1}(\omega) &= j\rho\omega\Phi_{S_1}(\omega) \\ &= \int_S -jk^3 \left\{ \frac{\Delta c}{c_0} + (1+\cos\theta_1)\frac{\Delta\rho}{2\rho_0} \right\} \frac{\boldsymbol{r}_{2a}\cdot\boldsymbol{n}_M}{r_{2a}n_M} \\ &\quad \frac{e^{-(\alpha_1+jk)(r_{1a}+r_{2a}+r_3)-(\alpha_2+jk)(r_{1b}+r_{2b})}}{8\pi^3(r_{1a}+r_{1b})(r_{2a}+r_{2b})r_3} A(\omega)\Delta V dS, \end{aligned} \tag{5.7}$$

where $\boldsymbol{r}_3 = \overrightarrow{MS_1}, r_3 = |\boldsymbol{r}_3|$.

The pressure variation in the time domain at S_1 is given by the inverse Fourier transformation of $p_{S_1}(\omega)$ as

$$P_{S_1}(t) = F^{-1}\left[p_{S_1}(\omega)\right]. \tag{5.8}$$

As it is difficult to calculate $p_{S_1}(\omega)$ of all angular frequencies, we introduce an assumption

$$e^{-\alpha_1(r_{2a}+r_3)-\alpha_2 r_{2b}} \simeq e^{-\alpha_1(r_{0b}+r_{0c})-\alpha_2 r_{0a}}, \tag{5.9}$$

where $r_{0a} = |\overrightarrow{T_aO}|, r_{0b} = |\overrightarrow{OM_0}|, r_{0a} = |\overrightarrow{U_2M}|$, S_0 is the center of the 2-D array, and M_0 is at the center in the visual angle of the mirror from S_0, as shown in Fig. 5.4. In Results, we evaluate the validity of this assumption.

By introducing this assumption, the following equations are given from Eq. 5.7.

$$p_{S_1}(\omega) \simeq p_{1S_1}(\omega)p_{2S_1}(\omega), \tag{5.10}$$

$$p_{1S_1}(\omega) = -jk^3 e^{-\alpha_1(r_{1a}+r_{0b}+r_{0c})-\alpha_2(r_{1b}+r_{0a})} A(\omega)\Delta V/(8\pi^3), \tag{5.11}$$

$$\begin{aligned} p_{2S_1}(\omega) &= \int_S \left\{ \frac{\Delta c}{c_0} + (1+\cos\theta_1)\frac{\Delta\rho}{2\rho_0} \right\} \frac{\boldsymbol{r}_{2a}\cdot\boldsymbol{n}_M}{r_{2a}n_M} \\ &\quad \frac{e^{-jk(r_{1a}+r_{1b}+r_{2a}+r_{2b}+r_3)}}{(r_{1a}+r_{1b})(r_{2a}+r_{2b})r_3} dS. \end{aligned} \tag{5.12}$$

$P_{S_1}(t)$ is given by the convolution of $F^{-1}\left[p_{1S_1}(\omega)\right]$ and $F^{-1}\left[p_{2S_1}(\omega)\right]$. Since $p_{1S_1}(\omega)$ is independent of the position of M, it is enough to calculate $p_{1S_1}(\omega)$ only one time. In the value $p_{2S_1}(\omega)$ only the term $e^{-jk(r_{1a}+r_{1b}+r_{2a}+r_{2b}+r_3)}$ is dependent on ω. Therefore $F^{-1}\left[p_{2S_1}(\omega)\right]$ is an impulse function. Then the following equations are given.

$$\begin{aligned} P_{S_1}(t) &\simeq P_{1S_1}(t) * F^{-1}\left[p_{2S_1}(\omega)\right] \\ &= \sum P_{1S_1}\left\{t - (r_{1a}+r_{1b}+r_{2a}+r_{2b}+r_3)/c_0\right\} \\ &\quad \left\{ \frac{\Delta c}{c_0} + (1+\cos\theta_1)\frac{\Delta\rho}{2\rho_0} \right\} \frac{\boldsymbol{r}_{2a}\cdot\boldsymbol{n}_M}{r_{2a}n_M} \frac{\Delta S}{(r_{1a}+r_{1b})(r_{2a}+r_{2b})r_3}, \end{aligned} \tag{5.13}$$

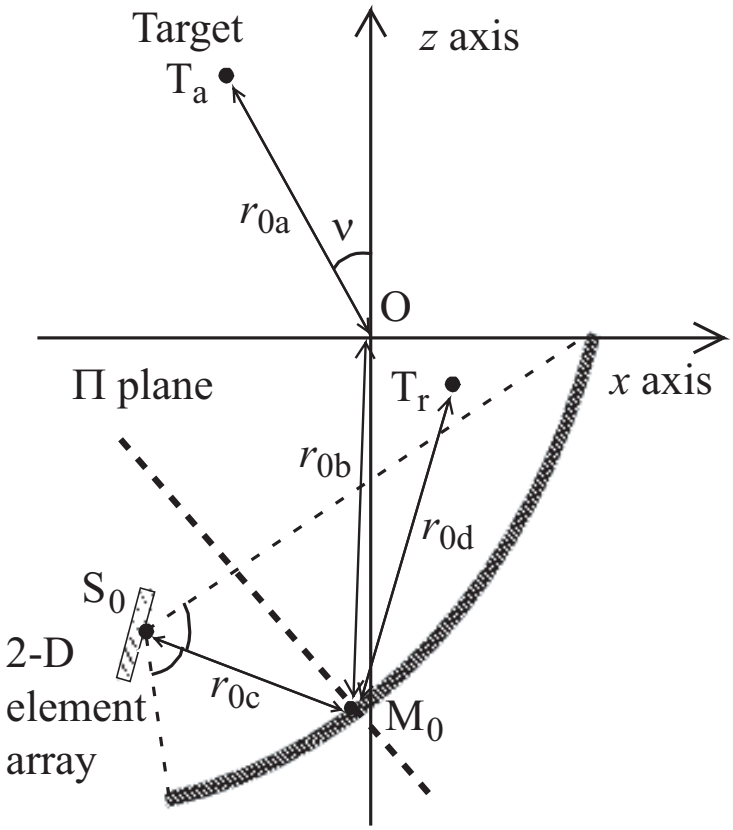

Figure 5.4: Schematic view of the mirror and array configuration for calculating in the time domain.

$$P_{1S_1}(t) \;=\; F^{-1}\left[p_{1S_1}(\omega)\right]. \tag{5.14}$$

The received signal on the element at S_1 is proportional to $P_{S_1}(t)$.

Image reconstruction

We reconstruct images of targets from the distributed images on the array by numerical back projection. Similar to the calculation of the received signal, we define an element and the measurement point existing, respectively, at S_{2m} and T_b, as shown in Fig. 5.5. Assuming that the received signal is proportional to the estimated volume velocity at S_{2m}, the estimated velocity potential at M is given by

$$\Phi_M(\omega)' \propto \sum_m \frac{p_m(\omega)'^* e^{-(\alpha_1+jk)r_3'}}{2\pi r_3'}, \tag{5.15}$$

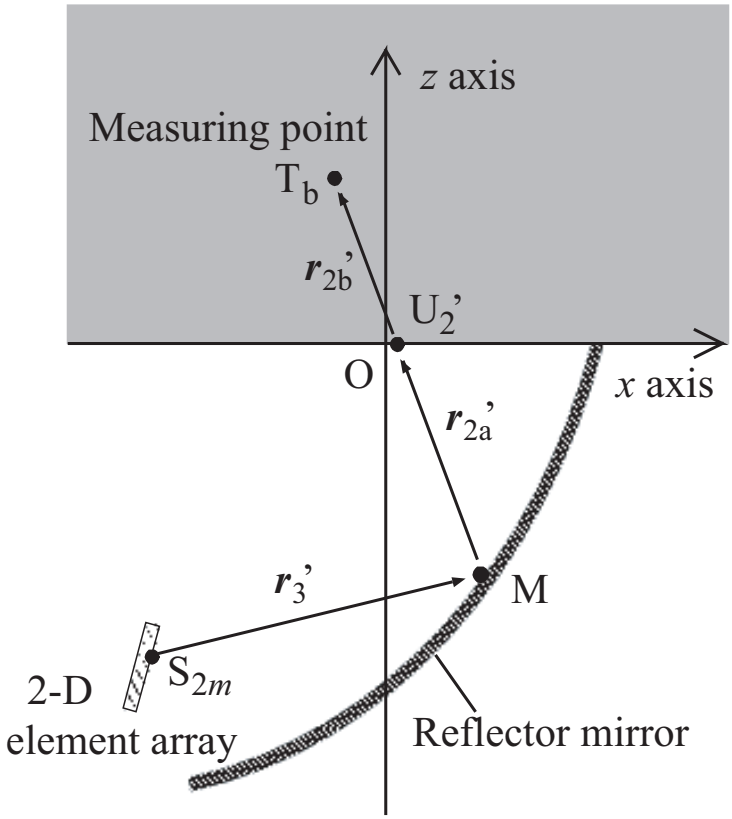

Figure 5.5: Arrangement of a 2-D element array and a mirror in the numerical back projection.

where $\boldsymbol{r}_3{}' = \overrightarrow{\mathrm{S}_{2m}\mathrm{M}}, r_3{}' = |\boldsymbol{r}_3{}'|$, $p_m(\omega)'^*$ is a complex conjugate of the received signal on the element. The estimated volume velocity at M is given by

$$V_{\mathrm{M}}{}' = -\frac{\partial \Phi_{\mathrm{M}}(\omega)'}{\partial r_3{}'} \frac{\boldsymbol{r}_3{}' \cdot \boldsymbol{n}_{\mathrm{M}}}{r_3{}' n_{\mathrm{M}}} \Delta S. \tag{5.16}$$

The estimated velocity potential and the estimated pressure variation at $\mathrm{T_b}$ are given by

$$\Phi_{\mathrm{T_b}}(\omega)' = \int_S \frac{V_{\mathrm{M}}{}' e^{-(\alpha_1+jk)r_{2\mathrm{a}}{}' - (\alpha_2+jk)r_{2\mathrm{b}}{}'}}{2\pi(r_{2\mathrm{a}}{}' + r_{2\mathrm{b}}{}')} dS, \tag{5.17}$$

$$\begin{aligned} p_{\mathrm{T_b}}(\omega)' &= j\rho\omega\Phi_{\mathrm{T_b}}(\omega)' \\ &\propto \int_S \sum_m \frac{-k^2 p_m(\omega)'^* e^{-(\alpha_1+jk)(r_{2\mathrm{a}}{}'+r_3{}') - (\alpha_2+jk)r_{2\mathrm{b}}{}'}}{4\pi^2(r_{2\mathrm{a}}{}' + r_{2\mathrm{b}}{}')r_3{}'} \frac{\boldsymbol{r}_3{}' \cdot \boldsymbol{n}_{\mathrm{M}}}{r_3{}' n_{\mathrm{M}}} dS, \end{aligned} \tag{5.18}$$

respectively, where $\boldsymbol{r}_{2\mathrm{a}}{}' = \overrightarrow{\mathrm{MU}_2{}'}, \boldsymbol{r}_{2\mathrm{b}}{}' = \overrightarrow{\mathrm{U}_2{}'\mathrm{T_b}}, r_{2\mathrm{a}}{}' = |\boldsymbol{r}_{2\mathrm{a}}{}'|, r_{2\mathrm{b}}{}' = |\boldsymbol{r}_{2\mathrm{b}}{}'|$.

The pressure variation in the time domain at $\mathrm{T_b}$ is given by the inverse Fourier transformation of $p_{\mathrm{T_b}}(\omega)'$ as

$$P_{\mathrm{T_b}}(t)' = F^{-1}\left[p_{\mathrm{T_b}}(\omega)'\right]. \tag{5.19}$$

We also introduce an assumption

$$e^{-\alpha_1(r_{2\mathrm{a}}'+r_3')-\alpha_2 r_{2\mathrm{b}}'} \simeq e^{-\alpha_1(r_{0\mathrm{b}}+r_{0\mathrm{c}})-\alpha_2 r_{0\mathrm{a}}}. \tag{5.20}$$

We evaluate this assumption in Results. By introducing this assumption, the following equations are given from Eq. 5.18.

$$\begin{aligned}
p_{\mathrm{T_b}}(\omega)' &\propto p_{1\mathrm{T_b}}(\omega)' p_{2\mathrm{T_b}}(\omega)', && (5.21)\\
p_{1\mathrm{T_b}}(\omega)' &= -k^2 e^{-\alpha_1(r_{0\mathrm{b}}+r_{0\mathrm{c}})-\alpha_2 r_{0\mathrm{a}}} p_m(\omega)'^*/(4\pi^2), && (5.22)\\
p_{2\mathrm{T_b}}(\omega)' &= \int_S \frac{e^{-jk(r_{2\mathrm{a}}'+r_{2\mathrm{b}}'+r_3')}}{(r_{2\mathrm{a}}'+r_{2\mathrm{b}}')r_3'} \frac{\boldsymbol{r}_3' \cdot \boldsymbol{n}_{\mathrm{M}}}{r_3' n_{\mathrm{M}}} dS. && (5.23)
\end{aligned}$$

As the equations 5.13 and 5.14, the following equations are obtained.

$$\begin{aligned}
P_{\mathrm{T_b}}(t)' &\propto P_{1\mathrm{T_b}}(t)' * F^{-1}\left[p_{2\mathrm{T_b}}(\omega)'\right]\\
&= \sum P_{1\mathrm{T_b}}\left\{t-(r_{2\mathrm{a}}'+r_{2\mathrm{b}}'+r_3')/c_0\right\}' \frac{\boldsymbol{r}_3' \cdot \boldsymbol{n}_{\mathrm{M}}}{r_3' n_{\mathrm{M}}} \frac{\Delta S}{(r_{2\mathrm{a}}'+r_{2\mathrm{b}}')r_3'}, && (5.24)\\
P_{1\mathrm{T_b}}(t)' &= F^{-1}\left[p_{1\mathrm{T_b}}(\omega)'\right]. && (5.25)
\end{aligned}$$

The estimated power at $\mathrm{T_b}$, the objective function, is given by

$$W_{\mathrm{T_b}}(t)' \propto P_{\mathrm{T_b}}(t)' P_{\mathrm{T_b}}(t)'^* \tag{5.26}$$

When an ultrasound wave, radiated from a point source, is measured at a surface and the phase is reversed, the reversed wave projected backward from the surface is focused at the radiation point. Therefore these functions are sufficient for a 3-D image construction.

Calculation parameters

To investigate spatial resolution of the proposed method, we set the parameters as follows: mean propagation velocity $c_0 = 1600$ m/s, density of the undisturbed medium $\rho_0 = 1.08 \times 10^3$ kg/m^3, the variation of the propagation velocity $\Delta c = -300$ m/s, and the variation of the density $\Delta\rho = -1.0 \times 10^2$ kg/m^3. The attenuation coefficients α_1 and α_2 are $2.0(\omega/2\pi)^2 \times 10^{-14}$ and $5.0(\omega/2\pi) \times 10^{-6}$ Np/m, respectively. In this method, similar to the digital beamforming method, the element pitch is 0.5 λ to prevent grating lobes, where $\lambda = c/f_0$ is the wavelength at the center frequency. Therefore the radiating high

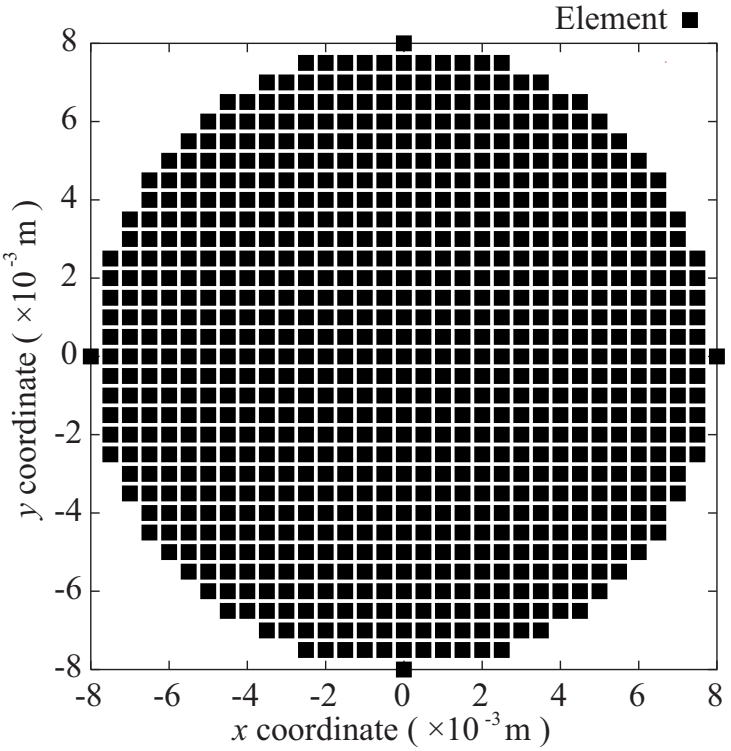

Figure 5.6: Element pattern for a 797-element array.

frequency ultrasound needs the miniaturization of the element size. In this paper, we set the element pitch as 5×10^{-4} m. This means that $\lambda = 0.001$ m; in other words, the center frequency $f_0 = 1.6$ MHz. Since the number of elements on the array is proportional to the cost, to employ a large array is unrealistic. Many researchers have investigate 2-D arrays with 500 to 1000 elements [49] [50]. We employ a circular array of 0.016 m in diameter with 797 elements, as shown in Fig. 5.6.

Fig. 5.7 shows the broad-band pulse transmitted by the elements in this paper, where -6 dB fractional bandwidth is 60 %. The spectrum of the pulse is expressed as

$$S(\omega) = A_{\mathrm{c}}\omega^2 e^{-B_{\mathrm{c}}(\omega-\mu)^2} \tag{5.27}$$

where A_{c} and B_{c} are coefficients and μ is the central angular frequency. Since we proposed that a wide transmit beam with high acoustic power can be synthesized using focusing method [83], we assume that the synthesized transmit beam is an omnidirectional spherical wave whose spectrum is proportional to $S(\omega)e^{-\alpha_1(r_{0\mathrm{c}}+r_{0\mathrm{d}})}$, where $r_{0\mathrm{d}} = |\overrightarrow{\mathrm{M_0T_r}}|$ and $e^{-\alpha_1(r_{0\mathrm{c}}+r_{0\mathrm{d}})}$ is caused by the attenuation through the impedance matching fluid.

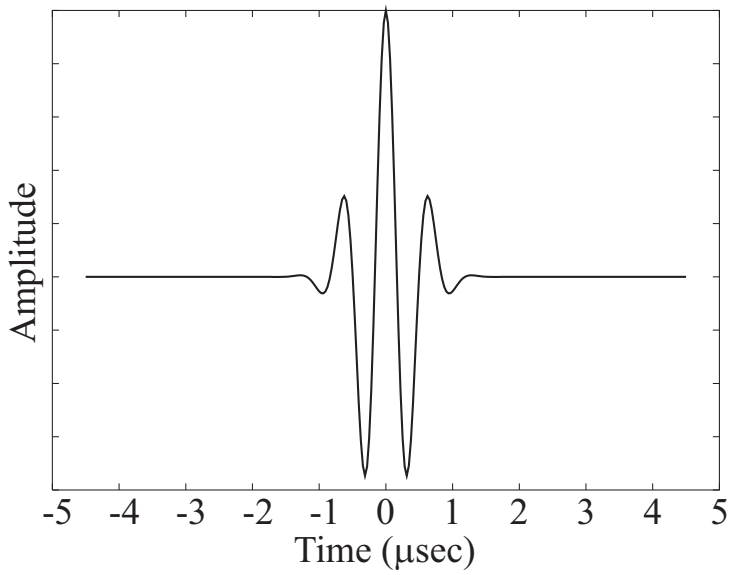

Figure 5.7: Waveform of the pulse used in this paper.

5.2.3 Optimization of the reflector shape and the array configuration

Since we reconstruct the received signal by numerical back projection, there is no need to focus it on the array. This indicates that the reflector shape suitable for this method may be different from traditional ones. Utilizing geometric optics we optimize the reflector shape and the array configuration for a wide measurement area with high spatial resolution.

Fig. 5.2 schematically shows the ray trace of an echo in geometric optics. Part of the echo reflected on the mirror is received on the array. We call the reflected region on the mirror the 'used area', and define φ_ν as the visual angle of the used area from the target position as follows.

$$\begin{aligned} \varphi_\nu &= \int_S \frac{g(\boldsymbol{r})}{r^3} \boldsymbol{r} \cdot d\boldsymbol{S} \\ &= \sum g(\boldsymbol{r}) \frac{\boldsymbol{r} \cdot \boldsymbol{n}_{\mathrm{M}}}{r^3 n_{\mathrm{M}}} \Delta S, \end{aligned} \tag{5.28}$$

$$g(\boldsymbol{r}) = \begin{cases} 1 & \text{if the point M is on the used area} \\ 0 & \text{else} \end{cases} \tag{5.29}$$

where $\boldsymbol{r} = \boldsymbol{r}_{2\mathrm{a}} + \boldsymbol{r}_{2\mathrm{b}}$, $r = |\boldsymbol{r}|$ and ν is the target direction from the z axis, as shown in Fig. 5.4.

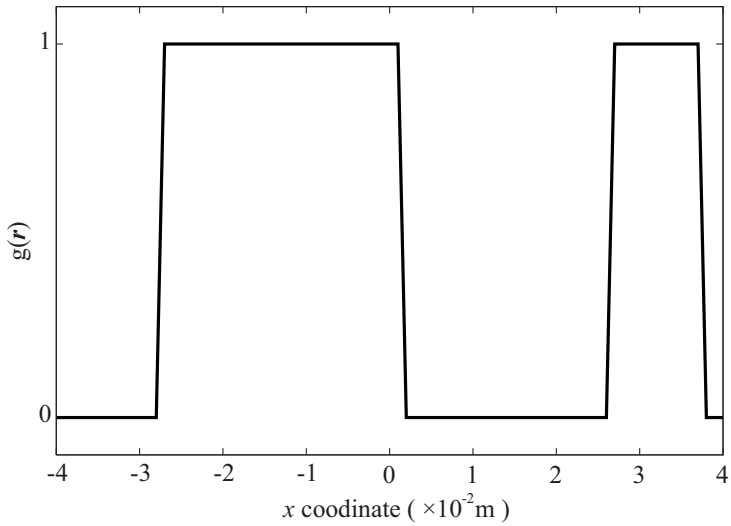

Figure 5.8: The area used on the mirror in the x-z section. The value of used area is 1 and that of non-used area is 0. The x, y and z coordinates of a target are 0.005, 0 and 0.07 m respectively.

First, in the case where the used area consists of plural groups, the sidelobe level is high because the main lobe divides. Below, we investigate an example of such a case. Fig. 5.8 is the used area on the mirror in the x-z section. The x, y and z coordinates of a target are 0.005, 0 and 0.07 m, respectively. The function value of 1 means that the region of the mirror is a used area, and 0 means that it is a non-used area. In this case the echo reflected on a region, whose x coordinate is more than 0.002 m and less than 0.026 m, is not received on the array. Thus the used area consists of two groups, one is the region on the mirror whose x coordinate is negative and the other is the right edge. Fig. 5.9 is the lateral resolution of this mirror for a depth of 0.07 m. The first sidelobe level is -5.9 dB, which disturbs the medical diagnoses. Therefore, we discard the mirror with a used area in the x-z plane or Π plane that consists of plural groups. The Π plane is perpendicular to both the x-z plane and the mirror, as shown in Fig. 5.4. The intersection of the Π plane and the mirror in the x-z plane is at the center in the visual angle of the mirror.

Next, we optimize the mirror shape under the above conditions. To realize sufficient lateral resolution and SNR using a small array, the echo should be gathered on the array. This means that the visual angle should be maximized. We set the evaluation function

$$E = E_{\mathrm{X}} + E_{\mathrm{Y}}, \tag{5.30}$$

$$E_{\mathrm{X}} = \int_{\nu_{\mathrm{Xmin}}}^{\nu_{\mathrm{Xmax}}} \varphi_\nu d\nu = \sum_x \varphi_\nu \Delta\nu, \tag{5.31}$$

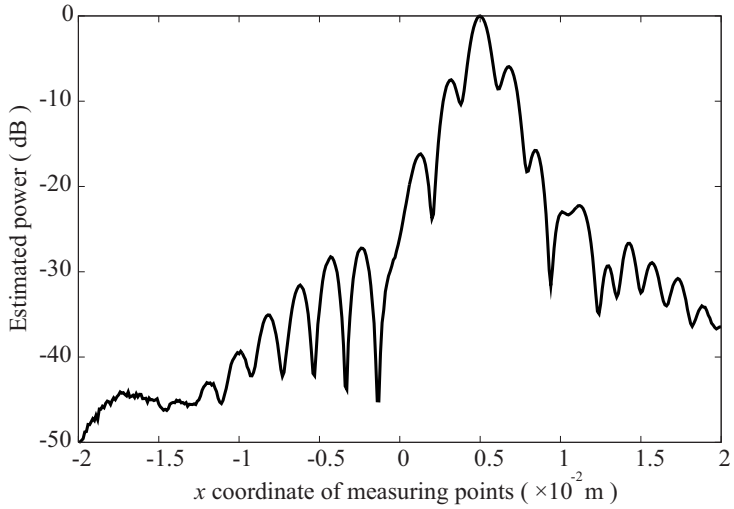

Figure 5.9: Lateral resolution where the used area consists of plural groups. The main lobe divides, and thus the sidelobe level becomes high.

$$E_{\mathrm{Y}} = \int_{\nu_{\mathrm{Ymin}}}^{\nu_{\mathrm{Ymax}}} \varphi_\nu d\nu = \sum_y \varphi_\nu \Delta\nu, \tag{5.32}$$

where E_{X} and E_{Y} are in cases where targets are in the x-z and y-z planes, respectively. As shown in Eq. 5.28, φ_ν is determined indirectly by the shape of the reflection mirror. Thus the maximization of E becomes a problem of finding the optimum shape function of a mirror that gives the highest value of E.

We call the shape functions of the optimized reflector in the x-z and Π planes f_x and f_y, respectively. These functions are given by

$$\begin{aligned} f_x &= l_{1x}\left[\{1-\cos(l_{3x}x + l_{3x}x_{\max} + l_{4x})\}^{l_{2x}} - \{1-\cos(l_{4x})\}^{l_{2x}}\right] \\ &\quad / \left[\{1-\cos(2l_{3x}x_{\max} + l_{4x})\}^{l_{2x}} - \{1-\cos(l_{4x})\}^{l_{2x}}\right] \qquad (5.33) \\ f_y &= l_{1y}\{1-\cos(l_{3y}y)\}^{l_{2y}} / \{1-\cos(l_{3y}y_{\max})\}^{l_{2y}}, \qquad (5.34) \end{aligned}$$

where $x_{\max}$ and $y_{\max}$ are half of the mirror width in the x-z and Π planes, respectively. They are in fact the heights from the bottom points of the reflector in each section.

Since we determine the visual angle of the measuring area as $\pi/3$, we set $\nu_{\mathrm{Xmax}} = \nu_{\mathrm{Ymax}} = \pi/6, \nu_{\mathrm{Xmin}} = \nu_{\mathrm{Ymin}} = -\pi/6$. Then we optimize $l_{1x}, l_{2x}, l_{3x}, l_{4x}, l_{1y}, l_{2y}, l_{3y}, x_{\max}, y_{\max}$ by maximizing the evaluation function E. The range of each variable is as follows: $0.025\ \mathrm{m} \le x_{\max} \le 0.04\ \mathrm{m}, 0.025\ \mathrm{m} \le y_{\max} \le 0.04\ \mathrm{m}, 0.01\ \mathrm{m} \le l_{1x} \le 0.1\ \mathrm{m}, 0.5 \le l_{2x} \le 3, \pi/40 \le l_{3x}x_{\max}, 0 \le l_{4x}, 2l_{3x}x_{\max} + l_{4x} \le \pi/2, 0.01\ \mathrm{m} \le l_{1y} \le 0.1\ \mathrm{m}, 0.5 \le l_{2y} \le 3, \pi/20 \le l_{3y}y_{\max} \le \pi/2$.

It is thought that many local maximums of E exist. We first optimize f_x and f_y by maximizing E_{X} and E_{Y}, respectively. At this optimization we deal with a 2-D problem. We set this as the initial value of the mirror shape, and optimize by maximizing E. We deal with a 3-D problem with this optimization.

The variables of the optimized reflector mirror are: $x_{\max} = 0.031$ m, $y_{\max} = 0.04$ m, $l_{1x} = 0.06$ m, $l_{2x} = 2.3, l_{3x} = \pi/124, l_{4x} = \pi/20, l_{1y} = 0.015$ m, $l_{2y} = 1.4, l_{3y} = 3\pi/160$.

Fig. 5.10 shows the used area on the optimized mirror in the x-z plane. x coordinates of the targets are -0.015, 0 and 0.015 m. The target range is 0.07 m. Fig. 5.11 shows the used area projected onto the x-y plane in the case where a target exists at the center for a 0.07 m depth.

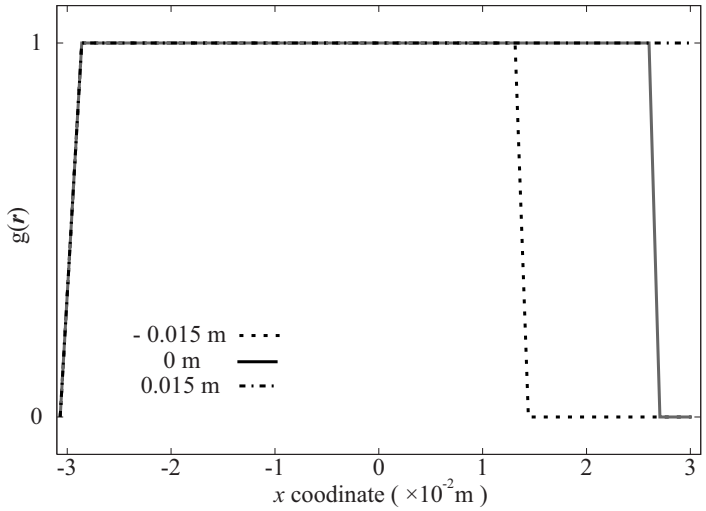

Figure 5.10: The used area on the optimized mirror in the x-z section. The value of the used area is 1 and that of the non-used area is 0. The x coordinates of targets are -0.015, 0 and 0.015 m. The target range is 0.07 m in the x-z section.

Since a large part of the echo reflected by the mirror returns to the array, the visual angle of the used area from the target, A_{H}, is larger than that of a same size array put at the center of the x-y plane, A_{DBF}. We call the ratio of A_{H} to A_{DBF} as the receive efficiency, R_{H}.

$$R_{\mathrm{H}} = A_{\mathrm{H}}/A_{\mathrm{DBF}}. \tag{5.35}$$

The echo reflected by the used area is received on the array, and thus R_{H} is close to the SNR improvement of the proposed method from that of a digital beamforming method with the same size array [66]. For example, where a target exists at the center for a depth of 0.07 m, R_{H} is 6.2. In this case the SNR improvement of the proposed method

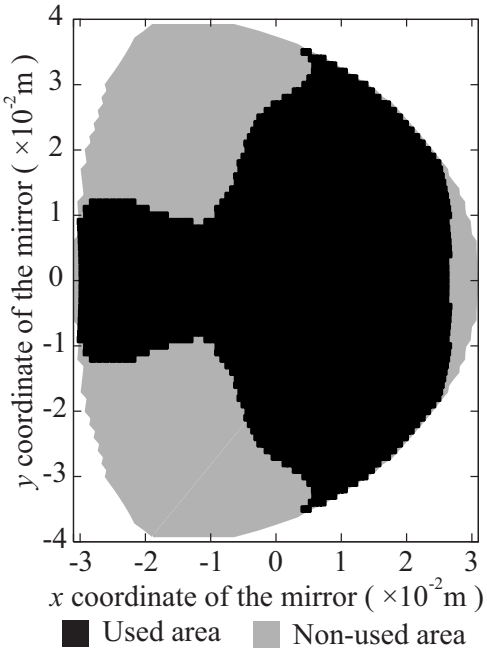

Figure 5.11: The used area on a mirror projected onto the x-y plane where a target exists at the center for a 0.07 m depth.

compared with a digital beamforming method is 7.8 dB, as shown in ‘ Considerations on signal-to-noise ratio ’, a subsection in Discussion. Henceforth, we normalize the estimated power at each measuring point to make the peak of it R_{H} when we calculate the lateral resolution of the proposed imager.

5.2.4 Sidelobe suppression in image reconstruction

For medical diagnoses, we should decrease the sidelobe levels of the proposed imager. In the proposed method only reflected echoes on the mirror are received on the array. Breaks of the received signal occur at the edge of the mirror and make for a high sidelobe level. While the reflection ratio of the mirror should taper off toward the edge, it is difficult to make such a mirror. Therefore, we employ a tapered reflection ratio for the mirror in image reconstruction from the received signal on the array. Since images are reconstructed from received signals by numerical back projection, the reflection ratio of the mirror can be set freely in image reconstruction. We now investigate the effect of tapering the reflection ratio of the mirror.

The used area on the reflector is distinctive for the target position. Therefore, weighting the reflection ratio of the mirror is useful to reduce the sidelobe level at the cost of some loss of SNR and lateral resolution. Because of the reflection ratio tapering off, the

functions 5.17 and 5.24 are changed as follows.

$$\Phi_{\mathrm{T_b}}(\omega)' = \int_S \frac{a_{\mathrm{M}} {V_{\mathrm{M}}}' e^{-(\alpha_1+jk){r_{2\mathrm{a}}}'-(\alpha_2+jk){r_{2\mathrm{b}}}'}}{2\pi({r_{2\mathrm{a}}}'+{r_{2\mathrm{b}}}')} dS, \tag{5.36}$$

$$P_{\mathrm{T_b}}(t)' = \sum P_{1\mathrm{T_b}} \{t-({r_{2\mathrm{a}}}'+{r_{2\mathrm{b}}}'+{r_3}')/c_0\}' \frac{{\boldsymbol{r}_3}' \cdot \boldsymbol{n}_{\mathrm{M}}}{{r_3}' n_{\mathrm{M}}} \frac{a_{\mathrm{M}} \Delta S}{({r_{2\mathrm{a}}}'+{r_{2\mathrm{b}}}'){r_3}'}, \tag{5.37}$$

where ${a_{\mathrm{M}}}^2$ is the reflection ratio of the mirror at the point M in the numerical back projection.

The first sidelobe level of a digital beamforming imager with a dense circular 2-D array is -18.3 dB. Therefore, we set the threshold as -18.3 dB. If the sidelobe level of a measuring direction is higher than the threshold, we use this method to decrease the sidelobe level to less than it.

For a depth of 0.07 m in the x-z section, the first sidelobe level is highest in the case that the x coordinate of a target is 0.015 m. Fig. 5.12 shows the used area on an optimized reflector in such a case. A break occurs in the received signal at the right edge of the mirror, and thus we set the reflection ratio of the mirror to taper off at the right edge, as shown in Fig. 5.13. The visual angle decrease of the used area from the target is -0.18 dB. This means that tapering makes for a slight decrease in the estimated power. Fig. 5.14 shows the lateral resolution of the proposed method with and without tapering. The sidelobe level is suppressed to less than -21 dB at the cost of some slight deterioration of the SNR and lateral resolution.

5.3 Results

In this section, we examine the spatial resolution of the proposed image. First, we compare the spatial resolution of a phased array imager with a liner array to that of the proposed one. When using a linear or convex array for 3-D imaging, the receive beams can be dynamically focused in the section parallel to the longitudinal axis of the array. On the other hand, in the perpendicular section, transmit and receive beams are focused by acoustic lenses. This means that the focal distance is fixed. Fig. 5.15 shows the spatial resolution of a phased array imager in a perpendicular section when the array width is 0.016 m and the focal length is 0.07 m. A target exists at the center for depths of (a) 0.02 m and (b) 0.07 m. If targets exist near the focal zone, spatial resolution is high but spurious images of high amplitude appear in a wide area when the distance between the focal zone and the targets is large, as shown in this figure. This significantly disrupts medical diagnoses.

Fig. 5.16 shows the spatial resolution of the proposed method where the optimized reflector mirror is used. The target ranges are (a) 0.02 m and (b) 0.07 m. In this method,

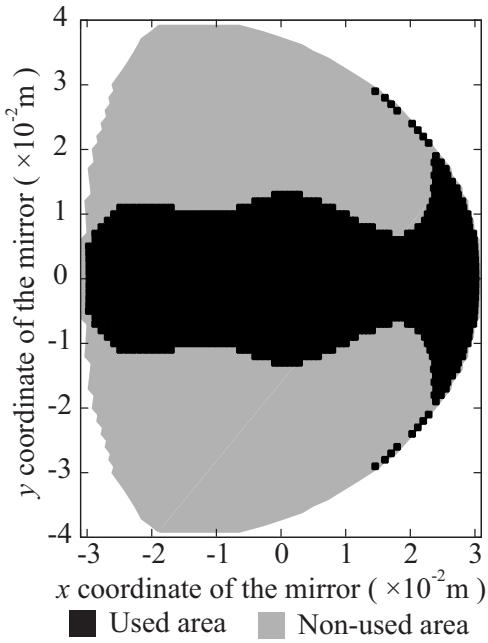

Figure 5.12: The used area on a mirror projected onto the x-y plane where the x coordinate of a target is 0.015 m in the x-z section for a 0.07 m depth.

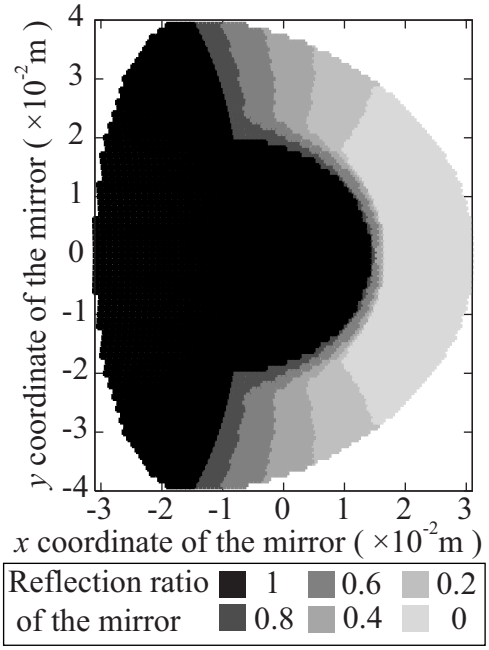

Figure 5.13: The taper function for the reflection ratio on the mirror in numerical back projection.

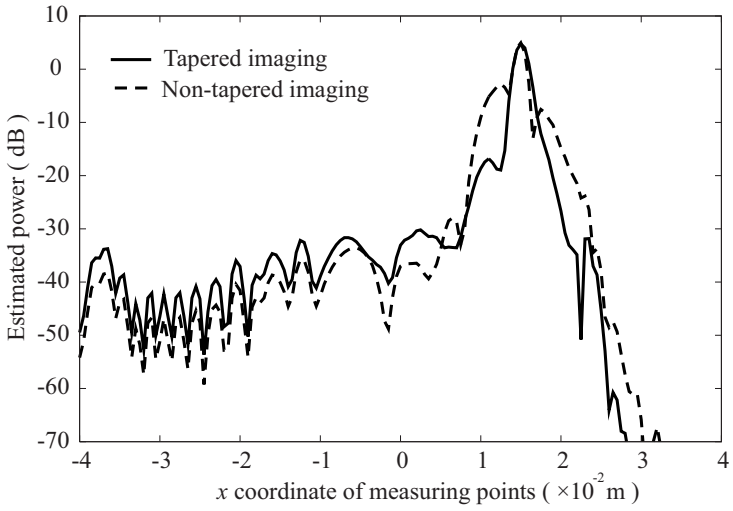

Figure 5.14: Lateral resolution of a tapered and non-tapered proposed imager with a 0.016 m width array in a 3-D problem. The x coordinate of a target is 0.015 m, and those of the measuring points are -0.04 to 0.04 m.

receive beams are dynamically focused to all measuring points and good spatial resolution can be acquired.

Fig. 5.17 shows lateral resolution of the proposed imager with a 0.016 m width array at the range of 0.07 m in the (a) x-z and (b) y-z sections. The x coordinates of targets in the x-z section are $-0.03, -0.015, 0, 0.015$ and 0.03 m, and the y coordinates in the y-z section are 0, 0.015 and 0.03 m. Sidelobe levels in all these situations are less than -21 dB.

To evaluate the validity of the assumptions eqs. 5.9 and 5.20, we calculate the estimated power without the assumption. The calculation in the frequency domain utilizing eqs. 5.8 and 5.19 costs a lot of computational load, and thus we calculate the estimated power at two measurement points. They are placed at $y = 0$ and 0.004 m in the y-z plane for a 0.07 m depth when a point target exists at the center for a 0.07 m depth. That is, we have compared two measurement points of Fig. 5.17(b) when a point target is placed at the center. The differences between with and without the assumption about attenuation at the measurement points of $y = 0$ and 0.004 m are 0.216 dB and 0.208 dB, respectively. This indicates that the assumptions of equations 5.9 and 5.20 are valid.

The lateral resolution of $y = 0.015$ m in the y-z section has swells at $y = 0.013$ and 0.017 m. This is made by the small used area separated from the main used area, as shown in Fig. 5.18. In the case where images are reconstructed using a taper function to remove the small used area, -3 dB lateral resolution deteriorates slightly and the swells vanish.

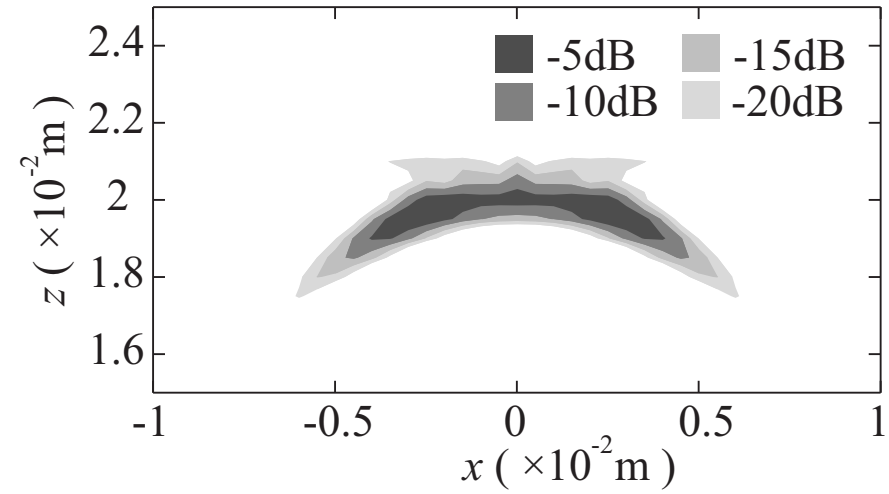

(a)

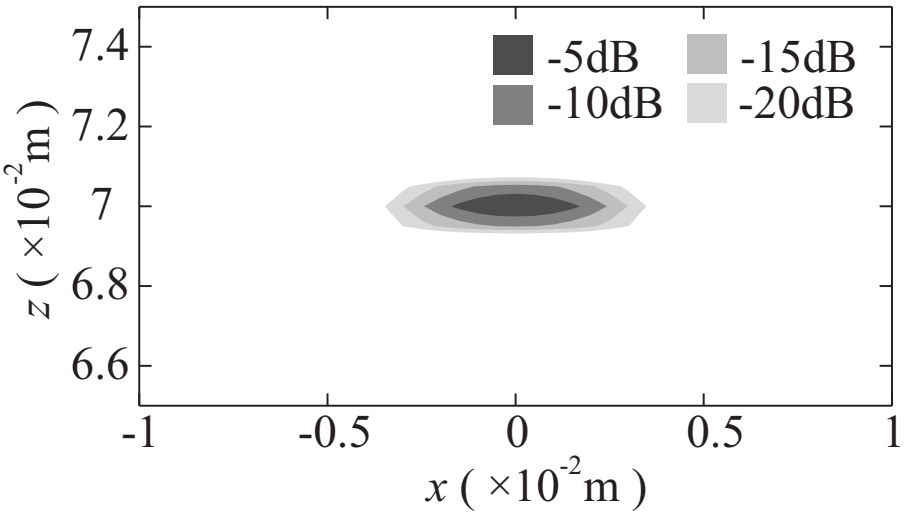

(b)

Figure 5.15: Spatial resolution of a phased array imager with a 1-D array. The focal length of the acoustic lenses is 0.07 m, and the targets exist at the center for depths of (a) 0.02 m and (b) 0.07 m. This section is perpendicular to the longitudinal axis of the linear array.

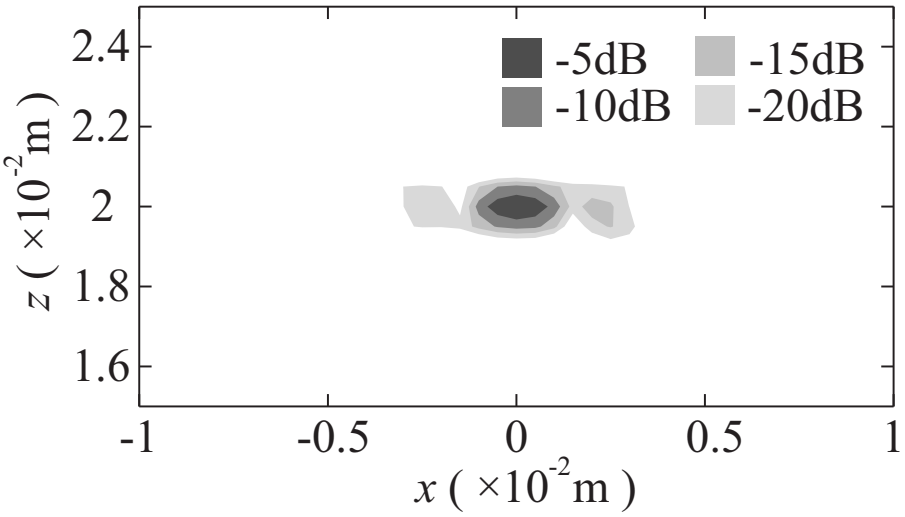

(a)

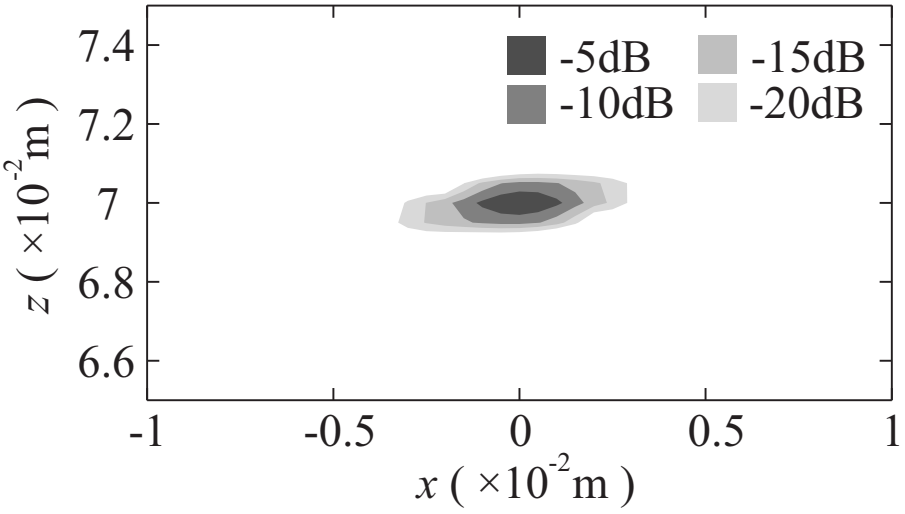

(b)

Figure 5.16: Spatial resolution of the proposed imager in the x-z section. Targets exist at the center for depths of (a) 0.02 m and (b) 0.07 m.

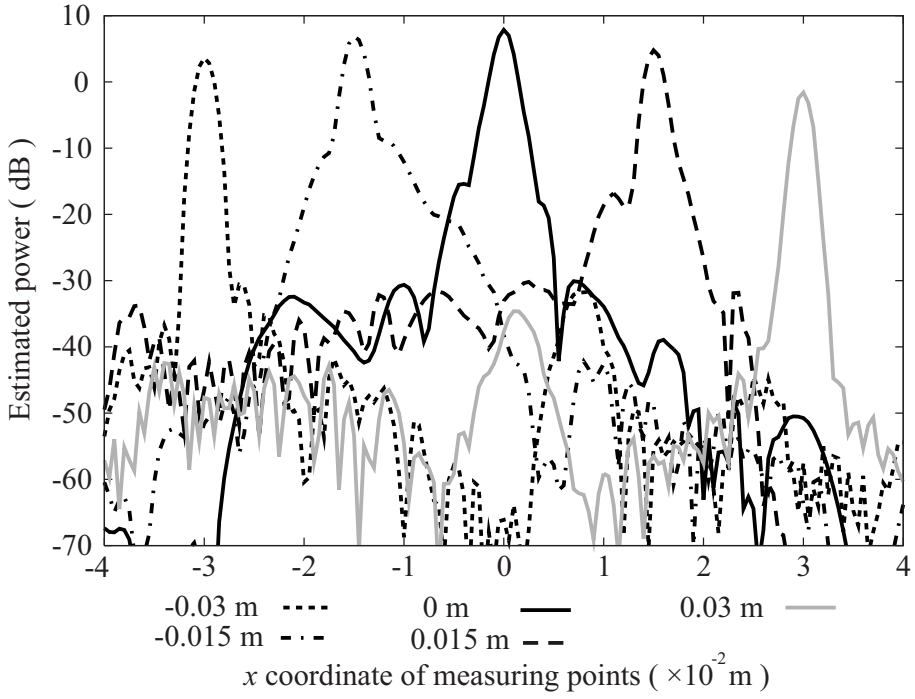

(a)

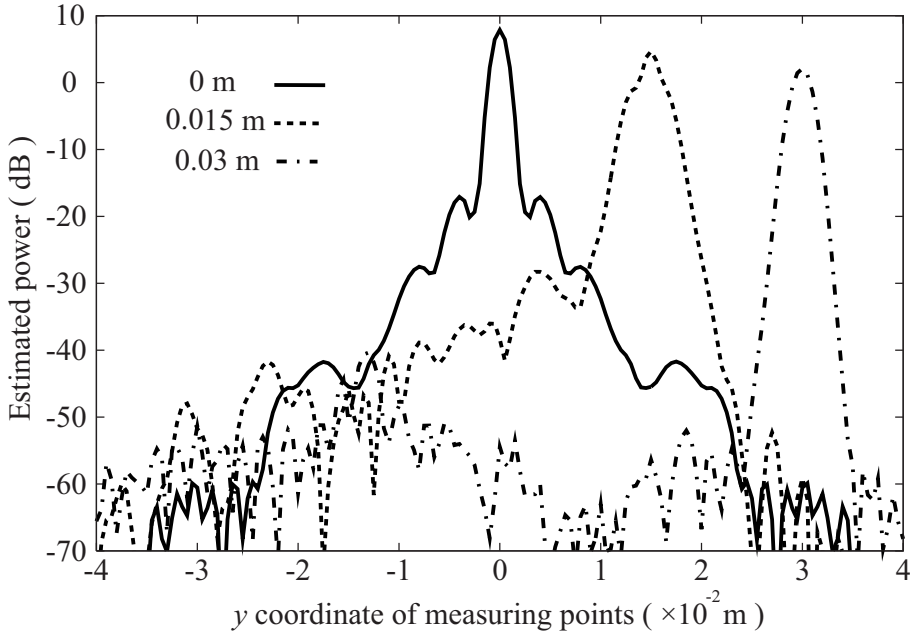

(b)

Figure 5.17: Lateral resolution of the proposed imager with a 0.016 m width array in the (a) x-z and (b) y-z sections for a 0.07 m depth. (a) x coordinates of targets are $-0.03, -0.015, 0, 0.015$ and 0.03 m. (b) y coordinates of targets are 0, 0.015 and 0.03 m.

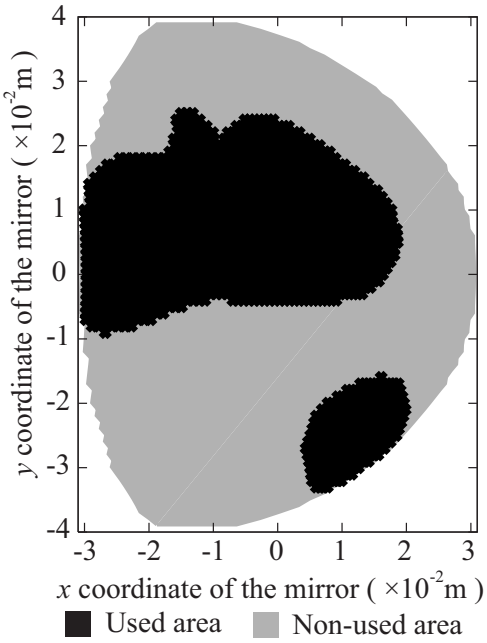

Figure 5.18: The used area on a mirror projected onto the x-y plane where the y coordinate of a target is 0.015 m in the y-z section for a 0.07 m depth.

5.4 Discussion

5.4.1 Evaluation of the radiation pattern

In this session, we compare the spatial resolution of the proposed imaging scheme from that of the digital beamforming method. The x-z and y-z section -3 dB lateral resolutions at the center for a 0.07 m depth are about 1.70 λ and 1.41 λ, respectively, which is the same as that of a digital beamforming imager with an elliptic array sized 0.041 m long and 0.051 m wide, as shown in Fig. 5.19. Because the elements are spaced at intervals of one-half of a wavelength on the array, the area of the array is proportional to the number of elements. Therefore, the number of elements can be reduced to about 1/8.2 of a dense 2-D array having the same spatial resolution.

5.4.2 Considerations on signal-to-noise ratio

A common problem for a digital beamforming imager is the low signal-to-noise ratio due to the wide transmit beam. Since this proposed method also uses wide transmit beams, we need to investigate the SNR with this method. In this section we compare the SNR of phased array, digital beamforming and proposed methods.

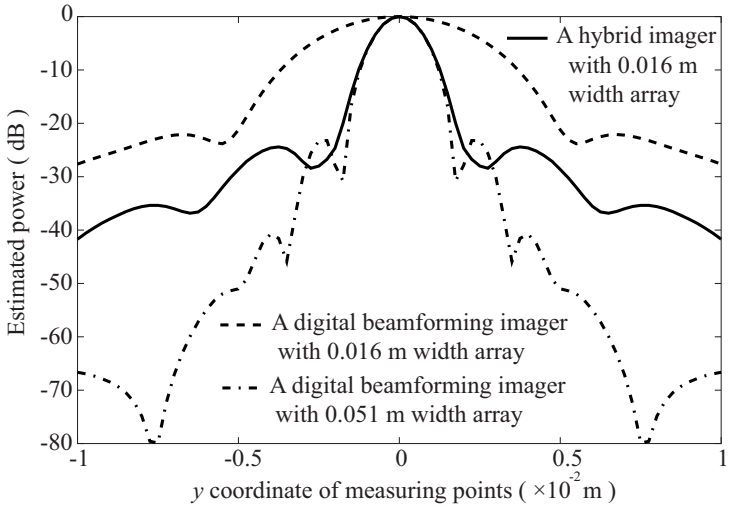

Figure 5.19: Lateral resolution of the proposed imager with a 0.016 m width array and digital beamforming imagers with 0.016 m and 0.051 m width arrays. A target exists at the center for a 0.07 m depth.

Noise in an acoustic image is primary determined by uncorrelated electronic noise in the receiver. For this discussion we follow the investigation of Karaman *et al.* [42].

For a phased array imager all transmit pulses are focused and the signal power is proportional to ${N_\mathrm{t}}^2$ at the focal region, where N_t is the number of transmit elements. Assuming uncorrelated noise, a multi-element receiver causes a SNR improvement of $10\log(N_\mathrm{r})$ dB, where N_r is the number of receive elements. Consequently the SNR of a phased array imager, $\mathrm{SNR_{PA}}$, satisfies the following equation.

$$\mathrm{SNR_{PA}}/\mathrm{SNR_0} = 10\log({N_\mathrm{t}}^2 N_\mathrm{r}), \tag{5.38}$$

where $\mathrm{SNR_0}$ is the SNR of a single-element imager.

For a digital beamforming imager, a defocused multi-element transmitter synthesizes single-element spatial resolution, and the signal power is N_t times that of a single-element transmitter. Consequently the SNR of a synthetic aperture imager, $\mathrm{SNR_{DBF}}$, satisfies the following equation.

$$\mathrm{SNR_{DBF}}/\mathrm{SNR_0} = 10\log(N_\mathrm{t} N_\mathrm{r} N_\mathrm{c}), \tag{5.39}$$

where N_c is the number of coherently integrated pulses.

For the proposed imager a multi-element transmitter with proper time delay synthesizes a single-element spatial response, similar to a digital beamforming imager with defocusing, and it is expected that the signal power is N_t times as intensive as that of a

single element transmitter. R_{H} is the SNR improvement of the proposed method compared with the digital beam forming method. Because a large part of the echo reflected by the mirror returns to the array, usually R_{H} is larger than 1. We further define $P_{\mathrm{H}l}, P_l$, and b_l, satisfying the following expression.

$$P_{\mathrm{H}l} = \sqrt{R_{\mathrm{H}} b_l} P_l D_{\mathrm{t}} D_{\mathrm{r}}, \tag{5.40}$$

where $P_{\mathrm{H}l}$ is the received signal amplitude in the proposed method, P_l is that in the digital beamforming method, and b_l is a coefficient. D_{t} and D_{r} are caused by the attenuation through the impedance matching fluid at the transmit and receive phase. Since the power summation of received signals is proportional to the power of returned echoes, the following expressions are given.

$$W_{\mathrm{H}} \propto \sum_l {P_{\mathrm{H}l}}^2 = R_{\mathrm{H}} \sum_l (b_l {P_l}^2) {D_{\mathrm{t}}}^2 {D_{\mathrm{r}}}^2, \tag{5.41}$$

$$W_{\mathrm{DBF}} \propto \sum_l {P_l}^2. \tag{5.42}$$

The coefficient b_l satisfies the following equation.

$$\sum_l (b_l {P_l}^2) = \sum_l {P_l}^2. \tag{5.43}$$

Because of reconstruction based on numerical back projection, the estimated signal amplitude, S_{HA}, is given by

$$S_{\mathrm{HA}} \propto \sum_l (\sqrt{R_{\mathrm{H}} b_l} P_{\mathrm{H}l}) e^{-2\alpha_1 (r_{0\mathrm{a}} + r_{0\mathrm{b}})}, \tag{5.44}$$

where we introduce the approximation that $D_{\mathrm{t}} = D_{\mathrm{r}} = e^{-\alpha_1 (r_{0\mathrm{a}} + r_{0\mathrm{b}})}$.

The estimated signal power, S_{HP}, satisfies the following equation.

$$S_{\mathrm{HA}} \propto {R_{\mathrm{H}}}^2 (\sum_l P_l)^2 e^{-4\alpha_1 (r_{0\mathrm{a}} + r_{0\mathrm{b}})}. \tag{5.45}$$

Assuming uncorrelated noise, the SNR of the proposed imager, $\mathrm{SNR_H}$, is given by the relation

$$\mathrm{SNR_H}/\mathrm{SNR_0} = 10 \log(N_{\mathrm{t}} N_{\mathrm{r}} R_{\mathrm{H}} N_{\mathrm{c}} e^{-4\alpha_1 (r_{0\mathrm{a}} + r_{0\mathrm{b}})}). \tag{5.46}$$

For example, with an 800-element array ($N_{\mathrm{t}} = N_{\mathrm{r}} = 800$), the impedance matching fluid is water ($\alpha_1 = 2.0(\omega/2\pi)^2 \times 10^{-14}$ Np/m), $r_{0\mathrm{a}} + r_{0\mathrm{b}} = 0.085$ m, if the receive efficiency R_{H} is 6.2, and the number of coherently integrated pulses N_{c} is 260, a proposed imager realizes the following SNR.

$$\mathrm{SNR_H/SNR_{SA}} = 7.8\ [\mathrm{dB}]\,, \tag{5.47}$$
$$\mathrm{SNR_H/SNR_{PA}} = 3.0\ [\mathrm{dB}]\,. \tag{5.48}$$

In this case 3-D images can be acquired at the rate of 19 3-D images/s. In the case of the impedance matching fluid being ultrasound jelly, the SNR improvements are 6.7 and 1.9 dB, respectively.

For cardiology, higher time resolution is needed. Assuming a heart rate of 80 beats/min and a moving distance in a beat cycle of 0.02 m, the maximum speed is about 0.04 m/s. To improve the SNR we can use coherent integration when the target moves 1/4 of a wavelength. Where that wavelength is 0.001 m, the maximum coherent integration time is 1/160 second; in other words, $N_\mathrm{c} = 30$. This means that more than 160 images/s are needed to measure the heart when the wavelength is less than 0.001 m. The proposed scheme is suited for such purposes.

5.5 Conclusion

For a high resolution acoustic real-time 3-D imaging system, we proposed a system based on a hybrid method with a reflector mirror and a small dense array. Utilizing this scheme, images of the whole measuring area can be reconstructed from a single transmit and receive event; so enabling real-time 3-D imaging. Receiving a large part of the echo focused by the mirror has the same effect as using a large array. This method realizes lateral resolutions of 1.70 λ in the x-z and 1.41 λ in the y-z sections for a depth of 0.07 m, where the center frequency is 1.6 MHz, the width of the reflector is 0.062 m long and 0.08 m wide, and the array is a circle 0.016 m in diameter. This shows that the number of elements can be reduced to about 1/8.2 of a dense 2-D array having the same spatial resolution but using a digital beamforming method. Because we make the reflection ratio of the mirror taper off in the numerical back projection, the sidelobe level is suppressed to less than -21 dB. The maximum theoretical frame rate is 5000 frames/s, when the SNR is sufficiently high. Since the transmit beam is synthesized by all elements on the array, a sufficiently high SNR is achieved. In cases where the frame rate is 19 images/s, the SNR improvements compared to a conventional phased array method and a digital beamforming method with defocusing are 3.0 dB and 7.8 dB, respectively.

Chapter 6

Improvement of the Spatial Resolution of a 3-D Acoustic Medical Imaging System Based on Hybrid Method Using Synthetic Aperture Technique

6.1 Introduction

A volumetric 3-D real-time high-resolution acoustic imaging system is needed for medical diagnosis. A 3-D imager that employs a linear array measures one target plane at a time, and then moves mechanically for 3-D imaging [74][76]. However, this method has insufficient time resolution for the medical examination of a fast-moving organ such as the heart. The use of acoustic lenses on the elements to focus the transmit and receive beams to a target plane results in serious deterioration in spatial resolution both in front of and behind the focus. A digital beamforming imager that incorporates a 2-D array enables measurement of the entire target field as a single transmit and receive event. This system, therefore, has high time resolution; however, the number of elements on the 2-D array is enormous and the signal-to-noise ratio (SNR) is low [42][52][84]. Though a myocardial motion imager is useful for medical diagnoses [85], it has insufficient lateral resolution.

We proposed a system based on a hybrid array-refrector configuration, shown in Fig. 6.1 [86]-[88]. This system employs a wide transmit beam that is radiated over the entire measurement field. The angular resolution and SNR of the proposed method are improvements over those of a digital beamforming imager with a similarly-sized 2-D array. This is because in the current method most of the echo reflected by the mirror is gathered to the array.

In this paper, we propose a method for the improvement of the spatial resolution of

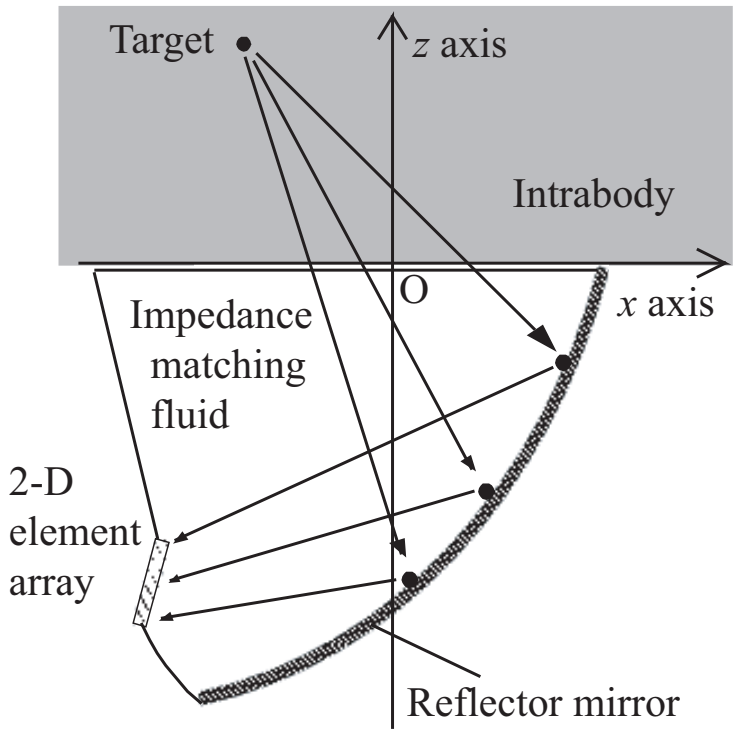

Figure 6.1: Schematic view of the system in the receive phase.

a 3-D acoustic medical imaging system based on a hybrid method that uses a synthetic aperture technique. Since a 3-D imager based on a hybrid method aquires a 3-D image as single transmit and receive event, the image reconstruction from multiple transmit and receive events realizes sufficient time resolution to measure a fast moving organ such as a heart.

In section 2, we outline the framework of the 3-D acoustic imaging system based on the hybrid method. The parameters for calculating spatial resolution are set out in section 3. In the proposed imager all elements on the 2-D array radiate ultrasound pulses at proper time delays for synthesizing a wide transmit beam. In section 4, we propose a method to employ proper time delays. The radiation pattern of the transmit beam is calculated in section 5. In section 6, we evaluate the effect of the coherent integration of multiple transmit and receive events on the improvements in spatial resolution of the proposed method. In section 7, we examine the spatial resolution of the proposed imager in the case that the time resolution is 300 3-D images/s. Finally, we draw conclusions.

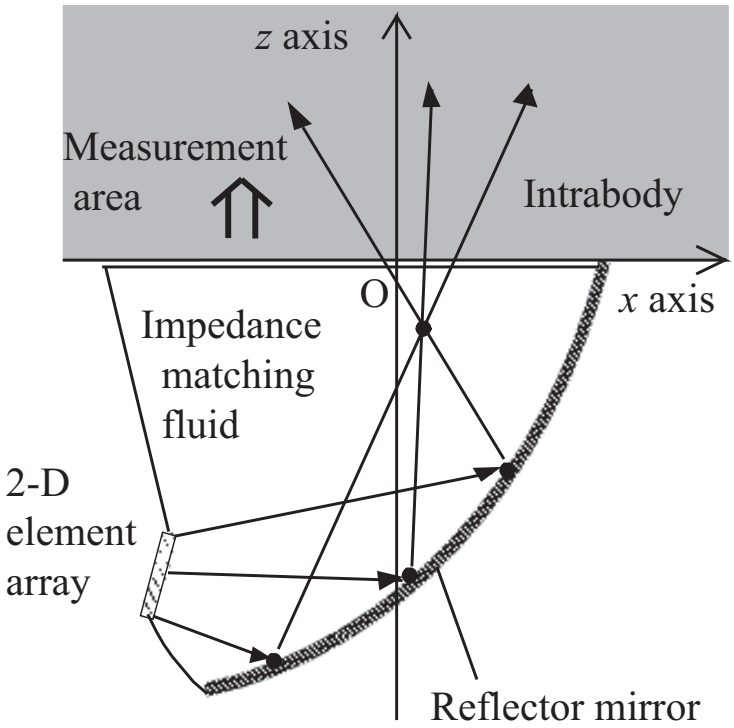

Figure 6.2: Schematic view of the system in the transmit phase.

6.2 Formation of the transmit beam using a focusing method

With this method, a transmit beam is radiated over the entire measurement field before any echoes from the targets are received on the 2-D array. The image of the target is reconstructed from the received signals using numerical back-projection. The image reconstruction based on numerical back-projection is processed as follows: the phase of the received signal is reversed before being projected backward from the receive point. The waves projected backward are focused at the target points.

To measure the entire target field as a single transmit and receive event, the transmit beam must be radiated sufficiently widely over the target field. As well, high transmit power is desirable to improve the SNR. A method to form a wide transmit beam is shown in [88]. Fig. 6.2 is a schematic view of the proposed imager in the transmit phase. All elements on the array radiate ultrasound pulses at appropriate time delays to enable the pulses to be focused by the reflector. As a single element response placed at the focus is synthesized, a wide transmit beam with high acoustic power is radiated over the entire target field.

6.3 Calculation parameters

A set of parameters for investigating spatial resolution of a 3-D acoustic imager based on a hybrid method is shown in [88]. We follow this set in this paper: mean propagation velocity $c_0 = 1600$ m/s, density of the undisturbed medium $\rho_0 = 1.08 \times 10^3$ kg/m^3, the variation of the propagation velocity $\Delta c = -300$ m/s, and the variation of the density $\Delta\rho = -1.0 \times 10^2$ kg/m^3. The attenuation coefficients of the intrabody and the impedance matching fluid are $2.0(\omega/2\pi)^2 \times 10^{-14}$ and $5.0(\omega/2\pi) \times 10^{-6}$ Np/m, respectively. The element pitch is half the wavelength λ at the center frequency, where the center frequency is 1.6 MHz and -6 dB fractional band width is 60 %. A circular 2-D array of 0.016 m in diameter is employed, where the element pitch is 0.0005 m. The number of elements is 797. The reflector size is 0.062 m long and 0.08 m wide.

6.4 Transmit time delays for focusing the transmit beam

In this section, we first propose a method that utilizes numerical back-projection to calculate the transmit waveform for focusing the transmit pulses at a point. In this case, we assume that a spherical wave is radiated backward from the focus; we then calculate the received signal at each element on the array. The phase of the transmit pulse is the reverse of the received signal.

The waveform of the received signal is particular to each element because the transmission pass from the focus is unique to the element position. As radiating different individual waveforms from all elements is impractical because the number of elements is 797, all elements radiate ultrasound pulses of the same waveform with different time delays. We introduce the assumption that the waveform radiated backward from the focus is the same as that radiated from all elements. We calculate the time delay by maximizing

$$E(\tau) = \int p(t-\tau)q(t)dt, \tag{6.1}$$

where $p(t)$is the waveform radiated backward from the focus, $q(t)$ is the waveform received at an element, and t is the transmit time delay of the element. The transmit waveform radiated from the element is $p(t+\tau)$.

6.5 The region with a guaranteed focus

In this section we evaluate the region in which the focus is guaranteed for radiating an ultrasound beam in a direction. In the geometric optics shown in Fig. 6.3, a transmit pulse from an element is reflected by the mirror and then radiated to the measurement point (T_a) after passing through the focus (T_r). In the same way, the inverse pass T_aT_r

arrives at the array after being reflected by the mirror. For radiating a transmit beam to T_a, it is therefore necessary that the focus exists in the region between T_a and the used area. The used area is the region on the mirror where the echo from T_a is reflected and arrives at the array. We call this as the region with a guaranteed focus (RGF), as shown in Fig. 6.4.

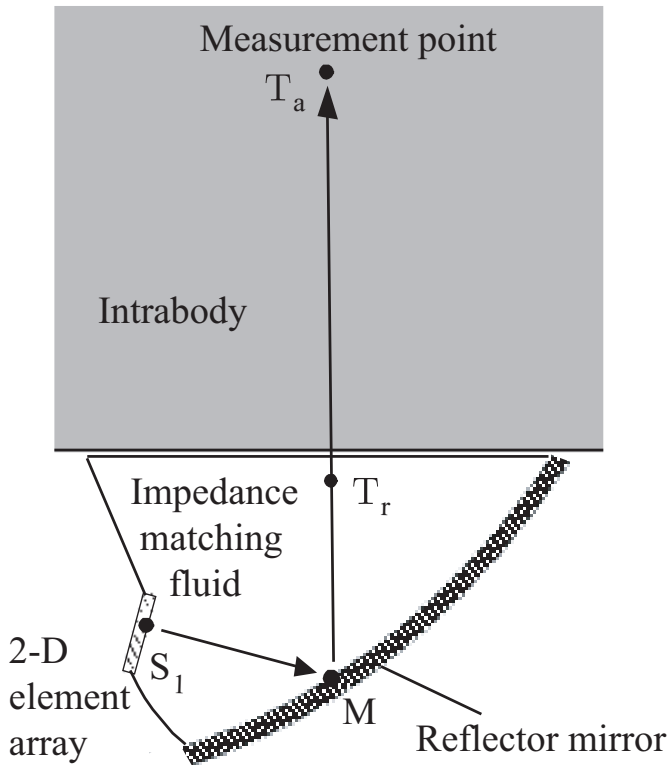

Figure 6.3: A transmit pass in geometric optics. In geometric optics a transmit pulse from an element is reflected by the mirror, and then radiated to the measurement point T_a after passing through the focus T_r.

Fig. 6.5 shows the radiation pattern of the proposed imager. In this calculation we set the focus at the origin. The -6 dB transmit beam width is 1.8λin the x-y section. This indicates that the transmit power is gathered at the focus; that is, the time delays employed to the elements are proper. At a 0.07 m depth in a region with an x coordinate of more than -0.013 m and less than 0.03 m, the transmit power is greater than -6 dB compared with the peak power: the amplitude half-width is 33.7 degrees. Therefore, the proposed imager measures a target field of 33.7 degrees of visual angle as a single transmit and receive event.

Fig. 6.6 shows the RGFs on the x axis. The regions, whose x coordinates of measure-

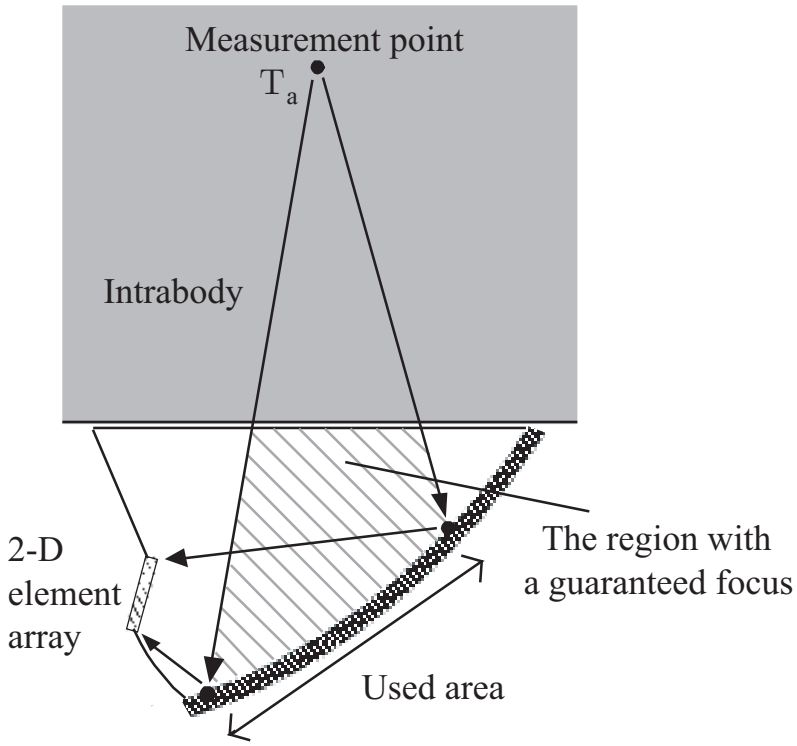

Figure 6.4: The Region with a guaranteed focus. When the focus is contained within the region, the transmit wave is radiated to the measurement point T_a.

ment points are -0.015 m to 0.03 m, contain the origin and that whose x coordinate is -0.03 m does not contain the origin. This corresponds to the radiation pattern shown in Fig. 6.5. Therefore to radiate a certain measurement point, the focus should be arranged in the RGF of the point.

6.6 Improvement of the spatial resolution by multiple transmit and receive events

Since a single transmit and receive event can make a 3-D image in the proposed method, the time resolution is 5000 images/s when the measurement range is 0.16 m. For medical diagnoses a lower time resolution is sufficient, and so the spatial resolution and SNR can be improved from multiple transmit and receive events. Utilizing a synthetic aperture technique, the coherent integration of multiple receive signals of different transmit points equivalently enlarges the aperture size, and thus the spatial resolution is improved. With this method we can change the focal position by employing proper time delays.

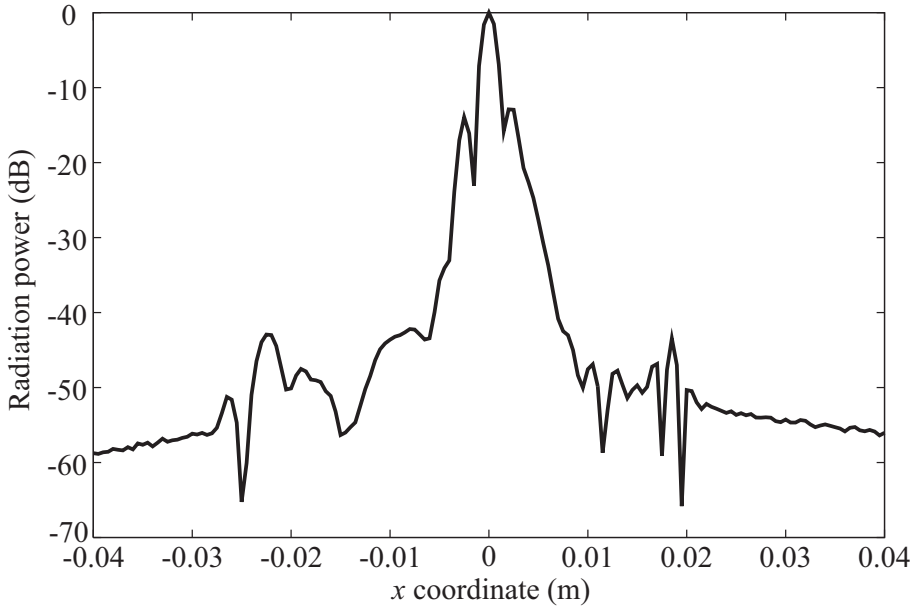

(a)

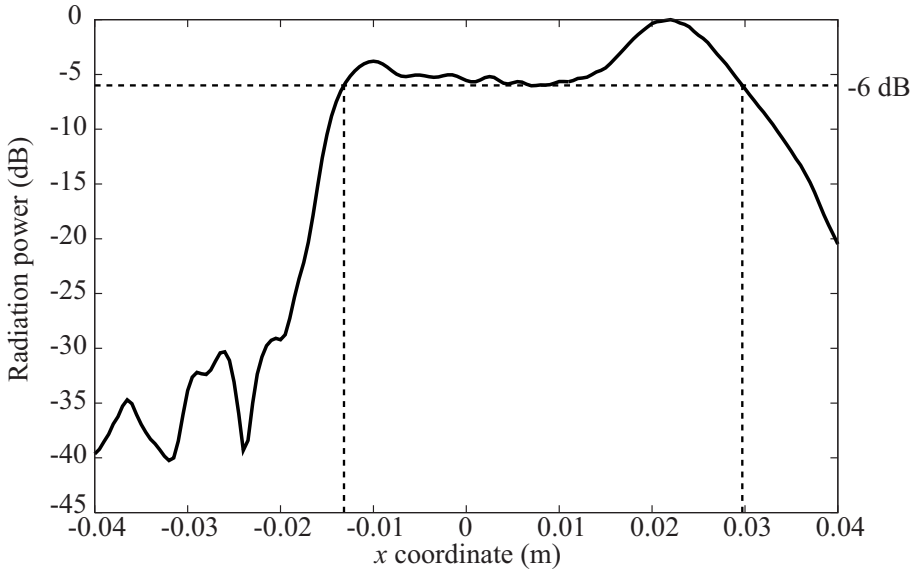

(b)

Figure 6.5: Radiation pattern of the proposed imager in the x-z section for (a) 0 m and (b) 0.07 m depths.

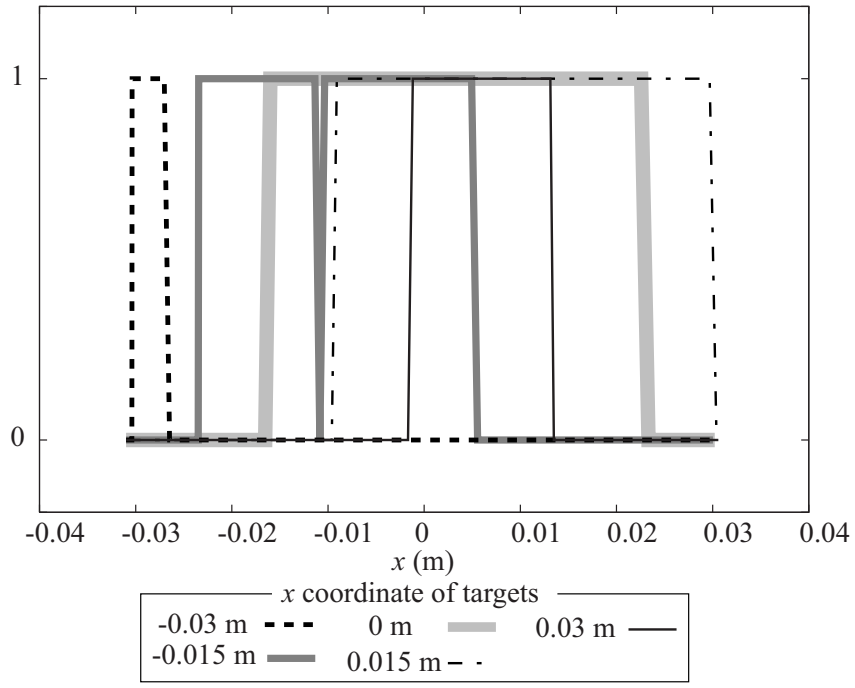

Figure 6.6: The regions with a guaranteed focus on the x axis. The regions, whose x coordinates of measurement points are -0.015 m to 0.03 m, contain the origin and that whose x coordinate is -0.03 m does not contain the origin. This corresponds to the radiation pattern shown in Fig. 6.5(b).

When measuring a fast moving organ, such as the heart of a fetus, a time resolution of 300 3-D images/s is needed. In this case, the spatial resolution can be improved from 16 transmit and receive events by using a synthetic aperture technique. As shown in Fig. 6.7, we arrange the 16 focuses for a -0.01 m depth. The transmit wave is radiated in the direction where the RGF contains the focus. Therefore, the spatial resolutions for point targets at the x coordinates of -0.015, 0, 0.015 m are improved respectively from 10, 14, 8 transmit and receive events. Receiving a large part of the echo reflected on the mirror has the same effect as using a large array. As shown in [87], the echo passing through a section of the RGF are received on the array; thus the spatial resolution of the proposed imager is equivalent to that of a digital beamforming imager with an array of the same size as the section of the RGF. Then we call the section of the RGF as the effective aperture. Fig. 6.8 shows the synthesized aperture from 14 events when measuring the center for a 0.07 m depth; where we introduce the approximation that a spherical wave is radiated from the focus. The coherent integration utilizing the synthetic aperture technique realizes a spatial resolution equivalent to that of an aperture given by the convolution of the focuses and the effective aperture.

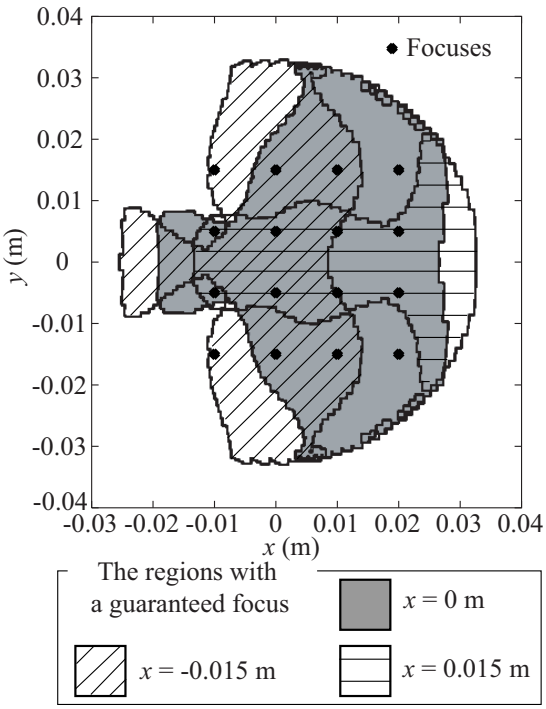

Figure 6.7: Arrangement of the focuses and the regions with a guaranteed focus for a -0.01 m depth.

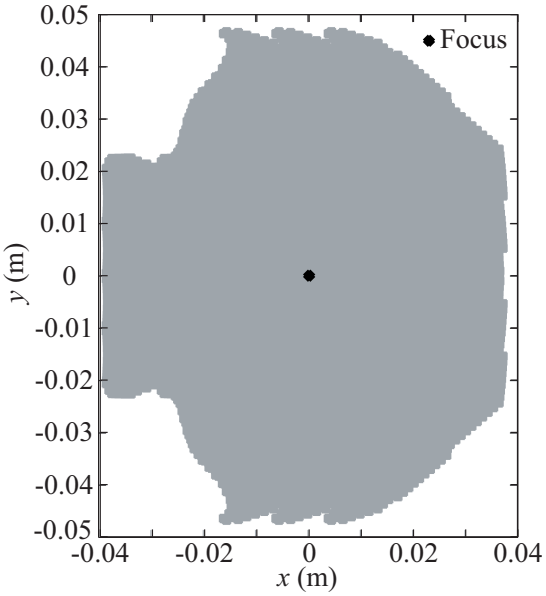

Figure 6.8: The synthesized aperture from 14 transmit and receive events when measuring the center for a 0.07 m depth.

6.7 Results and discussion

Fig. 6.9 shows the spatial resolution of the proposed imager acquired from single and 16 transmit and receive events. As noted above, the spatial resolutions of the x coordinates of -0.015, 0, 0.015 m are improved, respectively, from 10, 14, 8 transmit and receive events by utilizing a synthetic aperture technique.

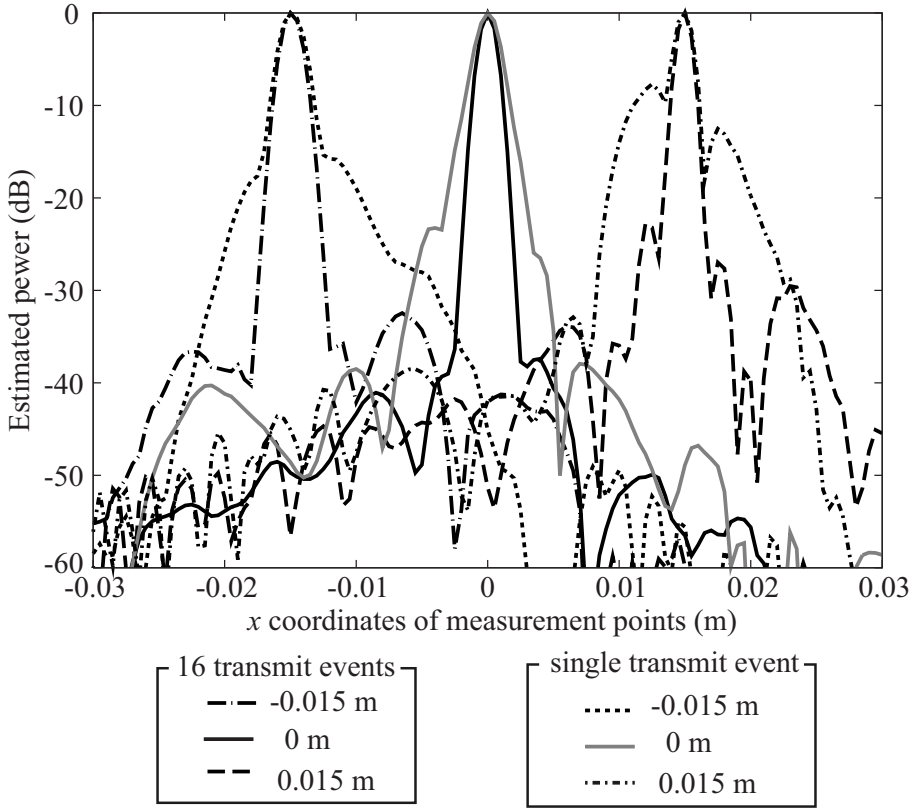

Figure 6.9: Lateral resolution of the proposed imager acquired from single and 16 transmit and receive events in the x-z section for a 0.07 m depth. The x coordinates of point targets are -0.015, 0 and 0.015 m.

We compare the spatial resolution of the proposed imaging method with that using the digital beamforming method. The spatial resolution of digital beamforming imagers is improved from 16 transmit and receive events. As shown in Fig. 6.10, the x-z and y-z section -3 dB lateral resolutions are about 1.30λ and 1.17λ, respectively. A target exists at the center for a 0.07 m depth. They are the same as those of a digital beamforming imager with an elliptic array of 0.041 m long and 0.047 m wide. Because the elements are spaced at intervals of one-half of a wavelength on the array, the area of the array is proportional to the number of elements. Therefore, the number of elements can be

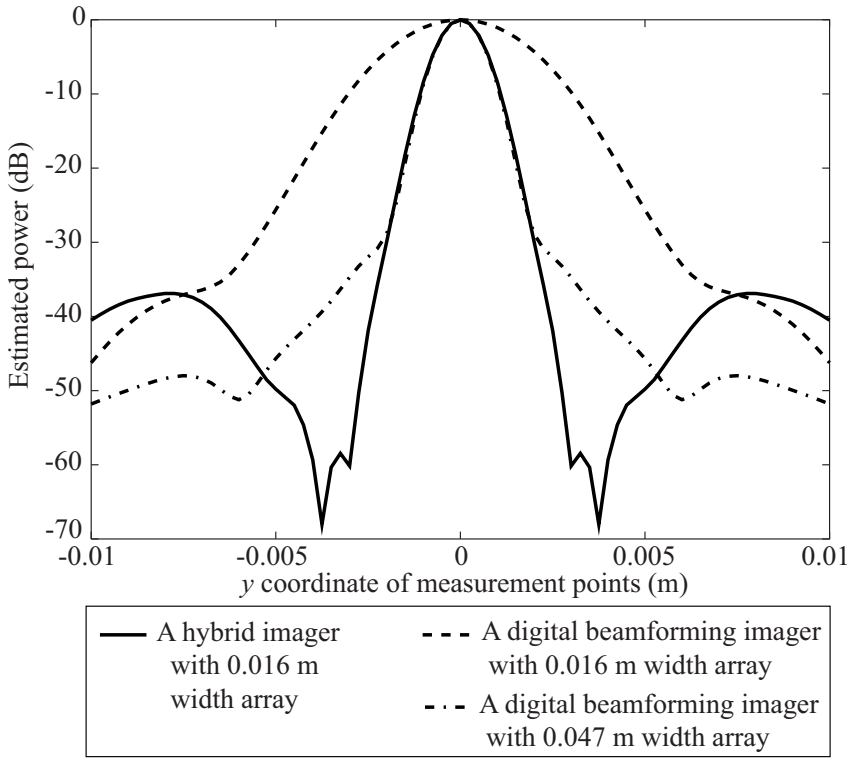

Figure 6.10: Lateral resolution of the proposed imager with a 0.016 m width array and digital beamforming imagers with 0.016 and 0.047 m width arrays. A point target exists at the center for a 0.07 m depth. The spatial resolutions of the proposed imager and digital beamforming imagers are improved, respectively, from 14 and 16 transmit and receive events.

reduced to about 1/7.5 of a dense 2-D array having the same spatial resolution.

6.8 Conclusion

To realize a high resolution acoustic real-time 3-D imaging system, we proposed one based on a hybrid method utilizing a synthetic aperture technique. Since images of the entire measurement field are reconstructed as single transmit and receive event, we can reconstruct a 3-D image from multiple transmit and receive events with sufficient time resolution. When the time resolution is 300 3-D images/s, by utilizing the synthetic aperture technique the coherent integration of 16 transmit and receive events improves the spatial resolution. Image reconstruction from 16 events realizes a lateral resolution of 1.30λ in the x-z and 1.17λ in the y-z sections for a 0.07 m depth, where the center frequency is 1.6 MHz, the width of the reflector is 0.062 m long and 0.08 m wide, and

the array is a circle 0.016 m in diameter. This shows that the number of elements can be reduced to about 1/7.5 of a dense 2-D array having the same spatial and time resolution but using a digital beamforming method with a synthetic aperture technique.

Appendix A

Production of the coefficient used in Eq. 2.1.

The particle velocity $v_{\mathrm{T}_1 0}$ is given by

$$v_{\mathrm{T}_1 0} = b_{\mathrm{v}} \frac{1 + jkr}{r^2} e^{-(\alpha + jk)r}, \tag{A.1}$$

where we assume the transmit element as a point source and b_{v} is a constant value. In the far field, that is, in the condition that the particle velocity $kr \gg 1$ and the pressure variety $v_{\mathrm{T}_1 0}$ have the same phase, and the following equation is satisfied.

$$p_{\mathrm{T}_1 0} = \frac{\rho\omega}{k} p_{\mathrm{T}_1 0}. \tag{A.2}$$

Therefore, the acoustic power I is given by

$$I = \frac{1}{2} p_{\mathrm{T}_1 0} {v_{\mathrm{T}_1 0}}^* = \frac{k\rho\omega b_{\mathrm{v}}^2}{2r^2} e^{-2\alpha r}. \tag{A.3}$$

When the attenuation coefficient $\alpha = 0$, the transmit power is given by $W = 4\pi r^2 I$, and thus the following equations are obtained.

$$W = 2\pi b_{\mathrm{v}}^2 k\rho\omega, \tag{A.4}$$

$$b_{\mathrm{v}} = \sqrt{\frac{W}{2\pi k\rho\omega}}. \tag{A.5}$$

Therefore, the particle velocity is obtained by

$$v_{\mathrm{T}_1 0} = \sqrt{\frac{W}{2\pi k\rho\omega}} G_{\mathrm{r}} R_{\mathrm{r}}(x, y, z) \frac{1 + jkr}{r^2} \cdot e^{-(\alpha + jk)r}. \tag{A.6}$$

Bibliography

[1] R. E. Hoover, "The cane as a travel aid," In P. Zahl (Ed.) Blindness: Modern approaches to the unseen environment. New York: Hafner Publishing Company, 1963.

[2] C. A. Shingledecker, and E. Foulke, "A human factors approach to the assessment of the mobility of blind pedestrians," Human Factors, vol. 20, pp. 273-286, 1978.

[3] J. M. Benjamine, N. A. Ali, and A. F. Schepis, "A laser cane for the blind," Proc. San Diego Biomedical Symp., vol. 12, pp. 53-57, 1973.

[4] N. Pressey, "Mowat sensor," Focus, vol. 11, no. 3, pp. 35-39, 1977.

[5] L. Rusell, "Travel path sounder," Proc. Rotterdam Mobility Res. Conference, Smer. Foundation for the Blind, 1965.

[6] L. Kay, "A sonar aid to enhance spatial perception of the blind; Engineering design and evaluation," Radio, Electron, Eng., vol. 44, no. 11, pp. 605-627, 1974.

[7] S. Shoval, J. Borenstein, and Y. Koren, "The Navbelt - A computerized travel aid for the blind based on mobile robotics technoloby," IEEE Trans. Biomed. Eng., vol. 45, no. 11, 1998.

[8] J. G. Linvill, and J. C. Bliss, "A direct translation reading aid for the blind," Proc. IEEE, vol. 54, pp.40-51, 1966.

[9] R. Farcy, and R. Damaschini, "Triangulating laser profilometer as a three-dimensional space perception system for the blind," Applied Optics, vol. 36, no. 31, pp. 8227-8232, 1997.

[10] D. Yuan, and R. Manduchi, "A Tool for Range Sensing and Environment Discovery for the Blind," Computer Vision and Pattern Recognition Workshop, 2004.

[11] S. Saida, Y. Shimizu, and T. Wake, "Computer-controlled TVSS and some characteristics of vibrotactile letter recognition," Percept-Mot-Skills, vol. 55, no. 2, pp. 651-653, 1982.

[12] Y. Yanagida, "Vibrotactile letter reading using a low-resolution tactile array," Proc. of the 12th Symp. on Haptic Interfaces for Virtual Environment and Teleoperator Systems, pp. 400-406, 2004.

[13] G. Brindley, and W. Lewin, " The sensation produced by electrical stimulation of the visual cortex," Journal of Physiology, vol. 196, pp. 479-493, 1968.

[14] M. S. Humayun, "Visual perception elicited by electrical stimulaion of retina in blind humans," Arch Ophthalmol, vol. 114, pp. 40-46, 1996.

[15] M. Mahadevappa, J. D. Weiland, D. Yanai, I. Fine, R. J. Greenberg, and M. S. Humayun, "Perceptual thresholds and electrode impedance in three retinal prosthesis subjects," IEEE Trans. Neural Syst. Rehabil. Eng., vol. 13, no. 2, pp. 201-206, 2005.

[16] L. Hesse, T. Schanze, M. Wilms, and M. Eger, "Implantation of retina stimulation electrodes and recording of electrical stimulation responses in the visual cortex of the cat," Graefe's Archive for Clinical and Experimental Ophthalmology, vol. 238, No. 10, pp. 840-845, 2000

[17] C. C. Collins, "Tactile television - mechanical and electrical image projection," IEEE Trans. Man Machl. Syst., vol. MMS-11, pp. 65-71, 1970.

[18] P. Bach-y-Rita, "Brain mechanisms in sensory substitution," Academic Press, 1972.

[19] C. C. Collins and P. Bach-y-Rita, "Transmission of pictorial information through the skin," Adv. Biol. Med. Phys., vol. 14, pp. 285-315, 1973.

[20] P. Bach-y-Rita, L. A. Scadden, and C. C. Collins, "Tactile television system," Smith-Kettlewell Institute of Visual Sciences, 1975.

[21] J. L. Coffey, "The development and evaluation of the battele aural reading device," proc. Int. Congr. on Technology and Blindness, Clark, L. L. ed., American Foundation for the Blind, vol. 1, pp. 343-360, 1963.

[22] G. C. Smith and H. A. Mauch, "Summary report on the development of reading machine for the blind," Bull. Proshetic Res., BPR 10-12, Dept.of Medicine and Surgery, Veterans Admin, Washington D. C., pp. 243-271, 1969.

[23] R. M. Fish, "An audio display for the blind," IEEE Trans. Biomedical Engineering, vol. 23, no. 2, pp. 144-154, 1976.

[24] K. A. Kaczmarek, J. G. Webster, P. Bach-y-Rita, and W. J. Tompkins, "Electrotactile and vibrotactile displays for sensory substitution systems," IEEE Trans. Biomed. Eng., vol. 38, no. 1, 1991.

[25] C. A. Perez, A. J. Santibanez, C. A. Holzmann, P. A. Estevez, and C. M. Held, "Power requirements for vibrotactile piezo-electric and electromechanical transducers," Med. Biol. Eng. Comput., vol. 41, no. 6, pp. 718-726, 2003.

[26] K. A. Kaczmarek, J. G. Webster, and R. G. Radwin, "Maximal dynamic range electrotactile stimulation waveforms," IEEE Trans. Biomed. Eng., vol. 39, no. 7, pp. 701-715, 1992.

[27] K. A. Kaczmarek and S. J. Haase, "Pattern identification and perceived stimulus quality as a function of stimulation waveform on a fingertip-scanned electrotactile display," IEEE Trans. Neural Syst. Rehabil. Eng., vol. 11, no. 1, pp. 9-16, 2003.

[28] C. J. Poletto and C. L. Van-Doren, "A high voltage, constant current stimulator for electrocutaneous stimulation through small electrodes," IEEE Trans. Biomed. Eng., vol. 46, no. 8, pp. 929-936, 1999.

[29] C. J. Poletto and C. L. Van-Doren, "Elevating pain thresholds in humans using depolarizing prepulses," IEEE Trans. Biomed. Eng., vol. 49, no. 10, pp. 1221-1224, 2002.

[30] C. A. Perez, and P. A. Munoz, "Optimization of the power targeted to the frequency region of maximum tactile sensitivity," Med. Prog. Technol., vol. 21, no. 2, pp. 67-76, 1995.

[31] J. Radon, "Uber die bestimmung von funktionen durch irhe integralwerte langs gewisser mannigfaltigkeiten", Ber. Saechs. Akad. Wiss. Leipzig, Math.-Phys. Kl, 1917

[32] A. M. Cormack, "Representation of a function by its line integrals, with some radiological applications. II", J. Appl. Phys. Vol 35, no.10 pp.2908-2913, 1964.

[33] R. A. Brooks, and G. Di-Chiro, "Principles of computer assisted tomography (CAT) in radiographic and radioisotopic imaging," Phys. Med. Biol., vol.21, no. 5, pp. 689-732, 1976.

[34] R. N. Bracewell, "Numerical transforms," Science, vol. 248, no. 697-704, 1990.

[35] J. J. Flaherty, K. R. Erikson, and V. M. Lund, "Synthetic aperture ultrasonic systems," U.S. Patent 3 548 642, 1967.

[36] J. W. Goodman, "Digital image formation from detected holographic data," in Acoustical Holography, vol. 1, A. F. Metherell *et al.*, Eds. New York: Plenum, pp. 173-185, 1969.

[37] J. T. Ylitalo, and H. Ermert, "Ultrasound synthesis aperture imaging: monostatic approach," IEEE Trans. Ultrason. Ferroelectr. Freq. Contr., vol. 41, no. 3, pp. 333-339, 1994.

[38] Z. M. Benenson, A. B. Elizarov, T. V. Yakovleva, and W. D. O'Brien, Jr., "Approach to 3-D ultrasound high resolution imaging for mechanically moving large-aperture transducer based upon Furier transform," IEEE Trans. Ultrason. Ferroelectr. Freq. Contr., vol. 49, no. 12, pp. 1665-1685, 2002.

[39] B. Delannoy, R. Torguet, C. Bruneel, E. Bridous, J. M. Rouvaen, and H. LaSota, "Acoustical image reconstruction in parallel-processing analog electronic systems," J. Appl. Phys., vol. 50, pp. 3153-3159, 1979.

[40] D. P. Shattuck, M. D. Weinshenker, S. W. Smith, and O. T. von Ramm, "Explososcan: A parallel processing technique for high speed ultrasound imaging with linear phased arrays," J. Acoust. Soc. Amer., vol. 75, pp. 1273-1282, Apr. 1984.

[41] O. T. Ramm, S. W. Smith, and H. G. Pavy, Jr, "High-speed ultrasound volumetric imaging system - Part ii: parallel processing and image display," IEEE Trans. Ultrason. Ferroelectr. Freq. Contr., vol. 38, no. 2, pp. 109-115, 1991.

[42] M. Karaman, P. C. Li, M. O'Donnell, "Synthetic aperture imaging for small scale systems," IEEE Trans. Ultrason. Ferroelectr. Freq. Contr., vol. 42, no. 3, pp. 429-442, 1995.

[43] G. R. Lockwood, J. R. Talman , S. S. Brunke, "Real-time 3-D ultrasound imaging using sparse synthetic aperture beamforming," IEEE Trans. Ultrason. Ferroelectr. Freq. Contr., vol. 45, pp. 980-988, 1998.

[44] T. A. Shoup and J. Hart "Ultrasonic imaging systems," Proc. IEEE Ultrasonics Symposium, pp. 863-871, 1988.

[45] D. H. Turnbull, and F. S. Foster, "Beam steering with pulsed two-dimensional transducer arrays," IEEE Trans. Ultrason. Ferroelectr. Freq. Contr., vol. 38, no. 4, pp. 320-333, 1991.

[46] T. S. Sumanaweera, J. Schwartz, and D. Napolitano, "A spiral 2D phased array for 3D imaging," Proc. IEEE Ultrason. Symp., pp. 1271-1274, 1999.

[47] S. W. Smith, H. G. Pavey , O. T. Ramm. "High speed ultrasound volumetric imaging system - Part i: Transducer design and beam steering," IEEE Trans. Ultrason. Ferroelectr. Freq. Contr., vol. 38, pp. 100-108, 1991.

[48] G. R. Lockwood, P-C Li, M. O 'Donnell, *et al.*, "Optimizing the radiation pattern of sparse periodic linear arrays," IEEE Trans. Ultrason. Ferroelectr. Freq. Contr., vol. 43: pp. 7-14, 1996.

[49] G. R. Lockwood and F. S. Foster, "Optimizing the radiation pattern of sparse periodic two-dimensional arrays," IEEE Trans. Ultrason. Ferroelectr. Freq. Contr., vol. 43, pp. 15-19, 1996.

[50] A. Austeng and S. Holm, "Sparse 2-D arrays for 3-D phased array imaging - design methods," IEEE Trans. Ultrason. Ferroelectr. Freq. Contr., vol. 49, pp. 1073-1086, 2002.

[51] J. E. Snyder, J. A. Kisslo, and O. T. Ramm, "Real-time orthogonal mode scanning of the heart. I. System design," J. Amer. Coll. Cardiol., vol. 7. pp. 1279-1285, 1986.

[52] B. D. Steinberg, "Digital beamforming in ultrasound," IEEE Trans. Ultrason. Ferroelectr. Freq. Contr., vol. 39, no. 6, pp. 716-721, 1992.

[53] H. R. Everett, "Sensors for Mobile Robots," Theory and Application. pp.139-150, A K Peters, 1995.

[54] L. Korba, "Variable Aperture Sonar for Mobile Robots," Proc. IEEE International Conference on RA, San Diego, USA, pp.3136-3141, 1994.

[55] T. Yata, A. Ohya, and S. Yuta, "A fast and accurate reflecting points measurable sonar-ring system," J. Robotics Soc. Jpn, pp. 1173-1182, vol. 17, no. 8, 1999 [in Japanese].

[56] S. R. Freemam, M. K. Quick, M. A. Morin, R. C. Anderson, C. S. Desilets, T. E. Linnenbrink, and M. O'Donnell, "Delta-sigma oversampled ultrasound bemformer with dynamic delays," IEEE Trans. Ultrason. Ferroelectr. Freq. Contr., vol. 46, no.2, pp. 320-331, Mar. 1999.

[57] M. Inerfield, G. R. Lockwood, and S. L. Garverick, "A sigma-delta-based sparse synthetic aperture beamformer for real-time 3-D ultrasound," IEEE Trans. Ultrason. Ferroelectr. Freq. Contr., vol. 49, no. 2, pp. 243-254, Feb. 2002.

[58] H. Taki and T. Sato, "A High-resolution Ultrasound Guidance System for Visually Handicapped Using a Reflector and a Sensor Array," IEICE Tech. Rep., 101-377, 2001 [in Japanese].

[59] H. Taki, H. Yashima, and T. Sato, "Optimization of the Sensor Array Position and Study of the Reconstructed Image for a High-resolution Ultrasound Guidance System for Visually Handicapped," Proc. IEICE General Conf., A-11-13, 2003 [in Japanese].

[60] E. Yamashita, "Analysis Methods for Electromagnetic Wave Problems," Artech House, 1990.

[61] E. Yamashita, "Application of Electromagnetic Wave Analysis",IEICE Japan, 1993 [in Japanese].

[62] P. Bach-y-Rita, C. C. Collins, F. A. Saunders, B. White, and L. Scadden "Vision Substitution by tactile image projection," Nature, vol. 221, pp. 963-964, 1969.

[63] C. C. Collins, "On mobility aids for the blind, in Electronic Spatial Sensing for the Blind," Warren and E. R. Strelow, Eds. Dordrecht, The Netherlands; Matinus Nijhoff, pp.35-64, 1985.

[64] M. Shinohara, Y. Shimizu, and A. Mochizuki, "Three-dimensional tactile display for the blind," IEEE Trans. Rehab. Eng., vol. 6, pp. 249-256, Sept. 1998.

[65] L. H. D. Poll, and R. P. Waterham, "Graphical user interfaces and visual disabled users," IEEE Trans. Rehab. Eng., vol. 3, pp. 65-69, 1995.

[66] H. Taki, H. Yashima, and T. Sato, "Study of the hybrid method and the sensor for a high-resolution ultrasound vision substitute system for visually handicapped," IEICE Trans. Fundamentals, J88-A, pp. 568-576, 2005 [in Japanese].

[67] G. Jansson, "Tactile guidance of movement," International Journal of Neuroscience, vol. 19, no. 1-4, pp. 37-46, 1983.

[68] S. Weinstein, "Intensive and extensive aspects of tactile sensitivity as a function of body part, sex and laterality," Skin Senses, D. R. Kenshalo, Ed. Springfield, I11: Charles C. Thomas, pp. 195-222, 1968.

[69] Y. Shimizu, "Psychophysical characteristics due to tactile stimuli," Journal of the Robotics Society of Japan, vol. 2, no. 5, pp.61-66, 1984 [in Japanese].

[70] B. Christine, *et al.*, "Facial sensibility in patients with unilateral facial nerve paresis," Otholaryngology-head and neck surgery, vol. 109, no. 3, pp. 506-513, 1993.

[71] P. McIsaac, A. Craig, Y. Tran, and P. Boord, "The mind switch environmental control system: Remote hands free control for the severely disabled," Techn. Dis., vol. 14, pp. 15-20, 2002.

[72] J. M. Loomis, and C. C. Collins, "Sensitivity to shifts of a point stimulus : An instance of tactile hyperacuity," Perception and Psychophysics, vol. 24, pp. 487-492, 1978.

[73] Y. Shimizu, "Shikaku joho no shokkaku ni yoru daiko dentatsu hoshiki ni kansuru kenkyu," Dissertation at Waseda University, 1982 [in Japanese].

[74] T. R. Nelson and D. H. Pretorius, "Three-dimensional ultrasound imaging," Ultrasound Med. Biol., vol. 24, pp. 1243-70, 1998.

[75] S. Berg, H. Torp, D. Martens, *et al.* "Dynamic three-dimensional freehand echocardiography using raw digital ultrasound data," Ultrasound Med. Biol., vol. 25, pp. 745-753, 1999.

[76] R. Canals, G. Lamarque, and P. Chatain, "Volumetric ultrasound system for left ventricle motion imaging," IEEE Trans. Ultrason. Ferroelectr. Freq. Contr., vol. 46, pp. 1527-38, 1999.

[77] D. H. Turnbull and F. S. Foster, "Simulation of B-scan images from two-dimensional transducer arrays: Part 2 Comparison between linear and two-dimensional phased arrays," Ultrason. Imaging, vol. 14, pp. 334-353, 1992.

[78] P. K. Weber, R. M. Schmitt, B. D. Tylkowski, *et al.*, "Optimization of random sparse 2-D transducer arrays for 3-D electronic beam steering and focusing," Proc. IEEE Ultrasonics Symposium, pp. 1503-1506, 1994.

[79] S. Holm, B. Elgetun, and G. Dahl, "Weight- and layout- optimized sparse arrays," Proc. International Workshop on Sampling Theory and Applications, pp. 97-102, 1997.

[80] J. L. Schwartz and B. D. Steinberg, "Ultrasparse ultrawideband arrays," IEEE Trans. Ultrason. Ferroelectr. Freq. Contr., vol. 45, pp. 376-393, 1998.

[81] G. R. Lockwood, J. R. Talman, and S. S. Brunke, "Real-time 3-D ultrasound imaging using sparse synthetic aperture beamforming," IEEE Trans. Ultrason. Ferroelectr. Freq. Contr., vol. 45, pp. 980-988, 1998.

[82] M. Ueda and H. Ichikawa, "Analysis of an echo signal reflected from a weakly scattering volume by a discrete model of the medium," J. Acoust. Soc. Am., vol. 70, pp. 1768-1775, 1981.

[83] H. Taki and T. Sato, "A study on the radiation pattern using focusing method for the 3-D medical acoustic imaging system with a reflector and a 2-D array," Proc. Symp. Ultrason. Electron. vol. 27, pp. 149-150, 2006.

[84] R. M. Lutolf, A. Vieli, and S. Basler, "Ultrasonic phased-array scanner with digital echo synthesis forDoppler echocardiography," IEEE Trans. Ultrason. Ferroelectr. Freq. Contr., vol. 36, Sept. pp. 494-506, 1989.

[85] H. Kanai, H. Hasegawa and K. Imamura, "Spatial distribution measurement of heart wall vibrations generated by remote perturbation of inner pressure," Jpn. J. Appl. Phys. vol. 45 , pp. 4718-4721, 2006.

[86] H. Taki and T. Sato, "3-D ultrasound medical imaging system based on hybrid method using synthetic aperture technique," Jpn. J. Med Ultrasonics 33 Suppl. S280, 2006 [in Japanese].

[87] H. Taki and T. Sato, "High-resolution real-Time 3-D acoustic imaging system based on hybrid method: Improvement of the spatial resolution by multiple transmit and receive event," IEICE Tech. Rep. US106-109, 2006 [in Japanese].

[88] H. Taki and T. Sato, "High-resolution real-Time 3-D acoustic imaging system with a reflector" submitted to J. Medical Ultrasonics.

Major Publications

1. H. Taki, H. Yashima, and T. Sato, "Study of the Hybrid Method and the Sensor for a High-Resolution Ultrasound Vision Substitute System for Visually Handicapped," IEICE Trans. Electron., vol. J88-A, No.5, pp. 568-576, 2005 [in Japanese].

2. H. Taki, and T. Sato, "High-Resolution Real-Time 3-D Acoustic Imaging System with a Reflector," Proc. 3rd IASTED international conference on Biomedical Engineering, Feb., 2005.

3. H. Taki, and T. Sato, "Human Interface and Transmit Frequency Control for the Through-Air Acoustic Real-Time High Resolution Vision Substitute System," Proc. 27th IEEE Annual International Conference of the Engineering in Medicine and Biology Society, 2005.

4. H. Taki, and T. Sato, "Transfer Information Enhancement with a 2-D Tactile Stimulator Array for Acoustic Vision Substitute System," Proc. 28th IEEE Annual International Conference of the Engineering in Medicine and Biology Society, 2006.

5. H. Taki, and T. Sato, "Transfer Information Enhancement with a 2-D Tactile Stimulator Array for an Acoustic Vision Substitute System," IEICE Trans. Electron., Accepted.